Durham University

Durham E-Theses

Using NIR spectral features in an SDSS sample of early-type galaxies to constrain the low-mass Initial Mass Function

Helen Jermak

How to cite:

Jermak, Helen (2013) Using NIR spectral features in an SDSS sample of early-type galaxies to constrain the low-mass Initial Mass Function. Masters thesis, Durham University.

Use policy

The full-text may be used and/or reproduced, and given to third parties in any format or medium, without prior permission or charge, for personal research or study, educational, or not-for-profit purposes provided that:

- a full bibliographic reference is made to the original source
- a https://etheses.durham.ac.uk/id/eprint/7269/ is made to the metadata record in Durham E-Theses
- the full-text is not changed in any way

The full-text must not be sold in any format or medium without the formal permission of the copyright holders.

Please consult the full Durham E-Theses policy for further details.

Academic Support Office, The Palatine Centre, Durham University, Stockton Road, Durham, DH1 3LE
e-mail: e-theses.admin@durham.ac.uk Tel: +44 0191 334 6107
https://etheses.durham.ac.uk

Using NIR spectral features in an SDSS sample of early-type galaxies to constrain the low-mass Initial Mass Function

Helen Jermak

Supervisors : Dr. J. Lucey & Dr. R. Smith

A thesis submitted to the University of Durham
in accordance with the regulations for
admittance to the Degree of Master of Science.

Department of Physics
University of Durham
October 2012

Abstract

The stellar initial mass function (IMF) is a major component in galaxy formation theory, it describes the original distribution of stars as a function of mass at the epoch of formation of the population.

To investigate the form and possible variation of the IMF at low stellar-masses, features are measured in spectra from the Sloan Digital Sky Survey DR7 for a sample of $\sim$2000, low-redshift (0.010 - 0.057) red sequence galaxies and in simple stellar population models that cover a range of elemental abundances and IMFs. Particular attention is paid to the calcium triplet (at $\sim$8600 Å) and the sodium doublet (at $\sim$8200 Å) which are characteristic of high-mass ($\gtrsim$8 $M_{\odot}$) and low-mass ($\lesssim$0.5 $M_{\odot}$) stars respectively and the NaD (at 5895 Å) and CaI (at 4227 Å) features which show a strong response to their respective elemental abundances. The combination of these spectral features is a useful technique for separating the effects of elemental abundance and IMF on the size of the measured spectral features, allowing the form and variation of the IMF to be investigated individually.

The sodium abundance is constrained from the NaD index, popularly disregarded as an abundance indicator due to the effect of interstellar absorption on this feature. In this work there is no strong evidence to suggest that interstellar absorption has a detrimental effect on the abundance constraints from the NaD index.

Evidence is found for an increasing sodium abundance ([Na/Fe] $\propto \sigma^{1.654\pm0.050}$) and marginally decreasing calcium abundance ([Ca/Fe] $\propto \sigma^{-0.19\pm0.12}$) with increasing galaxy mass. With these abundances taken into consideration, the IMF variation found is slightly shallower at higher masses but also consistent with zero; Δx = -0.111$\pm$0.071 Δ log σ (where x is the power-law index describing the slope of the IMF).

Taking into consideration the average abundances, the best-fitting IMF is found to be approximately Chabrier-like, with outlying galaxies that correspond to more extreme environments including high sodium abundances and bottom-heavy IMFs.

Contents

List of Figures

List of Tables

Declaration

The work described in this thesis was undertaken between 2011 and 2012 while the author was a research student under the supervision of Dr. Russell Smith and Dr. John Lucey in the Department of Physics at the University of Durham. This work has not been submitted for any other degree at the University of Durham or any other university. The copyright of this thesis rests with the author. No quotation from it should be published without the author's prior written consent and information derived from it should be acknowledged.

Acknowledgements

I would like to thank Dr. John Lucey and Dr. Russell Smith for giving me the opportunity to undertake a part-taught part-research masters at Durham University. I am very grateful to Dr. Smith for listening and advising me and being patient when I had questions. I thank Dr. Lucey for his helpful conversations and for his comments on my thesis.

I thank Paul Evans for going abroad for six months which allowed me time to dedicate to my masters without distraction and for his support when he was close to- and far from- home.

Special thanks goes to my friends and family who have stood by me and given me encouragement when I needed it the most.

I am grateful to my colleagues at Durham University who over the last twelve months have given me computational advice, solved my `laTeX` problems and generally kept me smiling.

Chapter 1

Introduction

In order to fully understand the structure and evolution of galaxies it is crucial to gain knowledge about their stellar content. The structure and evolution of a galaxy is controlled by its quantities of brown dwarfs (<0.072 $M_\odot$ that do not undergo hydrogen burning), very-low- mass (0.072 $M_\odot$ to 0.5 $M_\odot$), low- mass (0.5 $M_\odot$ to 1 $M_\odot$), intermediate- mass (1 $M_\odot$ to 8 $M_\odot$) and high- mass (>8$M_\odot$) stars Kroupa (2002), with the evolution of individual stars primarily being dictated by their initial masses. The mass of a star controls how quickly hydrogen is burned. The more massive a star, the higher the temperature and pressure needed to prevent it from gravitational collapse which means that the more massive stars convert hydrogen into helium at a greater rate and the depletion of the hydrogen occurs more rapidly compared to stars of lower masses. The mass of the star therefore dictates its main sequence lifetime; stars populating the low-mass end of the main sequence can have main sequence lifetimes hundreds of times greater than the age of the universe, whilst high- mass stars can deplete their hydrogen supply and move onto subsequent evolutionary phases in a few million years. The mass of a star also dictates how the star contributes to the chemical enrichment of the galaxy. Stars with masses >8$M_\odot$ end their lives in supernovae and enrich the interstellar medium with metals, becoming a neutron star or black-hole. Stars with initial masses <8$M_\odot$ end their lives with a planetary nebula; enriching the interstellar medium with carbon from the outer shells, leaving behind a white dwarf. If a white dwarf begins accreting from a binary companion, it can eventually exceed the Chandrasekhar limit and begin collapsing as it is no longer supported by electron degeneracy pressure. This collapse heats the core and allows carbon fusion to occur. The process of nuclear fusion continues as it would in a higher mass star (e. g. >8$M_\odot$) and eventually the star undergoes a type 1a supernova explosion, enriching the interstellar medium with elements formed during nuclear fusion, and becomes a neutron star. The distribution of the masses of stars at the beginning of the star formation epoch is a useful tool for dictating the evolution of the galaxy containing those stars.

1.1 The Initial Mass Function

The initial mass function (IMF) is an empirical function that describes the distribution of stars in a given population at a certain occurance of star formation. It can be defined as

$$dN = \xi(m)dm \tag{1.1}$$

where m is the stellar mass and N is the number of stars in the mass interval m,m+dm. At specific masses the IMF is proportional to a power law; ξ(m) $\propto$ $m^{-\alpha}$.

Theoretical considerations suggest that the intrinsic, stellar IMF follows a power law slope with α $\approx$2 (Oey (2011)). The slope represents the formation of stars from clumps which are made up of molecular clouds. Extensive studies carried out in spiral galaxies such as the Milky Way and local stellar populations (Kroupa (2001), Chabrier (2003), Kroupa et al. (1993)), along with more distant, older galaxies (Spiniello et al. (2011)), find a similar value for the slope of the IMF for stars with masses $\gtrsim$1 $M_{\odot}$, prompting the idea that the IMF may be universal. Bastian et al. (2010) conclude in their review paper that there is no clear evidence for a non-universal IMF in the Milky Way or in other galaxies. However, since then, it has also been reported that massive, old galaxies have been found to have bottom-heavy IMFs (Conroy & van Dokkum (2012a)) and that there is a trend with velocity dispersion that suggests that low-mass galaxies require Salpeter-like IMFs and the more massive galaxies require more bottom-heavy IMFs (Spiniello et al. (2012), Ferreras et al. (2012)). It is crucial to determine whether there is any variation in the IMF as many theoretical models rely on the assumption that the IMF is universal. This means that if the IMF is in fact found to be dependent on environment or other factors, the presence of a universal IMF in the theoretical models could be a source of substantial error.

The question of the universality of the IMF is one of the largest sources of uncertainty in the field of stellar population studies. Any variations detected in the IMF could provide information about the process of star formation in different stellar populations, along with providing an important constraint for theories of star formation as they would have to reproduce the various IMF values for different populations along with explaining why it varies.

Along with being used in galaxy formation models, the IMF can also be used to create model galactic spectra by combining individual stellar spectra from empirical and theoretical libraries according to the quantities specified by a given IMF slope. This, along with the current knowledge of stellar physics and evolution, is used to create a model spectrum of a stellar population at a certain epoch. Various model spectra can be created with different IMF slope values, ages and metallicities, which can then be compared to observational data to find the best-fitting IMF. The IMF can also be used to calculate the stellar mass of a population according to the total luminosity. The assumed IMF identifies the proportion of

different mass stars that make up the population and can therefore be used to calculate the total stellar mass. This technique is very sensitive to changes in the IMF, so if the IMF is proved to vary with galaxy mass it will affect the stellar masses calculated for different populations.

1.2 Determining the IMF

The IMF can be determined using a variety of techniques depending on the type of population being investigated. The first investigations of the IMF were carried out on Galactic stellar populations and those local to the Milky Way where the individual stars are resolvable. The study was then extended to more distant populations through a variety of techniques including gravitational lensing and dark matter density profiles, stellar kinematics and the measurement of spectral features in galaxy spectra.

1.2.1 Measuring the IMF in resolved populations

For stellar populations in and local to the Milky Way, it is possible to carry out stellar counts using a volume-limited survey and accurate distance measurements or using deep pencil-beam surveys that can extract hundreds of low-mass stars from stellar and galaxy images (Kroupa (2002)). The number of stars of different luminosities present in a given volume is called the present day luminosity function. This can be converted to a present day mass function (PDMF) using the established mass-to-light ratio of the stars. Once calculated, the PDMF can then be converted to an IMF by tracing the stars' evolution back along stellar evolutionary isochrones.

Edwin Salpeter of the Australian National University (Salpeter (1955)) was the first author to empirically evaluate the slope of the IMF, he referred to it as the 'Original Mass Function'. It appears that the concept of Salpeter's 'Original Mass Function' was first referred to as the 'initial mass function' in Warner (1961)'s paper 'The form of the initial mass function'. Salpeter presented his original mass function in a logarithmic form :

$$\frac{\mathrm{dN}}{\mathrm{d}\log \mathrm{m}} \propto \mathrm{m}^{-\Gamma} \tag{1.2}$$

where m is the stellar mass and N is the number of stars within the mass interval. Here Γ= α-1. [1]

He proposed a power law index value of Γ = 1.35 (i.e. α=2.35) for the initial distribution of stars in the mass range 0.4 $M_\odot$ to 10 $M_\odot$ in the solar neighbourhood. He used a proposed fraction of stars of certain spectral types, and using only main sequence stars, placed these stars on the HR-diagram and worked backwards to

[1] To clarify, in this work the slope of the IMF will be described in the power-law form ($\xi(\mathrm{m}) \propto \mathrm{m}^{-\alpha}$) rather than the logarithmic form used by Salpeter and other authors.

find an initial distribution. Once correction had been made for stars that were not on the main sequence, the resulting power-law index value was Γ = 1.35 (i.e. α=2.35). Despite it being almost 60 years since Salpeter's work on the IMF and the volume of work carried out by other authors, the Salpeter slope still stands as a good approximation for Galactic and many extragalactic stellar populations for stars with masses $\gtrsim 1\ \mathrm{M}_{\odot}$.

In the 1970s, authors proposed that the IMF was not the same over all mass ranges and could not be described by a single power law. Over the next thirty years they advanced from Salpeter's original work by finding a segmented IMF according to different mass ranges provides the best description of Galactic stellar populations. Using star-count data and models, Kroupa et al. (1993) propose a multi-segmented power-law relationship for the IMF according to three different mass ranges;

$$\begin{aligned} 0.70 < \alpha < 1.85 \quad &\text{for} \quad 0.08\ \mathrm{M}_{\odot} < \mathrm{M} \leq 0.5\ \mathrm{M}_{\odot} \\ \alpha = 2.2 \quad &\text{for} \quad 0.5\ \mathrm{M}_{\odot} \leq \mathrm{M} \leq 1\ \mathrm{M}_{\odot} \\ \alpha = 2.7 \quad &\text{for} \quad \mathrm{M} > 1\ \mathrm{M}_{\odot} \end{aligned}$$

In Scalo's review paper (Scalo (1998)), the Galactic IMF is presented as a three-segment logarithmic power law. For clarity, here, the results are presented in the non-logarithmic form with the IMF slope steepest at intermediate masses:

$$\begin{aligned} \alpha = 1.2 \pm 0.3 \quad &\text{for} \quad 0.1\ \mathrm{M}_{\odot} < \mathrm{M} \leq 1\ \mathrm{M}_{\odot} \\ \alpha = 2.7 \pm 0.5 \quad &\text{for} \quad 1\ \mathrm{M}_{\odot} < \ \mathrm{M}\ \leq 10\ \mathrm{M}_{\odot} \\ \alpha = 2.3 \pm 0.5 \quad &\text{for} \quad 10\ \mathrm{M}_{\odot} < \mathrm{M} \leq 100\ \mathrm{M}_{\odot} \end{aligned}$$

The Galactic-field IMF proposed by Kroupa (2001) differs from the value of Scalo (1998) as the correct structure in the luminosity function below 1 $\mathrm{M}_{\odot}$ is accounted for by Kroupa. The Kroupa (2001) IMF is segmented into four mass ranges :

$$\begin{aligned} \alpha_0 = 0.3 \pm 0.7 \quad &\text{for} \quad 0.01\ \mathrm{M}_{\odot} \leq \mathrm{M} < 0.08\ \mathrm{M}_{\odot}, \\ \alpha_1 = 1.8 \pm 0.5 \quad &\text{for} \quad 0.08\ \mathrm{M}_{\odot} \leq \mathrm{M} < 0.50\ \mathrm{M}_{\odot}, \\ \alpha_2 = 2.7 \pm 0.3 \quad &\text{for} \quad 0.50\ \mathrm{M}_{\odot} \leq \mathrm{M} < 1.00\ \mathrm{M}_{\odot}, \\ \alpha_3 = 2.3 \pm 0.7 \quad &\text{for} \quad 1.00\ \mathrm{M}_{\odot} \leq \mathrm{M}. \end{aligned}$$

Zoccali et al. (2000) derived the slope of the IMF for low-mass Galactic bulge stars using stellar counts and found an overall IMF slope of α = 1.33 $\pm$ 0.07 for stars with masses $0.15 \lesssim \mathrm{M}/\mathrm{M}_{\odot} \lesssim 1$. This was also represented as a segmented IMF with two stellar mass ranges, in good agreement with Kroupa et al. (1993) :

$$\alpha = 1.3 \quad \text{for} \quad 0.15\,\mathrm{M}_\odot \leq \mathrm{M} < 0.50\,\mathrm{M}_\odot,$$
$$\alpha = 2.2 \quad \text{for} \quad 0.50\,\mathrm{M}_\odot \leq \mathrm{M} < 1.00\,\mathrm{M}_\odot.$$

Zoccali et al. (2000) found a luminosity function for the lower main sequence stars in the Galactic bulge and converted this to a mass function (which is the same as the IMF as the stars have not evolved far along the main sequence from where they formed) using a mass-luminosity relation established by Henry & McCarthy (1993) for solar metallicity stars. The stars in the Milky Way's bulge are the best resolvable stellar population that could be similar to elliptical galaxies, with regards to age and abundance. The bulge and disk of the Milky Way have very different star formation histories and conditions, if the slope of the IMF for these two populations are found to be similar, then it would give strong evidence for a robust and non-varying IMF.

Chabrier (2003) looked at stars in the Galaxy disk, spheroid, young and globular clusters and suggested the IMF is segmented with a log normal slope below 1 $\mathrm{M}_\odot$ and a power-law form for stars with masses $\gtrsim 1\ \mathrm{M}_\odot$, with the form :

$$\xi = \begin{cases} 0.158 \text{ exp } [-(\log \mathrm{M} - \log 0.079)^2/2(0.69)^2], & \text{for M} \lesssim 1\mathrm{M}_\odot \\ 0.0443\ \mathrm{M}^{-2.3}, & \text{for M} \gtrsim 1\mathrm{M}_\odot. \end{cases}$$

In their review, Bastian et al. (2010) summarise the recent findings with regard to the possibility of a varying IMF. Their main conclusion is the high-mass end (i.e. $\sim$0.5-2 $\mathrm{M}_\odot$ to $\simeq$ 150 $\mathrm{M}_\odot$) is well approximated by a power law slope of $\alpha \simeq$2.35. At lower masses they suggest an approximation of a log-normal distribution, with a peak at $\sim$0.2 - 0.3 $\mathrm{M}_\odot$ and a dispersion of $\sim$0.5 - 0.6 $\mathrm{M}_\odot$ or a series of broken power laws with a similar shape. Despite the large uncertainty, they suggest a substellar IMF of a $\alpha \lesssim$1.5 power law and the extrapolation of the log-normal distribution to lower masses.

1.2.2 External galaxies

For external galaxies whose stars are not resolvable, it becomes more complicated to establish an IMF. The individual stars cannot be separated from each other so it is not possible to carry out stellar counts, instead analysis has to be done using the integrated light from the galaxy. There are three main methods for establishing the IMF in non-resolvable stellar populations; two are often used together and involve establishing a stellar mass-to-light ratio as a constraint on the IMF.

Gravitational lensing of a galaxy occurs when the light travelling from a distant source, which is aligned correctly with respect to the observer, is bent around the galaxy creating arcs of distorted light (see Einstein (1936)) . Gravitational lensing is predicted by general relativity and is used to constrain the mass within the radius of the cylinder enclosed by the arcs of light. Gravitationally lensed galaxies

are extremely useful for many aspects of astrophysics; such as calculating galactic mass, constraining cosmological parameters and exploring dark matter and dark energy. The gravitational lens model allows the constraint of the total mass within the Einstein radius of a lensed galaxy, which is made up of the stellar and dark matter components. For the purpose of investigating the IMF and establishing a stellar mass-to-light ratio, it is important to separate the stellar and dark matter contribution. This is often done using an established form for the dark matter density profile and marginalizing over the possible inner slope of the density profile to provide estimates of the stellar and dark matter contribution to the total mass within the Einstein ring. With the proposed stellar mass a stellar mass-to-light ratio is created and can be compared to those mass-to-light ratios predicted by different IMFs. Sonnenfeld et al. (2012) use a particularly powerful gravitational lens known as the 'Jackpot' which is special because it lenses two sources at different redshifts. They use the Jackpot lens to constrain the total mass within two Einstein rings and the findings agree with a Salpeter IMF. Treu et al. (2010) and Spiniello et al. (2011) use gravitational lensing along with stellar dynamics and stellar population synthesis models to constrain the IMF and both find evidence for a Salpeter IMF also.

Another method used to constrain the mass-to-light ratio of a galaxy and subsequently the IMF, is stellar dynamics. Using Integral Field Spectroscopy a telescope fibre is pointed at each part of a galaxy and a spectrum is taken for every pixel. This allows the distribution of velocity dispersions to be mapped and therefore constrain the mass within multiple radii. In the same way as the gravitational lensing method, the dynamics constrains the total mass within a radius and a dark matter density profile is then used to constrain the stellar mass fraction within that radius. This stellar mass fraction is used to calculate the stellar mass-to-light ratio and is compared to those predicted by various IMFs. Cappellari et al. (2012) used dynamical models and integral-field maps of stellar kinematics and found that the IMF varies in early-type galaxies; from Kroupa-Chabrier like to more massive than Salpeter with increasing mass-to-light ratio. They attempt to explain this trend by suggesting that present-day massive early-type galaxies formed the majority of their stars in intense starbursts and at higher redshifts than spiral galaxies.

The main issue with the gravitational lensing and stellar dynamics methods is that they cannot provide a direct constraint on the low-mass star contribution to the IMF. To explore the specific low-mass star contribution to the total stellar budget, it is necessary to look at the galaxy's composite spectrum.

The features present in a galaxy's spectrum are representative of the different elements and molecules found in the stars' atmospheres. Some features are characteristic of different mass stars and can be explored to find the fraction of high- or low-mass stars and therefore constrain the IMF directly. There are also features that are characteristic of elemental abundances and can be combined with

the IMF indicative features to break the degeneracy between IMF and abundance effects. Observational spectra can be compared to model galaxy spectra which have been created using different ages, metallicities and IMFs. Comparison between the measured equivalent widths of the same spectral features from the observed and model spectra can determine the best fitting IMF, it is also possible to use this technique to determine whether there is a variation in the IMF with velocity dispersion. Using this method it is possible to constrain the low-mass IMF if features are measured in stellar populations that are devoid of the high-mass, fast-evolving stars; such as early-type galaxies. van Dokkum & Conroy (2010) use a similar method of comparing equivalent widths of IMF characteristic features in model spectra to observational data. Their method involves spectral fitting the model data to the observed spectra but adjusting the model parameters. They report a steeper than Salpeter, 'bottom-heavy' slope for massive, luminous, elliptical galaxies in the near Universe, with a power-law index value of α = 3.5, which suggests a large low-mass star population and therefore implies a difference in the star-formation history of these galaxies to that of the Milky Way (more detail to follow).

1.2.3 The low-mass IMF

A galaxy's spectrum is composed of the light from the different stars that make up that galaxy. Low-mass stars contribute substantially to the total mass budget, but have little contribution to the total luminosity (approximately 1%) (van Dokkum & Conroy (2010)). In late-type galaxies where star formation is on-going or recent, the stars that dominate the light are high mass stars ($\gtrsim 8 M_\odot$). High mass stars are more luminous than their lower mass companions and mask the contributory light from the less luminous stars. This leads to an IMF that does not adequately describe the distribution of low mass stars. In order to explore the shape of the low mass end of the IMF, it is important to focus on early-type galaxies, those that do not have on-going star formation and have not undergone recent star formation. Due to their comparatively short main sequence lifetimes, the high mass stars in early-type galaxies will have evolved off the main sequence and no longer dominate the total light output of the galaxy, making the light contribution from low mass stars easier to study.

The main problem with spectral analysis using early-type galaxy data is that the spectra of K and M giants and M dwarfs are very similar. K and M giant stars are, as the name suggests; large stars (with radii approximately 10 - 100 $R_\odot$). They are late in their evolution and populate the red giant branch on the HR diagram. They have the same effective temperature as M dwarf stars, but a much higher luminosity. The M dwarf stars are relatively cool and have low masses ($0.075\ M_\odot \lesssim M \lesssim 0.5\ M_\odot$). They burn hydrogen at a slower rate and have much longer lifetimes than high mass stars meaning that in early-type galaxies low mass stars dominate the main sequence. The spectra of K and M giants and

M dwarfs are very similar due to their similar effective temperatures, however, they can be distinguished from each other by looking at certain spectral features that are characteristic of giant or dwarf stars.

1.2.4 Surface gravity effects

The discovery of spectral features characteristic of dwarf- or giant- stars allows the exploration of the low mass star contribution to the composite spectrum of a galaxy. The Wing-Ford (FeH) band (Wing & Ford (1969)) at 9896 Å was one of the first IMF indicative features discovered. The origin of the feature was an unknown until 1977 when Nordh et al. (1977) confirmed that it could be attributed to the iron hydride molecule. Jones et al. (1984) found that the calcium triplet (near 8600 Å) was strong in giants and weak in dwarfs, whereas the sodium doublet feature (8183 and 8195 Å) is conversely strong in dwarfs and weak or absent in giants. van Dokkum & Conroy (2010) utilised the fact that the Wing-Ford band and the Na I doublet are strong in stars with masses <0.3 $M_{\odot}$ to constrain the IMF in a selection of massive and luminous early-type galaxies in the nearby Universe. In Conroy & van Dokkum (2012a) they also explored the use of the calcium triplet feature to constrain the shape of the low mass IMF, and identified other features that are stronger in dwarfs than giants (CaI at 1.98 μm, KI at 1.17 μm and AlI at 1.31 μm) and stronger in giants than dwarfs (CO near 2.30 μm and various CO lines from $\sim$1.55 to 1.75 μm). Another feature which has been utilised to constrain the low- mass IMF is the titanium oxide feature at 6230 Å which is strong in giants and weak or absent in dwarfs (Spiniello et al. (2012)).

The discovery of these spectral features means, in principle, that it is possible to identify the relative contributions of M dwarfs or K and M giants in a galaxy spectrum. Conroy & van Dokkum (2012a) suggest the occurence of different features for different mass stars is due to surface gravity effects. As stars exhaust their supply of hydrogen their core starts to contract starting the hydrogen shell burning stage of the star's evolution. At the same time the radius of the star as a whole starts to increase. For stars with high initial masses (i.e. $\gtrsim$8 $M_{\odot}$), their evolution post-main sequence is quicker than that of their lower mass companions, and due to their greater temperatures and pressures they undergo nuclear synthesis reactions beyond carbon and oxygen creating elements up to and including iron. Their radii expand with the process of core contraction and they become supergiants. The post-main sequence evolution of intermediate mass stars ($\sim$1 - 8 $M_{\odot}$) is similar to that of the high mass stars but they do not undergo carbon-burning, their cores contract and their radii increase making them swell to giants. For stars with initial masses $\lesssim$1 $M_{\odot}$ their main sequence lifetime is considerably longer, for some stars ($\sim$0.5 $M_{\odot}$) their main sequence lifetime is greater than the age of the observed Universe. These stars are those still on the main sequence in early-type populations.

The increase in radius of giants and supergiants causes a decrease in the effect

of gravity at the surface, and therefore a decrease in electron pressure. This decrease in electron pressure, demonstrated by the Saha equation, causes the ratio of singly ionised to neutral species to increase (Conroy & van Dokkum (2012a)). Dwarf stars are of lower initial mass and at the same epoch are still on the main sequence undergoing hydrogen burning. They have a smaller radius than the giant and therefore a stronger surface gravity. It has been found that every neutral metal feature is strong in dwarfs and weak in giants, and conversely, every singly ionised metal feature is weak in dwarfs and strong in giants Conroy & van Dokkum (2012a). Conroy & van Dokkum (2012a) also state that for molecules, such as iron hydride (FeH), the increase in the partial pressure of atoms and molecules favours the side of a chemical reaction that produces fewer moles of gas. This means that iron hydride is prominent in dwarf stars rather than giants because the greater surface gravity in dwarfs causes a higher pressure meaning the formation of FeH is favoured over the individual atoms of iron and hydrogen.

van Dokkum & Conroy (2010) exploited the effect of surface gravity on certain spectral features to investigate the IMF in luminous and massive elliptical galaxies in the local Universe, as previously mentioned. They found evidence for a bottom-heavy IMF with a slope of α = 3.5, much steeper than the Salpeter-like IMF found in Galactic populations. Focusing on the Na I doublet and the Wing-Ford band they compared model spectra to averaged observed spectra from the Coma and Virgo cluster separately, finding the best fitting model for the Wing-Ford band to be the x = 3.0 (i.e. α = 3.0) IMF model, and the best fitting model for the NaI doublet being the even more dwarf-heavy x = 3.5 (α = 3.5) IMF model. This would suggest a much larger population of low mass stars in elliptical galaxies than in spiral galaxies like the Milky Way; therefore a greater mass-to-light ratio than that predicted by a Chabrier or Salpeter slope (the larger number of low mass stars contributing more mass than light) and an IMF that is not universal but depends on prevailing conditions at the time of star formation. van Dokkum & Conroy (2010) conclude that the IMF appears to be Kroupa-like in quiet, star-forming disks and more dwarf-heavy in the galaxies that evolved to become massive elliptical galaxies.

Conroy & van Dokkum (2012b) continue to explore the spectral lines characteristic of low mass stars (as discussed in their paper Conroy & van Dokkum (2012a)) using a new population synthesis model and spectra of 38 early-type galaxies and the nuclear bulge of M31. They find strong evidence for a varying IMF according to galaxy velocity dispersion and α-enhancement; with dwarf-heavy IMFs in more massive systems. Their new mass-to-light ratios do not violate dynamical or colour constraints and are a factor of ≈ 2 greater than that of a Kroupa-like IMF such as that found for the Milky Way. Conroy & van Dokkum take abundance variation into consideration as part of their analysis and find a high value for the sodium abundance ([Na/Fe] $\approx$ 1.0) for their best-fitting models. They do not use the NaD feature (at 5895 Å) to constrain their sodium abundance due to the sus-

pected effect of interstellar absorption of the feature, they instead use it to define an upper limit for the sodium abundance. They constrain the sodium abundance using the NaI feature at ($\sim$8200 Å) and the fact that the sodium abundance has an indirect effect on the entire spectrum due to its influence on the free electron abundance in stellar atmospheres (Conroy & van Dokkum (2012b)).

Spiniello et al. (2012) focus on the spectral features NaI and TiO as IMF indicators because for these features the effects of age and metallicity are orthogonal to the effects of the IMF. The authors focus on Sloan Digital Sky Survey spectra and an X-Shooter Lens Survey (XLENS) gravitational lens, comparing those to simple stellar population models (created by Conroy & van Dokkum (2012a)) to find a mildly steepening IMF with increasing mass from Salpeter (α = 2.35) to α = 3.0 for early-type galaxies in the range of σ = 200 - 335 km s^{-1}.

Smith et al. (2012) investigate the possibility of variations in the IMF in red-sequence galaxies in the Coma Cluster. They stack infrared spectra obtained from Subarau/FMOS to create composite spectra for galaxies grouped according to their velocity dispersion or [Mg/Fe] ratio. The spectral features focused on are the Ca I line at 10345 Å and the iron hydride (Wing-Ford) band. They find no clear evidence for an increase in dwarf-star content with velocity dispersion, but find the IMF slope changes from Chabrier-like in solar-abundance populations to Salpeter or heavier for highly α-enhanced populations, suggesting an IMF that depends on the mode of star formation.

Ferreras et al. (2012) measure spectral line strengths in the stacked spectra of local early-type galaxies and compare these to population synthesis models (MIUSCAT). They too find a correlation between the slope of the IMF and central galaxy velocity dispersion; the IMF increasing from a bottom-light, Kroupa-like function for low velocity dispersion galaxies (σ = 150 km s^{-1}), to a bottom-heavy IMF exceeding the Salpeter slope for higher velocity dispersion galaxies (σ = 200 km s^{-1}). They do not, however, take into consideration the possible change in abundances with galaxy mass, in particular the sodium abundance, which can have an effect on the predicted slope of the IMF.

1.2.5 Abundance effects

It is important that, along with the IMF, the effects of certain elemental abundances are taken into consideration for a particular stellar population. This is because the change in elemental abundances can affect the size of the spectral features' equivalent widths and therefore have an effect on the interpretation of the IMF for that population. Nelan et al. (2005) investigate the average stellar populations for a sample of red-sequence galaxies by fitting observed line-strength-σ relations according to the common trends of age, metallicity and α-abundance. They find positive scaling relations according to their galaxy sample and these relations can be combined with scaling relations from models to predict a line-strength-σ slope.

Smith et al. (2007) and Smith et al. (2009) also compare line-strength-σ slopes with Conroy & van Dokkum (2012a) model predictions and find scaling relations for their galaxy sample. The scalings constrained from their galaxy sample suggest a positive trend for age, α-abundance and metallicity with velocity dispersion. Due to the different galaxy samples and models used by the authors, the scaling relations, when used in this piece of work, predict different index-sigma slopes and are therefore used as a comparison with each other.

Graves et al. (2007) used stacked spectra of red-sequence galaxies, along with Schiavon models, to measure age, [Fe/H]- and a range of elemental- abundance ratios. They find [Ca/Fe] values that are roughly solar for their galaxy sample ([Ca/Fe] $\propto \sigma^{0.130\pm0.039}$).

Johansson et al. (2012) use Thomas et al. (2011) stellar population models based on the MILES stellar library to constrain abundance ratios (including [Ca/Fe]) in $\sim$4000 early-type galaxies from the Sloan Digital Sky Survey. They find [Ca/Fe] ratios that are close to solar over the whole range of velocity dispersions covered ($\sim$30 - 400 km s^{-1}).

1.3 Scope and structure

With regard to these recent findings, this work focuses on investigating the IMF variation for early-type galaxies with consideration for the effects of [Na/Fe] and [Ca/Fe]. It is thought that neglecting the abundance effects from IMF analysis can lead to misleading results. Equivalent widths of spectral features in model and observational data are measured with particular attention paid to the NaI doublet at 8183 and 8195 Å and the CaII triplet near 8600 Å which are exploited for their utility as dwarf and giant star indicators. The observational data is taken from the Sloan Digital Sky Survey and compared to model spectra constructed by Conroy & van Dokkum (2012a). The models cover a range of ages and abundances, along with a range of IMFs from dwarf-enriched to dwarf-depleted including Salpeter and Chabrier type IMFs. The variation of the IMF is explored through comparing index-sigma plots of various indices for both model and observational data, and the relationship between the line strengths from the models and observational data is also explored by doing index-index plots of spectral features associated with the same elements.

Section I covers the data and sample selection, Section II introduces the results of the data analysis and describes the models used, whilst Section III and IV, respectively, carry out a discussion of the results and conclude the findings of this work.

Chapter 2

Data and Sample Selection

The fundamental data for this work were taken from the Sloan Digital Sky Survey (SDSS), DR7 data release (Abazajian et al. (2009)). SDSS is a 2.5 metre telescope equipped with a 120 - megapixel camera and a pair of spectrographs, it is located at Apache Point Observatory in New Mexico, USA. The DR7 data release is the final section from the second survey (SDSS-II) which ran from 2005 - 2008, the first survey, SDSS-I, ran from 2000 - 2005. The data is publically available and although superseded by a further release, DR8, from the third and final survey (SDSS-III), it is the DR7 release which will be used in this work (for reasons that will be explained later in this section). The DR7 release has a wavelength coverage of 3800 - 9200 Å and a resolution of 1850 to 2200 for each spectrum.

The galaxy sample for use in this work was selected using the catalogue archive jobs system or 'Casjobs' which combines SDSS data and GalaxyZoo definitions for searching for specific types of data. GalaxyZoo (Banerji et al. (2010) and Lintott et al. (2008)) invites members of the public to identify features of the extensive galactic images from the SDSS library visually with the motivation that human-eye is better for identifying subtle features than a computer. Among other questions, users are asked to specify whether galaxies are smooth, have features or disks or whether they have a star or artifact in the image. Those galaxies that are selected by users to be 'smooth' are classed as elliptical galaxies. For the purpose of this work, early-type galaxies are required as they do not contain as many high-mass, main sequence stars that will dominate the light output. For this reason the sample was restricted to galaxies where all users have classed them as 'smooth'; with the aim of excluding the spiral galaxies that host on-going star formation.

The other criteria set for the CasJobs search were a signal-to-noise of >25 Å, and a redshift range of 0.01 to 0.057. The calcium triplet feature is the reddest spectral line used in this piece of work and is found at wavelengths 8498, 8542 and 8662 Å. This means that if the selected galaxies are at too high redshift then the feature of interest will be redshifted out of the measured region. The reddest wavelength covered by the calcium triplet is at 8725 Å. The maximum wavelength SDSS measures up to is approximately 9220 Å. This means that the largest redshift value that the sample can be selected from is z_{max} = 9220/8725 -1 = 0.057.

Local galaxies are also excluded from the data set; those galaxies at redshifts <0.01 appear too large on the sky meaning the projected aperture of the telescope fibre is very small, capturing light from a localised part of the galaxy and not being representative of the galaxy as a whole.

The syntax for the CasJobs search is shown below, the total number of galaxies found by the search was 9194.

```
select * from
public.galaxyzoo.GalaxyZoo1_DR_table2 as zoo, specobj as spec
where zoo.objid=spec.bestobjid
and spec.z>0.01 and spec.z<0.057 and zoo.elliptical=1 and sn_2>25
```

Following the CasJobs selection, subsequent filtering removed the galaxies that had erroneous velocity dispersions (SDSS assigned a value of -9999 to these galaxies), along with those galaxies that displayed Hα lines with equivalent widths >-10 Å (removing those galaxies with on-going star formation from the selection) and finally a further signal-to-noise cut of >48 per Å resulting in 2024 galaxies in the final sample. The Hα equivalent width selection value of >-10 Å was found by trial and error; looking at the scatter of the Hβ index values and visually inspecting some of the spectra excluded by the cut, the further signal-to-noise cut was found by similar methods; removing extreme outlier points.

Figure 2.1 shows the distribution of galaxies in the final sample; the lack of data at the low velocity dispersion, high redshift region is due to the fact that small galaxies at that distance would not be bright enough for good signal-to-noise detection. The low redshift region covers a smaller volume meaning that it is less likely to find the 'rarer' high velocity dispersion elliptical galaxies; explaining the lack of data in that region.

2.1 Skyline-subtraction

In this work the spectral features of interest occur in the near-infrared region of the spectrum. This is a particularly difficult area of the spectrum to study for two reasons. It is notoriously noisy due to the poor detection sensitivity at the red end of the spectrum, fortunately this has been improved by the advances in near-IR technology since the 1980s and 1990s. Also, the near- IR region is scattered with OH sky lines (longward of 6700 Å); disrupting the spectral features of interest. In an attempt to remove the telluric features from the spectra, SDSS has a custom-designed set of software pipelines, however, there has been a slight misalignment, leading to well-defined residual patterns that mask the spectrum and interfere with the features of interest. Wild & Hewett (2005) & Wild & Hewett (2010) have created a set of 'cleaner' spectra with the skyline residuals subtracted and have made them publically accessible. Wild & Hewett estimate a Poisson

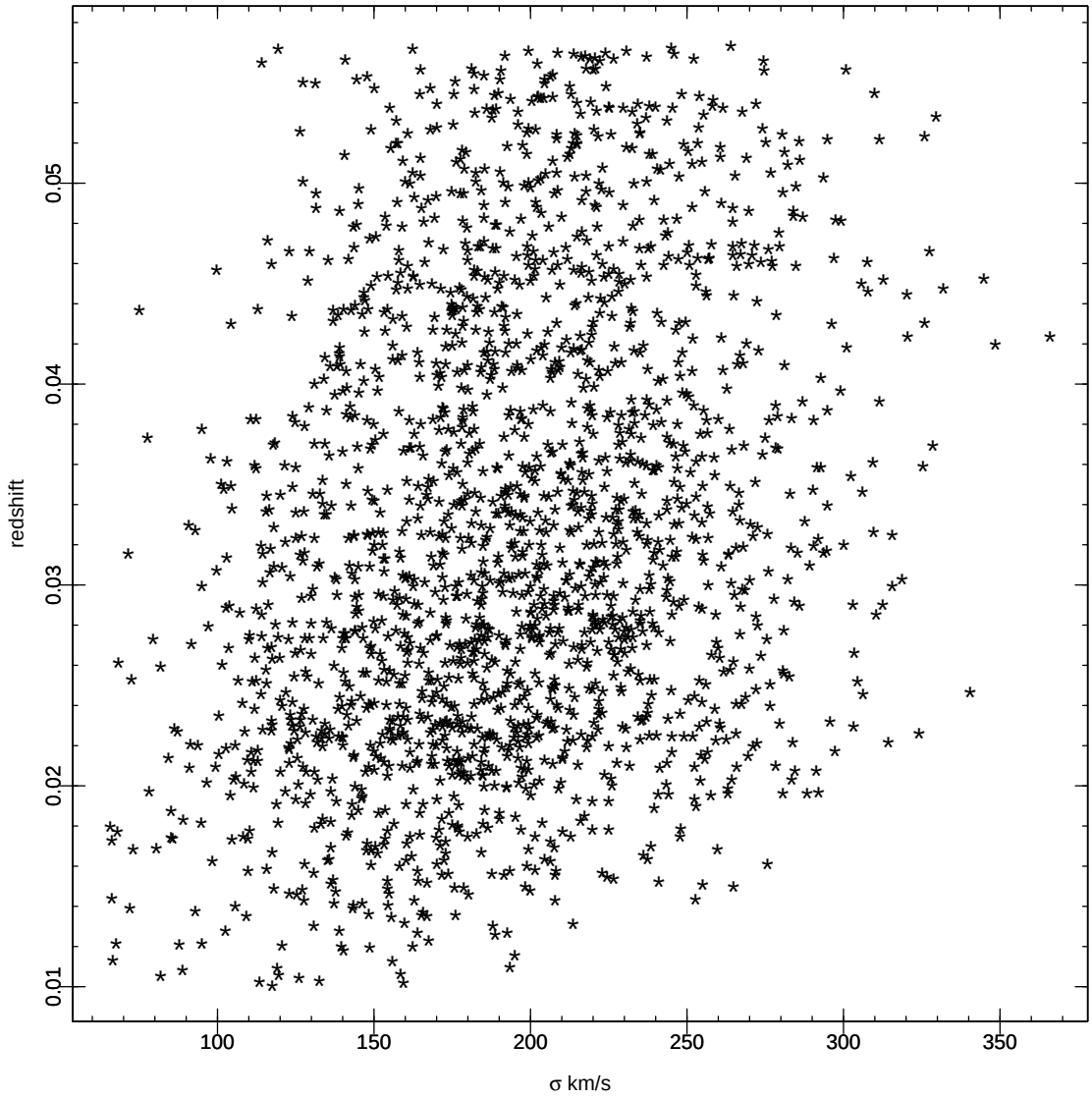

Figure 2.1: Selection of galaxies used in this work according to redshift and velocity dispersion. Lack of data at high redshift and low velocity dispersion is due to the fact that the sources are too small and faint at that distance to be detected. Lack of data at greater velocity dispersions and low redshift is due to the small volume of space at low-redshift therefore less 'rare' objects like high velocity dispersion elliptical galaxies.

noise spectrum for each SDSS plate; the Poisson noise spectrum is corrected for the rescaling that was applied by the SDSS reduction pipeline on the OH lines, and the sky spectrum is then normalised by the expected Poisson noise. A principal component analysis (PCA) is then performed on the Poisson error normalised sky spectra to produce a set of orthogonal components that represent the systematic residuals caused by the OH emission lines (Wild & Hewett (2010)). Once the galaxy sample had been selected using CasJobs, the corresponding galaxies were selected from the Wild & Hewett data online according to their fiber, plate and modified julian date (MJD) to create the final dataset.

2.2 The Models

The models used for comparison with observational data were created by Conroy & van Dokkum (2012a) as a function of age, abundance, metallicity and IMF. The models cover ages of 3 - 13.5 Gyr, abundances of solar, α-enhanced ([α/Fe] = 0.3), α-depleted ([α/Fe] = -0.3) along with the abundances of various other elements (including nitrogen, titanium, magnesium, silicon, sodium, calcium, iron and carbon) and IMFs ranging from extremely bottom-heavy x = 3.5, x = 3.0, Salpeter, Chabrier to a bottom-light IMF which is an extension of the Chabrier IMF (see Section 2.1.1) with a turnover at higher masses (i.e. $\sim$2 $M_\odot$ rather than the $\sim$0.08 $M_\odot$ used by Chabrier). The different IMFs used in the models are shown graphically in Figure 2.2.

The galaxy models were constructed by Conroy & van Dokkum (2012a) from stellar spectral libraries; the proportion of spectra for a certain stellar type is determined by selecting an IMF and adding the respective amounts of different stars accordingly. The age of the population is depicted using stellar isochrones which describe the behaviour of stars of different types as they move through evolutionary stages. The Conroy & van Dokkum (2012a) models used in this work were constructed from IRTF and MILES empirical spectral libraries with three separate isochrones to cover from the hydrogen burning limit to the asymptotic giant branch (AGB) stage of stellar evolution. These isochrones were the Dartmouth (main sequence and red giant branch) (Dotter et al. (2008)), Padova (horizontal branch and AGB) and Lyon isochrones for M<0.2 $M_\odot$ (due to application of surface boundary conditions at τ = 100 rather than T = T_{eff} which suits the environment of low-mass stars better) (Chabrier & Baraffe (1997), Baraffe et al. (1998)).

Each of the models were taken as tabulated data, converted into a spectrum and broadened to a range of velocity dispersions in order to provide better comparison with the observational data (where the spectral features are broadened due to the movement of the stars within the galaxy). Figure 2.3 shows the spectra for a range of models with differing IMFs (and ages of 13.5 Gyr and solar metallicity) within the region of 8000-9200 Å. The observed galaxy has a velocity

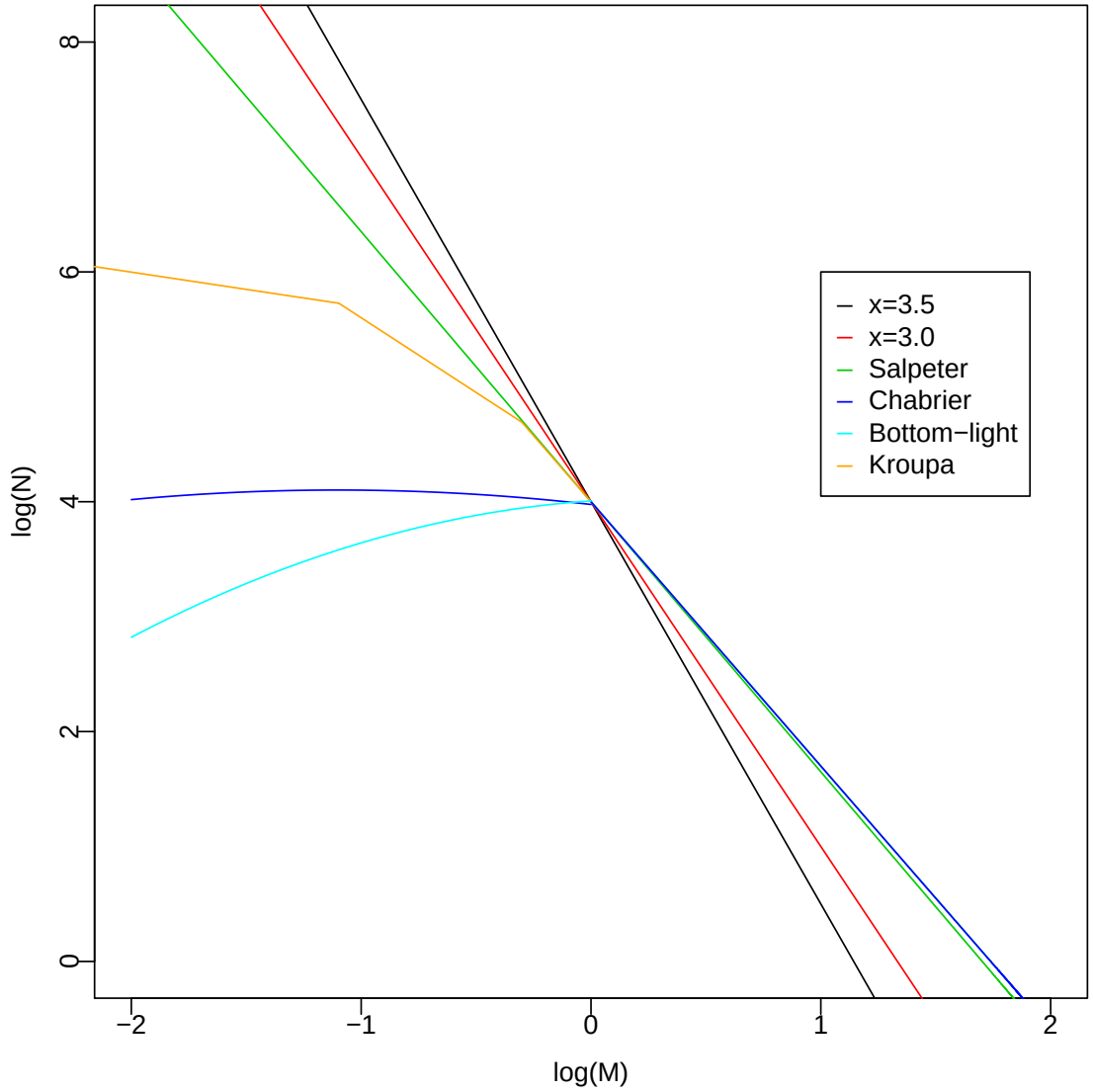

Figure 2.2: The standard stellar IMFs shown graphically; bottom heavy (x=3.5 and x=3.0), Salpeter, Chabrier, Kroupa and bottom-light (see text for details)

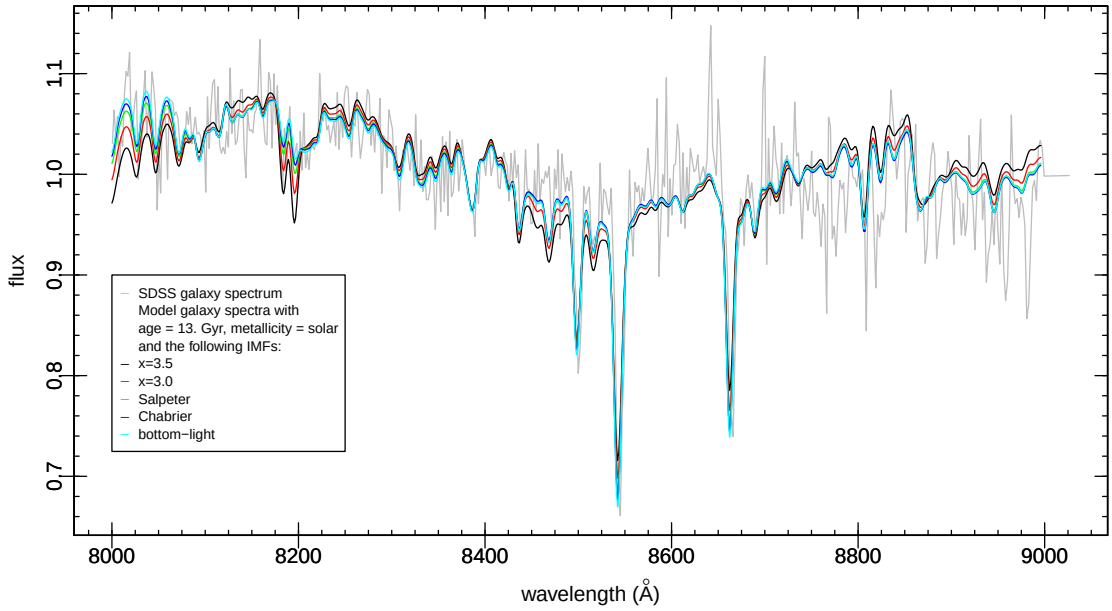

Figure 2.3: Examples of observed and model galaxy spectra. Grey spectrum is an observed galaxy with an SDSS measured velocity dispersion of 86 km s^{-1}. The models are the closest matched in velocity dispersion from the broadened range (at σ = 89 km s^{-1}). All models have solar metallicity and ages of 13.5 Gyr. The difference between the model spectra for different IMFs is apparent by comparing the different spectra; particularly for the NaI doublet near 8200 Å which shows a strong contrast between the size of the spectral features for the bottom-light (cyan) and the bottom-heavy (black) IMFs.

dispersion of 86 km s^{-1} and the models (with the closest value from the selected range) have a velocity dispersion of 89 km s^{-1}. The plot shows the region covering the calcium triplet (near ∼8500 Å) and the sodium doublet feature (near 8150-8170 Å). From the comparison of the different IMF models, it is clear to see which features are more prominent for dwarf-enriched IMFs. The sodium doublet is particularly prominent for the most bottom-heavy IMF (x = 3.5) and much smaller for the bottom-light IMF. The calcium triplet (as expected) is the converse; larger for the bottom-light IMFs and smaller for the bottom-heavy models.

2.3 Measuring the Indices

To measure the equivalent widths of selected indices in the model and observational data, continuum and central bands were placed at pre-assigned locations of the spectrum (see Table 2.1 for references) and the flux in the area of the feature under the continuum was measured. For the definition of the Lick feature continua, Faber et al. (1985) placed a straight line between the midpoints of the continua surrounding the feature and took the height of the line at the midpoint of the central bandpass to mark the local continuum. The widths of central and continuum bands were chosen to minimise the effect of velocity broadening on the measured absorption-line strengths (Burstein et al. (1984)). Figure 2.4 shows the central and continuum bandpasses used in this work. `indexf` was used to measure the indices; `indexf` is a program written in C++ to measure line-strength

TABLE A: SPECTRAL FEATURES

Index	blue bandpass Å	central bandpass Å	red bandpass Å	source
HdF	4057.250 - 4088.500	4091.000 - 4112.250	4114.750 - 4137.250	Hdelta F (Worthey & Ottaviani (1997))
CN2	4083.875 - 4096.375	4142.125 - 4177.125	4244.125 - 4284.125	Lick (Trager et al. (1998))
Ca4227	4211.000 - 4219.750	4222.250 - 4234.750	4241.000 - 4251.000	Lick (Trager et al. (1998))
HgF	4283.500 - 4319.750	4331.250 - 4352.250	4354.750 - 4384.750	Hgamma F (Worthey & Ottaviani (1997))
C4668	4611.500 - 4630.250	4634.000 - 4720.250	4742.750 - 4756.500	Lick (Trager et al. (1998))
Hbeta	4827.875 - 4847.875	4847.875 - 4876.625	4876.625 - 4891.625	Lick (Trager et al. (1998))
Mgb5177	5142.625 - 5161.375	5160.125 - 5192.625	5191.375 - 5206.375	Lick (Trager et al. (1998))
Fe5270	5233.150 - 5248.150	5245.650 - 5285.650	5285.650 - 5318.150	Lick (Trager et al. (1998))
Fe5335	5304.625 - 5315.875	5312.125 - 5352.125	5353.375 - 5363.375	Lick (Trager et al. (1998))
Fe5406	5376.250 - 5387.500	5387.500 - 5415.000	5415.000 - 5425.000	Lick (Trager et al. (1998))
Na5895	5860.625 - 5875.625	5876.875 - 5909.375	5922.125 - 5948.125	Lick (Trager et al. (1998))
TiO1	5816.625 - 5849.125	5936.625 - 5994.125	6038.625 - 6103.625	Lick (Trager et al. (1998))
TiO2	6066.625 - 6141.625	6189.625 - 6272.125	6372.625 - 6415.125	Lick (Trager et al. (1998))
CaII086a	8474.000 - 8484.000	8484.000 - 8513.000	8564.000 - 8577.000	(Conroy & van Dokkum (2012a))
CaII086b	8474.000 - 8484.000	8522.000 - 8562.000	8564.000 - 8577.000	(Conroy & van Dokkum (2012a))
CaII086c	8619.000 - 8642.000	8642.000 - 8682.000	8700.000 - 8725.000	(Conroy & van Dokkum (2012a))
NaI082	8170.000 - 8177.000	8177.000 - 8205.000	8205.000 - 8215.000	(Conroy & van Dokkum (2012a))
NaI082S	8150.000 - 8168.400	8168.500 - 8234.125	8235.250 - 8250.000	(Spiniello et al. (2012))

Table 2.1: Spectral features and bandpasses used for index equivalent width measurements with an additionally defined NaI082 index as used by Spiniello et al. (2012) (NaI082S).

indices in fully calibrated FITS spectra (Cardiel (2010)). It also measures errors on the indices according to the propagation of random errors such as photon statistics and read-out noise. This is done by supplying `indexf` with an addition error spectrum compiled by SDSS (as a FITS file) containing unbiased standard deviation for each pixel of the data spectrum.

Seventeen different spectral features were measured in total, these are shown in Table 2.1. The wavelengths for the continuum and central bandpasses are all Lick defined (Trager et al. (1998)), with the exception of Hdelta F and Hgamma F (Worthey & Ottaviani (1997)) and the calcium triplet and sodium doublet Conroy & van Dokkum (2012a). There is also an additional specification for the continuum and central bands of NaI082, used in the work by Spiniello et al. (2012).

Figure 2.4 shows the `indexf` measurements of the NaI082 doublet in various model spectra. The measurements are shown for models with three different velocity dispersions; 0, 100 and 300 km s^{-1} and four different IMFs (ranging from dwarf-rich to dwarf-deficient). The coloured bandpasses are those used by van Dokkum & Conroy and the black vertical lines are the newly defined bandpasses used by Spiniello et al. (2012). When the models are broadened by higher velocity dispersions (i.e. $\gtrsim$ 300 km s^{-1}) the resolution is reduced and the NaI doublet feature becomes smoothed into one broad peak. This peak is dissected by the index bandpass used by Conroy & van Dokkum so Spiniello et al. (2012) use wider bandpasses for measuring the feature which suits their data sample better as it contains more massive galaxies. The Spiniello central bandpass is wide enough to include the TiO1 feature which becomes more prominent the higher the velocity dispersion and blends with the sodium doublet in galaxies with velocity dispersions of $\gtrsim$ 300 km s^{-1}. The TiO1 feature also increases in size with decreasing dwarf concentration, this drags down the redder peak of the NaI doublet and is more noticeable at velocity dispersions $\lesssim$300 km s^{-1}. In Figure 2.4 it is evident

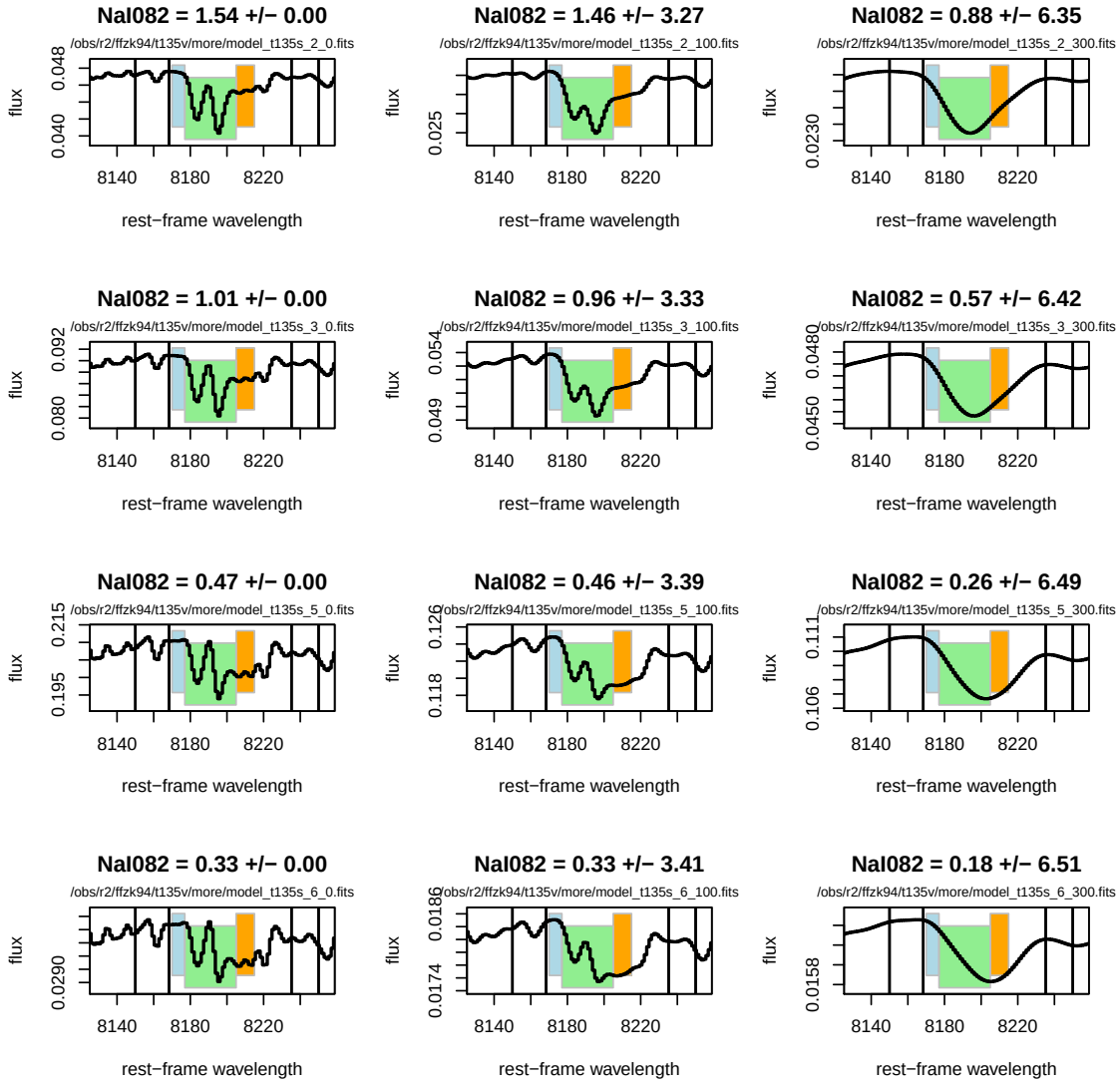

Figure 2.4: Model spectra showing measurement of NaI082 index. All models here have solar metallicity and ages of 13.5 Gyr. From left to right the velocity dispersions are 0, 100 and 300 km s^{-1}, from top to bottom the IMFs are x=3.5, x=3, Chabrier and bottom light. The black vertical lines represent the wider bandpasses set by Spiniello et al. (2011), the coloured blocks represent the bandpasses set by Conroy & van Dokkum (2012a). As the spectrum is broadened from zero velocity dispersion to 300 km s^{-1}, the NaI doublet is smoothed to a single peak instead of a doublet. For higher velocity dispersions the Conroy & van Dokkum (2012a) bandpass no longer covers the whole feature. The IMFs that describe an increasing dwarf-enriched content (bottom to top) have a stronger NaI feature. At lower resolution (models broadened by 300 km s^{-1}) the centre of the broadened line is shifted due to the TiO1 feature, no longer centering inside the bandpass set by Conroy & van Dokkum.

that the central bandpass used by Conroy & van Dokkum (2012a) is suitable for measuring the NaI082 index at lower velocity dispersions (e.g. $\sim$100 km s^{-1}), however, when the model is broadened to 300 km s^{-1} the centre of the feature is shifted and is no longer in line with the centre of the bandpass. Conroy & van Dokkum (2012a) used the bandpasses specified in Table 2.1 because the velocity dispersions in their sample ranged from 50 - 250 km s^{-1} and did not contain larger velocity dispersion galaxies like the sample used by Spiniello et al. (2012). The velocity dispersions used in this piece of work are similar to those used by Conroy & van Dokkum, with comparably few that are greater than $\sim$250 km s^{-1} (see Figure 2.1). For the galaxy sample used in this work, it would have been possible to use the same bandpasses as specified by Spiniello et al. (2012), however, it is believed that using the bandpasses specified by Conroy & van Dokkum (2012a) does not have a detrimental effect on the analysis of the sodium doublet equivalent widths.

2.4 Velocity dispersion corrections

The size of a feature in a galaxy spectrum is indicative of the abundance of a certain element or molecule in the stars that make up the galaxy. These spectral features are broadened by instrumental effects and the line-of-sight velocities of the stars. The broadening of these features generally has the effect of reducing the line-strength compared to the intrinsic values (Kuntschner (2000)). For this reason it is important to normalize all the observed galaxies by removing the effect of their different velocity dispersions on the size of their spectral indices. This is done by finding the relationship between the intrinsic index for a given velocity dispersion and its non-broadened equivalent width using the models.

The model spectra were broadened according to a range of velocity dispersion values using the Gauss function in `IRAF` (35 velocity dispersion values were randomly selected; ranging from 0 - 500 km s^{-1}). The equivalent widths for the spectral features in these models were measured using `indexf` and the relationship between the zero velocity dispersion model and the broadened models was used to calculate a non-broadened equivalent width for each spectral feature in the observed galaxy dataset. The relationship between the index measurements and the original and broadened models was used to calculate the index value for the observed galaxies at zero velocity dispersion. This was done by measuring the indices that corresponded with the different velocity dispersion models and selecting the closest models that were greater and less than the observed velocity dispersion and then extrapolating to find the corresponding zero velocity dispersion index measurement for the observed galaxy. Figure 2.5 shows the relationship between the broadened and non-broadened indices for the model spectra and the observed galaxies (with corrections constrained from the models). There is a good correlation between the observed data and the model ranges over 100,

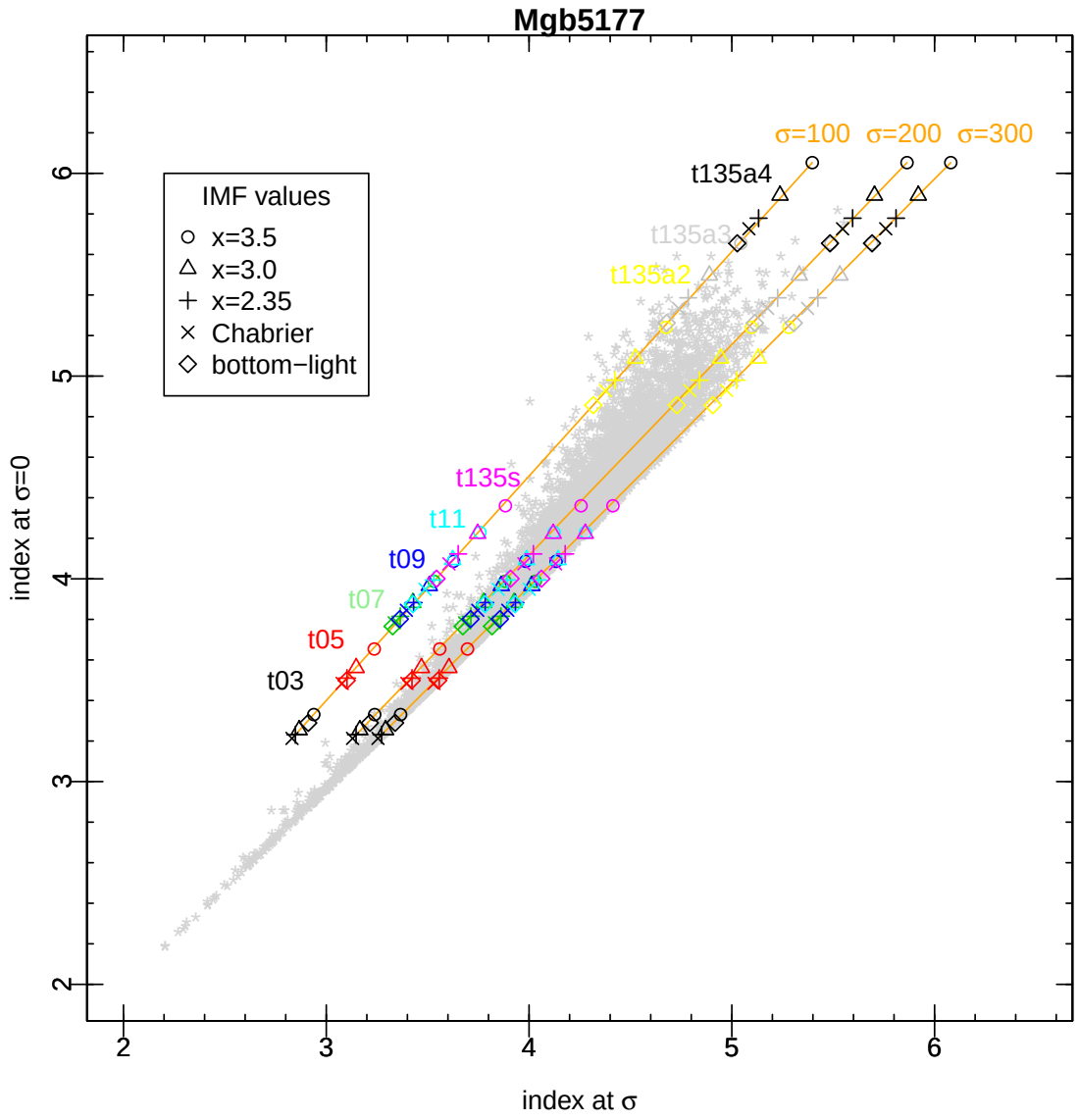

Figure 2.5: Plot of Mgb5177 index values (where σ = σ and σ = 0) for models and observed data. Showing distribution of observed galaxy data (grey points) in relation to models for three different velocity dispersions (100, 200 and 300 km s^{-1}), with different IMFs (shown by various symbols) and ages (different colours). The observational data fits the models well but would suggest a large quantity of galaxies have ages $\lesssim$3 Gyr.

200 and 300 km s^{-1} apart from at the smallest index values where the galaxy data seems to correspond with model spectra with ages $\lesssim$3 Gyr.

Figures 2.6 and 2.7 are plots of the correction between non-broadened and broadened indices for the models (i.e. equivalent width at σ=0 / equivalent width at σ) against their corresponding velocity dispersions. Comparison can be made with Figure B2 in Kuntschner (2000) for the common indices; Fe5270, Fe5335, Fe5406, Mgb5177, Hbeta, $C_2$4668 and HgF. Kuntschner (2000) used different models for their comparisons (Worthey (1994)) and despite their use of different velocity dispersion bins, there is a clear similarity between their corrections and those of the models used in this work.

From here onwards the measured indices will be quoted in their zero velocity dispersion value, unless specified otherwise.

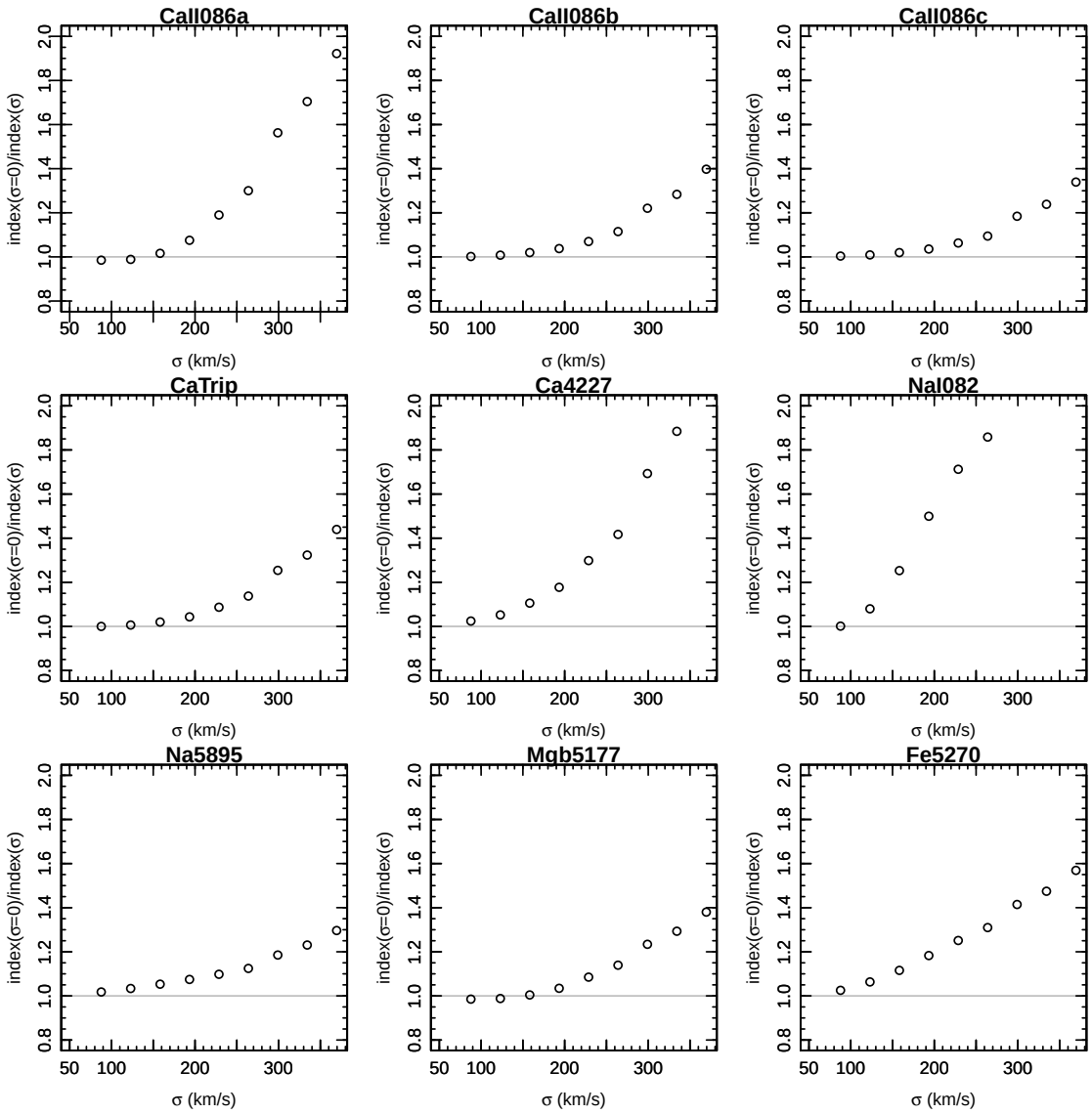

Figure 2.6: Velocity dispersion corrections for the model data (1). The open circles represent the average correction in each σ bin and the horizontal grey line represents the one-to-one ratio.

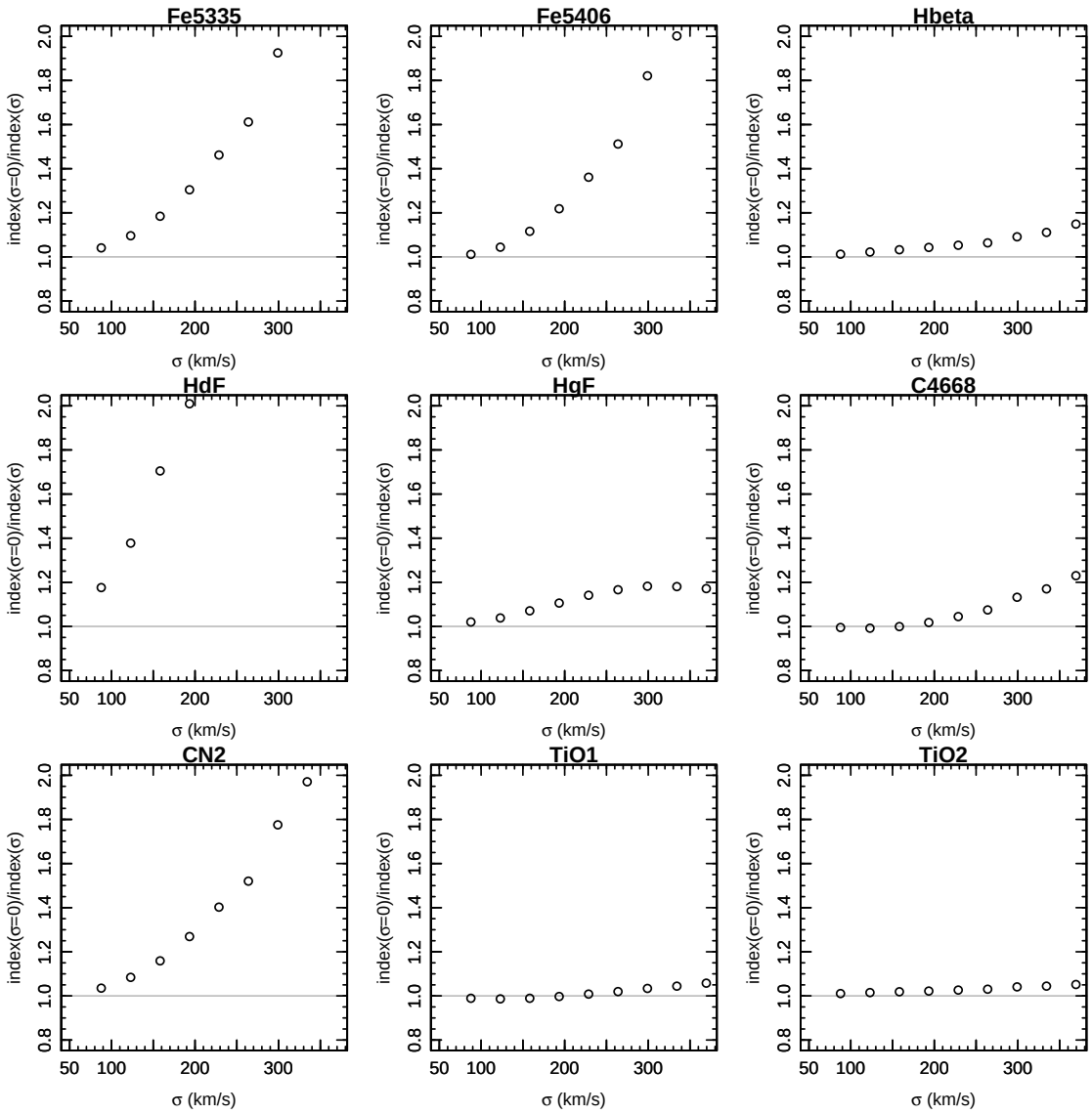

Figure 2.7: Velocity dispersion corrections for the model data (2). The open circles represent the average correction in each σ bin and the horizontal grey line represents the one-to-one ratio.

2.4.1 Errors

In order to conduct a fair and thorough analysis of the data, it is important to consider the errors on every result. Most errors in this work are the systematic errors obtained from linear fits to data, SDSS error spectra or quoted values in literature, however, some parameters have unknown errors (such as the model responses). In the following Results section, where appropriate, the corresponding error for the index-sigma scaling relations (calculated using a combination of model responses and literature scaling relations) is found by creating a vector of possible scaling relation values and taking the standard deviation of this dataset. The dataset is made up of the model responses from this work and a selection of literature values that are randomly selected from a Gaussian distribution, the distribution is created with a mean equal to the scaling relation value quoted in the literature and with a standard deviation equal to the literature-quoted error for the appropriate scaling relation.

Chapter 3

Results

This piece of work focuses on the NaI doublet and CaII triplet spectral features with the intent of exploiting their role as IMF characteristic features. Both indices show a strong response to the IMF but are also affected by their respective elemental abundances. In order to disentangle the effects of the IMF and abundance, the NaI doublet and the CaII triplet are combined with the NaD and CaI spectral features (which respond weakly to changes in the IMF but show a much stronger response to changes in the corresponding abundance).

A grid of model-predicted equivalent width values is compared to the measured equivalent widths of the observational data to determine what range of IMF values, elemental abundances and ages fit the observational data best. Whilst it may be possible to see the relationship between the observational data and the models, it still remains very hard to decouple the IMF from age and abundance effects with this method.

Investigation is then undertaken to explore whether effects of either abundance or IMF alone can account for variations in the index-sigma relations for the CaII triplet and NaI doublet. This is then extended by combining published scaling relations for age, α- and Fe- abundance with velocity dispersion (constrained from optical spectral features) and their corresponding model responses to create a predicted index-sigma scaling relation for each index. The predicted index-sigma relations for the abundance-characteristic indices (NaD and Ca4227) are then compared to the corresponding observed index-sigma relations to find the appropriate abundance-sigma variation for this galaxy sample. Once the literature constrained abundances and ages, along with the NaD and Ca4227 constrained abundances, have been combined to predict an index-sigma scaling relation, it is assumed that the remaining difference between the predicted and observed index-sigma scaling relations (for the IMF-characteristic indices) can be attributed to the IMF variation.

3.1 Index-index plots

3.1.1 Calcium

Figure 3.1 shows index-index plots of the measured equivalent widths for the two calcium features; Ca4227 and the CaII triplet, from both model and observational data. The model grid is plotted over the observational data and is made up of equivalent widths measured from models with IMFs ranging from bottom-heavy to bottom-light and with ages ranging from 3 - 13.5 Gyr. The models constructed with bottom-heavy IMFs predict CaII triplet equivalent width values that have a very slight negative correlation with age. For models constructed with a Salpeter IMF the predicted calcium triplet values vary only by 0.14 Å across the age range which is small in comparison to a variation of 0.47 Å for the most bottom-heavy IMF. For the bottom-light IMF the equivalent widths increase in size by 0.11 Å across the age range of 3 - 13.5 Gyr. In comparison, it is clear in Figure 3.1 that the Ca4227 index increases considerably with age (by $\sim$1 Å), with a greater range in equivalent widths for models with bottom-heavy IMFs. This shows that the Ca4227 index has a much stronger response to changes in age than the calcium triplet index. As expected, the model predicted calcium triplet equivalent widths decrease with increasingly dwarf-enriched IMFs (because the CaII species is only weakly present in the atmospheres of dwarf stars), whilst in comparison, the Ca4227 equivalent widths show minimal variations with changes in the IMF.

The observational data in Figure 3.1 are more widely dispersed than the range of the solar abundance models. A visual inspection of the plot in panel (a) of Figure 3.1 would suggest that the observational data fit a younger-aged model and cover a wide range of IMFs. Considering the GalaxyZoo selection criteria for the data distinguished only elliptical, and therefore older, galaxies, it is surprising to see the data seem to fit a younger aged model. However, this is just for a solar-metallicity model, without considering the calcium abundance.

The α-enhanced models (+0.2, +0.3 and +0.4 dex) predict equivalent widths that are much greater than the observational data range; with an increasing α-abundance both the calcium triplet and Ca4227 features are predicted to increase in size which indicates the two features show a strong response to α-abundance adjustments, this is intuitive as van Dokkum and Conroy treat calcium as an α-element in their models. Figure 3.1 shows that when [α/Fe]$\gtrsim$0.2 dex the models predict Ca4227 and calcium triplet values outside the range shown by the observational data.

Panel (b) of Figure 3.1 shows the index-index plot for the calcium indices with additional points representing the average equivalent width value in equally spaced velocity dispersion bins. By comparing the average equivalent widths for the observational data with the model grids it appears that the velocity dispersion-binned, observational data suit models with ages <3 Gyr for lower velocity dispersions ($\sim$66 km s^{-1}) and $\sim$7 Gyr for the largest velocity dispersions in this sam-

ple ($\sim$366 km s^{-1}). The best-fitting IMF for the velocity dispersion-binned data appears to become more bottom-heavy with increasing velocity dispersion, moving from an IMF where x = 3.0 to one where x = 3.5. The relationship of the observational data to the model grid may be affected when the calcium abundance is taken into consideration.

Figure 3.1 also shows equivalent widths for models in which the calcium is treated as a separate class from the α-elements. These models have enhanced and depressed calcium abundances ($\pm$ 0.15 dex), an age of 13.5 Gyr and a Chabrier IMF. The points represent the direction the grid would move (according to the fiducial solar metallicity, 13.5 Gyr, Chabrier point) to replicate the calcium abundance change. For the fiducial point to move to a [Ca/Fe] value of $\pm$0.15 dex the grid would move by approximately $\pm$1 Å along the x-axis and approximately $\pm$0.4 Å in the y-axis direction. Considering most of the observational data lie within an x-axis range of $\sim$11 Å and a y-axis range of $\sim$2 Å, this is quite a substantial adjustment of the grid, almost the full width of the data cloud. This could indicate that the larger distribution of observed galaxies compared to the models can be accounted for by the galaxies having a range of calcium abundances. The predicted equivalent width for the depressed calcium abundance model (-0.15 dex) is less on both the x- and y-axes as it represents a population with depleted calcium and therefore decreases the size of the two calcium features.

A crude transposition of the grid according to the [Ca/Fe] enhanced and depressed models is shown in Figure 3.2. It would seem that a calcium-enhanced (+0.15 dex) model is very incompatible with the observed data, whilst the calcium-depressed (-0.15 dex) model seems to provide better agreement with regards to the expected age of the galaxy sample. The direction the grid moves with respect to enhanced or depressed calcium abundance is anti-correlated with the trend shown by the velocity dispersion-binned data which indicates the calcium abundance of a certain galaxy does not correlate strongly with its mass.

With a depressed calcium abundance, the average velocity dispersion-binned data match a bottom-light or Chabrier IMF. Due to the proximity of the predicted model equivalent widths for the Salpeter, Chabrier and bottom-light IMFs, it is not possible to accurately comment on the trend with the velocity dispersion-binned data.

3.1.2 Sodium

Figure 3.3 is an index-index plot of the sodium indices, NaI and NaD, and is similar in structure to the calcium plots (Figure 3.1). In the calcium plot it is evident that the model predicted Ca4227 equivalent widths increase almost exclusively with age, this is not the case for the sodium features which both increase in size with increasing age. As expected, with the increasing NaI equivalent widths, there is a trend toward more bottom-heavy IMFs in the models; this is because the NaI index is characteristic of low-mass stars. As with the calcium indices,

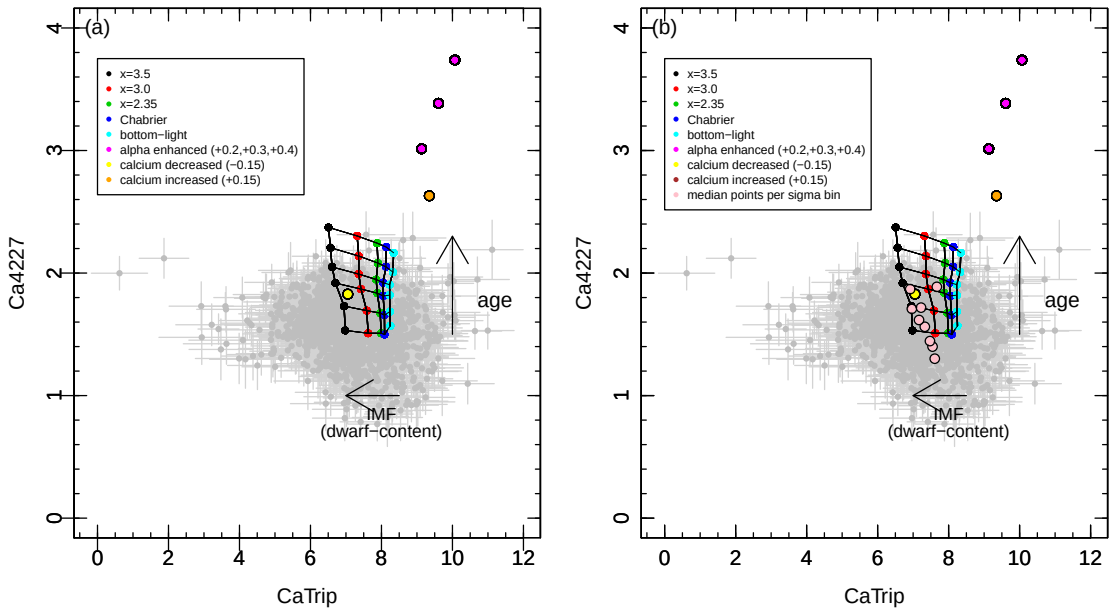

Figure 3.1: Index-index plot for the calcium features. Observational data is shown as grey points with light grey error bars. Grid of coloured points and black connecting lines represents the range of models in age and IMF. Orange and yellow points represent Ca- enhanced and depressed model values respectively. Magenta points represent α-enhanced models (positive correlation with index size; +0.2, +0.3 and +0.4 dex). Pale pink points in panel (b) represent average velocity dispersion binned equivalent widths for the observational data. The average velocity dispersion binned points suggest the data correspond with ages $\lesssim$7 Gyr, this does not agree with the sample selection criteria. See text for in-depth discussion

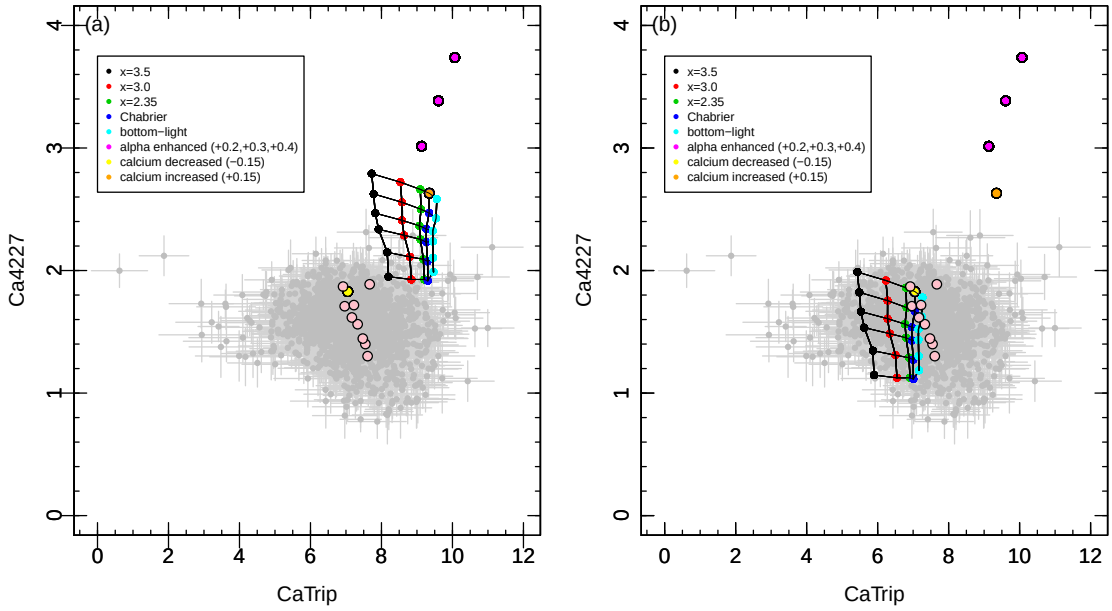

Figure 3.2: Index-index plots for the calcium indices, same as Figure 3.1 except the grid has been transposed according to enhanced and depleted calcium abundances. In panel (a) the whole grid has been moved according to the movement of the fiducial point (Chabrier IMF and age= 13.5 Gyr) moving to a depleted calcium abundance of -0.15 dex. Panel two shows the same transposition but to a calcium enhanced model value (+0.15 dex). The models require a negative calcium abundance of -0.15<[Ca/Fe]<0 dex in order to better match the expected age of the observational data. With a depressed calcium abundance, the velocity dispersion-binned points match a bottom-light or Chabrier IMF but it is difficult to ascertain precisely which IMF is the best match to the data due to the proximity of the predicted equivalent widths for the dwarf-depleted IMFs.

there is a smaller difference between the equivalent widths for the more dwarf-depleted IMFs (i.e. bottom-light, Chabrier) than the more dwarf-enriched IMFs (i.e. x = 3.5, x = 3.0), this is because the dwarf-depleted IMFs have a lower fraction of light coming from the stars that contribute most to the strength of the NaI spectral feature.

The relationship between the model data and the observed data is similar to that for the calcium indices whereby the observational data covers a much larger range than the models. Most of the observational data that fall within the range of the model grid are concentrated around the bottom-light IMFs and cover all ages. The most dwarf-enriched IMF (where x = 3.5) is almost completely out of the observational data range, with only a few galaxies corresponding to a bottom-heavy IMF.

The second panel in Figure 3.3 shows the additional velocity dispersion-binned points for the sodium indices. The change in velocity dispersion mimics the change in sodium abundance suggesting that the abundance changes from [Na/Fe] <-0.3 dex in low velocity dispersion galaxies to [Na/Fe]>0.3 dex for the high velocity dispersion galaxies (this can be seen even more clearly in Figure 3.4). It is not possible to interpret the relationship between the median velocity bin points and the trends of the model IMF predictions for the sodium indices. The similarity between the predicted equivalent widths for the bottom-light, Chabrier and Salpeter IMFs means that it is difficult to clarify whether the velocity dispersion-binned points tend toward more dwarf-enriched or depleted IMFs. The velocity dispersion-binned points move to increasingly large x- and y-axis values, this is different to the trend shown by the calcium σ-binned points which move to larger y-axis values and smaller x-axis values. The increase in size of both sodium indices as velocity dispersion increases is indicative of either a decreasing number of giant- and increasing number of dwarf- stars, or an increasing sodium abundance, or both as the galaxy mass increases.

An important point to take from Figure 3.3 (b) is that if the sodium abundance was increased, there would not be a change to the best-matching IMF. According to the fiducial point (solar metallicity, Chabrier IMF and age = 13.5 Gyr) in relation to the sodium-enhanced point ([Na/Fe] = 0.3, Chabrier IMF and age = 13.5 Gyr) the data would continue to suit the same IMF, as the fiducial point would move along the line of increasing velocity dispersion. Also note that Figure 3.3 also shows that the differences between the enhanced and depressed [Na/Fe] points and the fiducial point are not equal, the causes of this will be discussed later.

With the variation of the sodium abundance taken into consideration, the model grid in Figure 3.3 is a good representation of the data. Adopting a sodium abundance of [Na/Fe] = 0.3 dex, the grid would correspond roughly with the centre of the observational data. For the more massive galaxies in the observational sample, an even stronger sodium abundance is required in the models to replicate

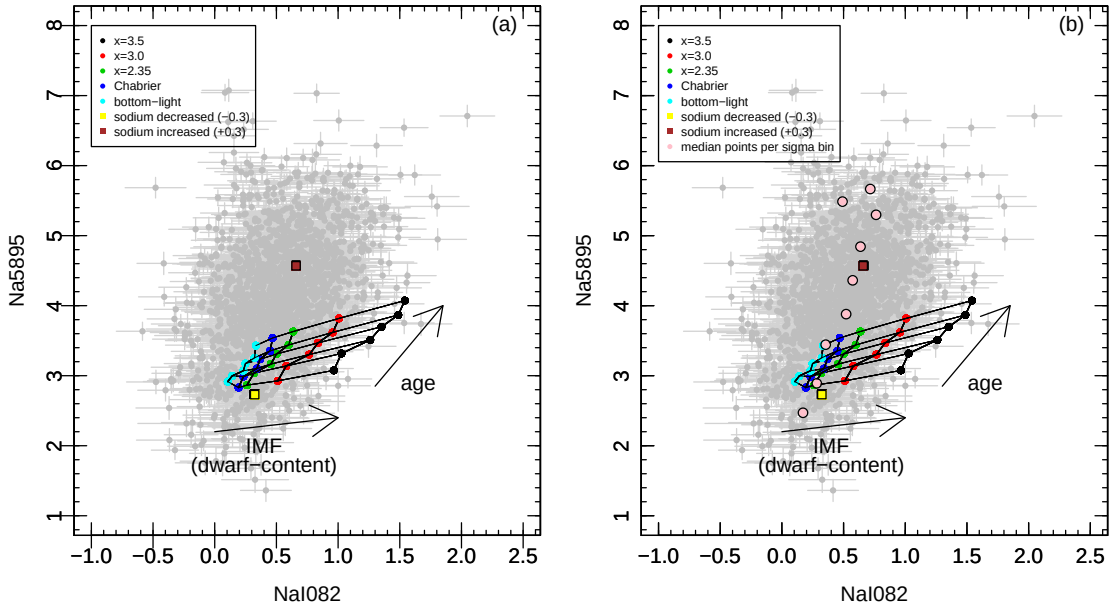

Figure 3.3: Index-index plots for the sodium indices. Both plots show a grid of model data (coloured circles and black lines) in comparison with observed data (grey points with light grey errors). The two square points represent model data for increased (+0.3 dex, orange) and decreased (-0.3 dex, yellow) sodium abundances. The order of the model IMFs changes in comparison to the calcium plot; the IMFs now become more bottom-heavy as the NaI082 line strength increases (as expected as NaI082 is strongest in stars $\lesssim$0.3 $M_{\odot}$). In addition to the other information, panel (b) also shows the median data points for ten equally space velocity dispersion bins (pink points). The change in velocity dispersion seems to be mimicked by the change in sodium abundance. The median data best fits a Salpeter IMF for lower-velocity dispersions $\lesssim$100 km s^{-1} and moves to a Chabrier IMF for galaxies with velocity dispersions $\gtrsim$100 km s^{-1}. Both of the sodium line strengths increase with age.

the equivalent widths, this would indicate that with increasing galaxy mass, the sodium abundance required to replicate the data needs to be $\sim$0.5 dex, and would subsequently require a less extreme IMF.

Figure 3.4 shows the same plot as Figure 3.3 but with the change in velocity dispersion highlighted with different colours. There is a clear trend in the size of the sodium indices with increasing velocity dispersion; both the NaI and NaD measured indices (on average) increase in size as the galaxy mass increases. The galaxies with velocity dispersions between 100 and 200 km s^{-1} seem the best match to the models. The data with velocity dispersions <100 km s^{-1} seem to best match a -0.3 dex sodium abundance decrease whilst the <300 km s^{-1} data seem to best match a +0.3 dex sodium abundance. For the galaxies in the sample with velocity dispersions >300 km s^{-1} an even greater sodium abundance is required for a match to the models. Some of the outlier galaxies require increased sodium abundances where [Na/Fe]>0.3 dex and also require more bottom-heavy IMFs, this is concurrent with the work by Spiniello et al. (2012) where they find two galaxies that suit increased sodium abundances and a very steep IMF slope.

In order to explore the statistical significance of the spread of points in Figure 3.4, a χ^2 test was performed to determine whether the scatter in NaI082 index measurements at fixed Na5895 index values is an underestimation of measure-

ment error, or whether there is real intrinsic scatter. For a fixed Na5895 index value (3.0<Na5895<3.5), the χ^2 for the corresponding NaI082 measurements is calculated according to

$$\chi^2 = \sum (\frac{\text{(NaI082 - mean(NaI082))}^2}{\text{NaI082}^2_{\text{error}}} = 1992 \tag{3.1}$$

The χ^2 value is greater than the number of degrees of freedom (1790) suggesting that if the errors are accurate the observed scatter in NaI082 index values at a fixed range of Na5895 index values is partly intrinsic. Calculating the probability distribution function of the NaI082 data suggests that in 99.94% of random trials with these error bars the resulting χ^2 would be lower than measured, suggesting there must be some intrinsic scatter.

The intrinsic scatter (sig) would equal the contribution to the errors that gives a χ^2 value equal to the number of degrees of freedom.

$$\chi^2 = \text{Ndof} = 1790 = \sum (\frac{\text{(NaI082 - mean(NaI082))}^2}{\text{NaI082}^2_{\text{error}} + \text{sig}^2}) \tag{3.2}$$

$$\text{sig} = 0.0911 \tag{3.3}$$

The fraction of the total intrinsic variance ($\text{sig}^2/\text{var(d)}$) for this range of Na5895 index values is 9% suggesting that the remaining 91% of variance is accounted for by the measurement errors. Continuing the same analysis to successive cuts of Na5895 index size through the sample suggests that the intrinsic scatter is greatest at low and high Na5895 index measurements (which in principle correspond to low and high velocity dispersions respectively). With equally sized bins of Na5895 index measurements the largest fraction of total intrinsic variance (16.7%) is found for the NaI082 index measurements that correspond with the smallest Na5895 measurements.

3.1.3 Summary

To clarify the results from this section;

Calcium

- The calcium index-index plot shows that with a solar-calcium abundance, the observational data correspond with models that have ages $\lesssim$7 Gyr and bottom-heavy IMFs.
- In order for the observational data to correspond with model ages that concur with the morphological constraints made when selecting the data sample, a sub-solar calcium abundance is required (-0.15 dex$\lesssim$[Ca/Fe]$\gtrsim$0 dex).
- With a sub-solar calcium abundance, the observational data correspond with a range of ages $\gtrsim$5 Gyr and more dwarf-depleted IMFs.

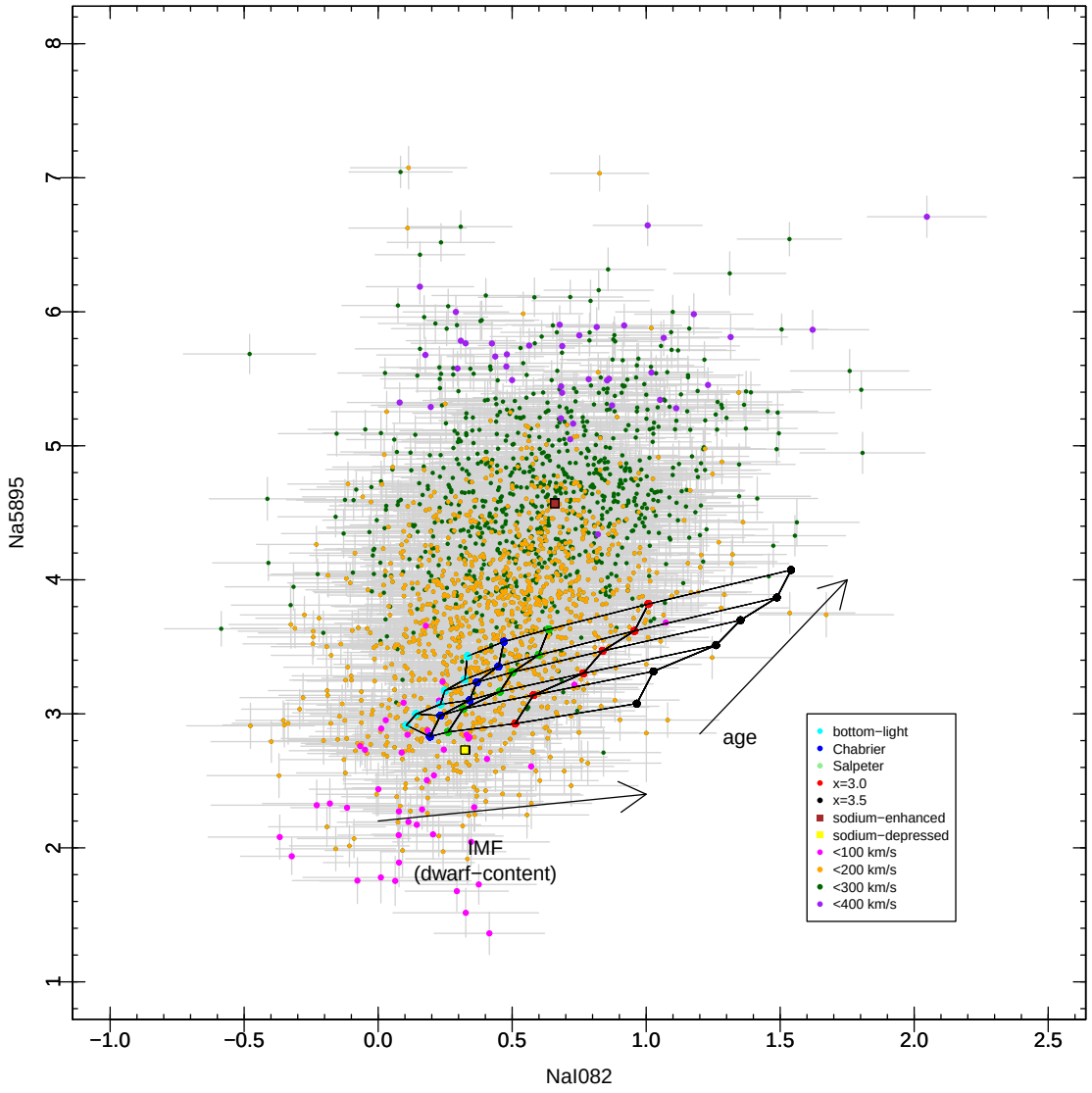

Figure 3.4: An Index-index plot of the sodium indices; NaI082 and Na5895, showing model and observational values. Observational values range from low velocity dispersions (<100 and <200 km s^{-1}; magenta and orange points respectively) to higher velocity dispersion values (<300 and <400 km s^{-1}; dark green and purple points respectively) with errors still shown in grey. The model grid is the same as in Figure 3.3 with square [Na/Fe] points (in brown (+0.3 dex) and yellow(-0.3 dex).

- There is no evidence for a strong correlation between velocity dispersion and calcium abundance.

Sodium

- The sodium index-index plot shows that the data correspond with a wide range of sodium abundances (-0.3 dex $\lesssim$[Na/Fe]$\lesssim$0.6 dex).
- For a solar-sodium abundance, the observational data best fit a $\sim$Chabrier or Salpeter-like IMF and cover a range of ages. If the sodium abundance is increased or decreased, it does not appear as though the best-fitting IMF would change for the majority of the data.
- There is a strong positive correlation between velocity dispersion and sodium abundance, but no evidence for a strong correlation between velocity dispersion and IMF.

3.2 Index-sigma scaling relations

As galaxies become more massive, the size of a certain spectral feature changes; this change can provide important information about the properties of galaxies. Combining the model index responses for certain parameters with literature scaling relations for constrained parameters such as age, metallicity and α-abundance, and making assumptions about the effect of IMF and abundance on certain indices; it is possible to attempt to reproduce observational data trends in order to gain insight into these galaxy properties.

Figures 3.5, 3.6 and 3.7 show the index-sigma relations for all seventeen indices measured in this work along with the combined CaII triplet index which is the total equivalent width of the three individual components of the feature. The slopes, normalisations and errors are shown in Table 3.1. Velocity dispersion is known to be well correlated with the properties of stellar populations. In this work velocity dispersion is used as a proxy for galaxy mass, it is not always the case that galaxy mass correlates strictly with velocity dispersion but for this purpose it will be sufficient to assume that the greater velocity dispersion values correspond with larger galaxies.

Figure 3.5 shows the combined calcium triplet feature, along with the combined components of the feature. Similar to trends found by other authors (Cenarro et al. (2003), Saglia et al. (2002)), the measured index for the calcium triplet decreases with increasing velocity dispersion. If attention is paid to the calcium triplet feature only, this could suggest a decrease in abundance of calcium with increasing size of a galaxy. The Ca4227 index does not show the same behaviour as CaII; it shows a positive correlation with galaxy mass. This opposing behaviour implies that there is something other than the calcium abundance having an effect on the size of the indices.

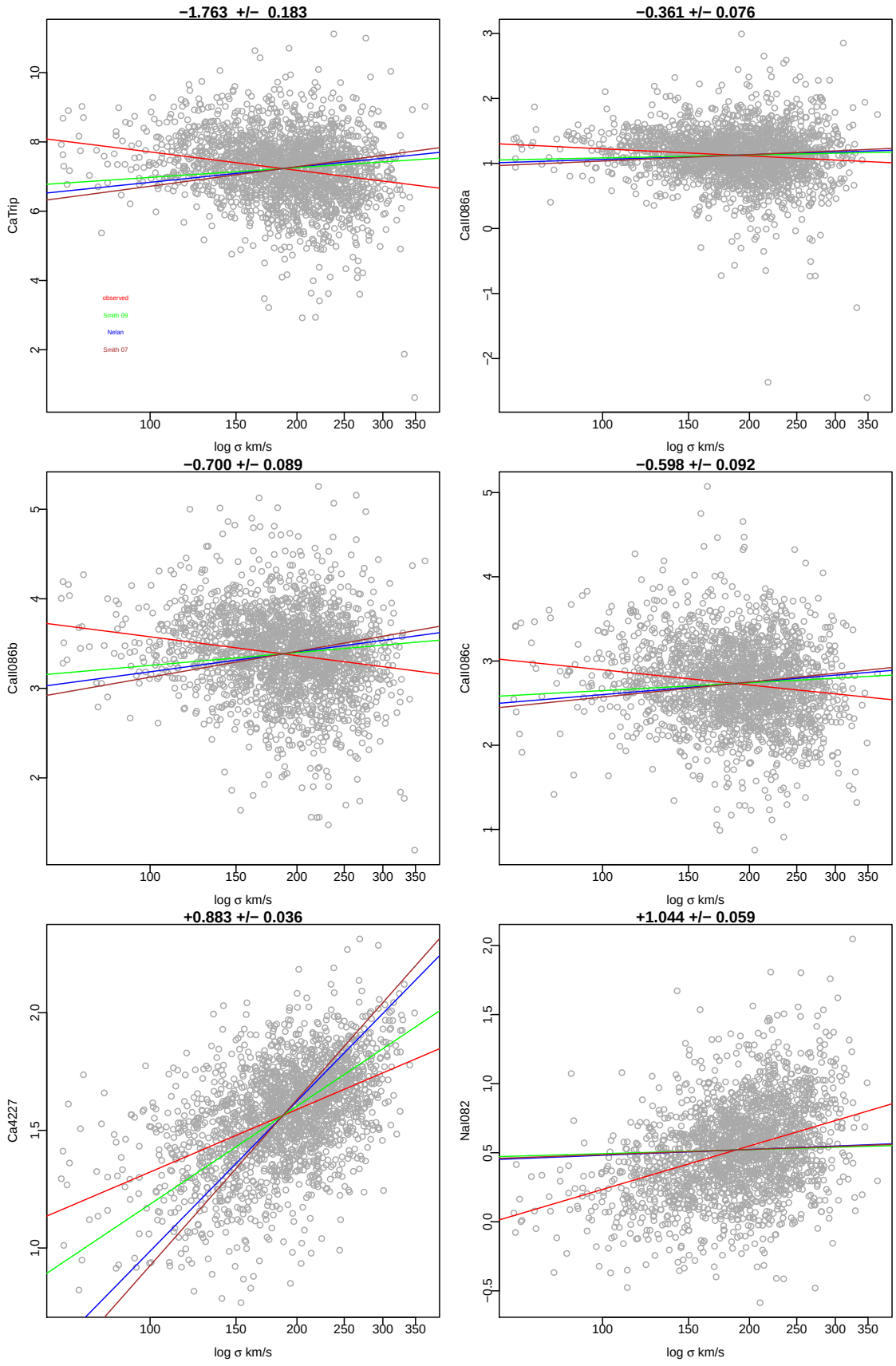

Figure 3.5: Index-sigma relations for calcium indices and NaI. Red lines are linear fits to the observational data (grey points). Blue, brown and green lines are predicted index-sigma slopes according to trends in age, α- and Fe-abundance from published values (Nelan et al. (2005), Smith et al. (2007) and Smith et al. (2009) respectively) , combined with model responses from Conroy & van Dokkum (2012a). See Figures 3.6 and 3.7 for other indices and text for discussion.

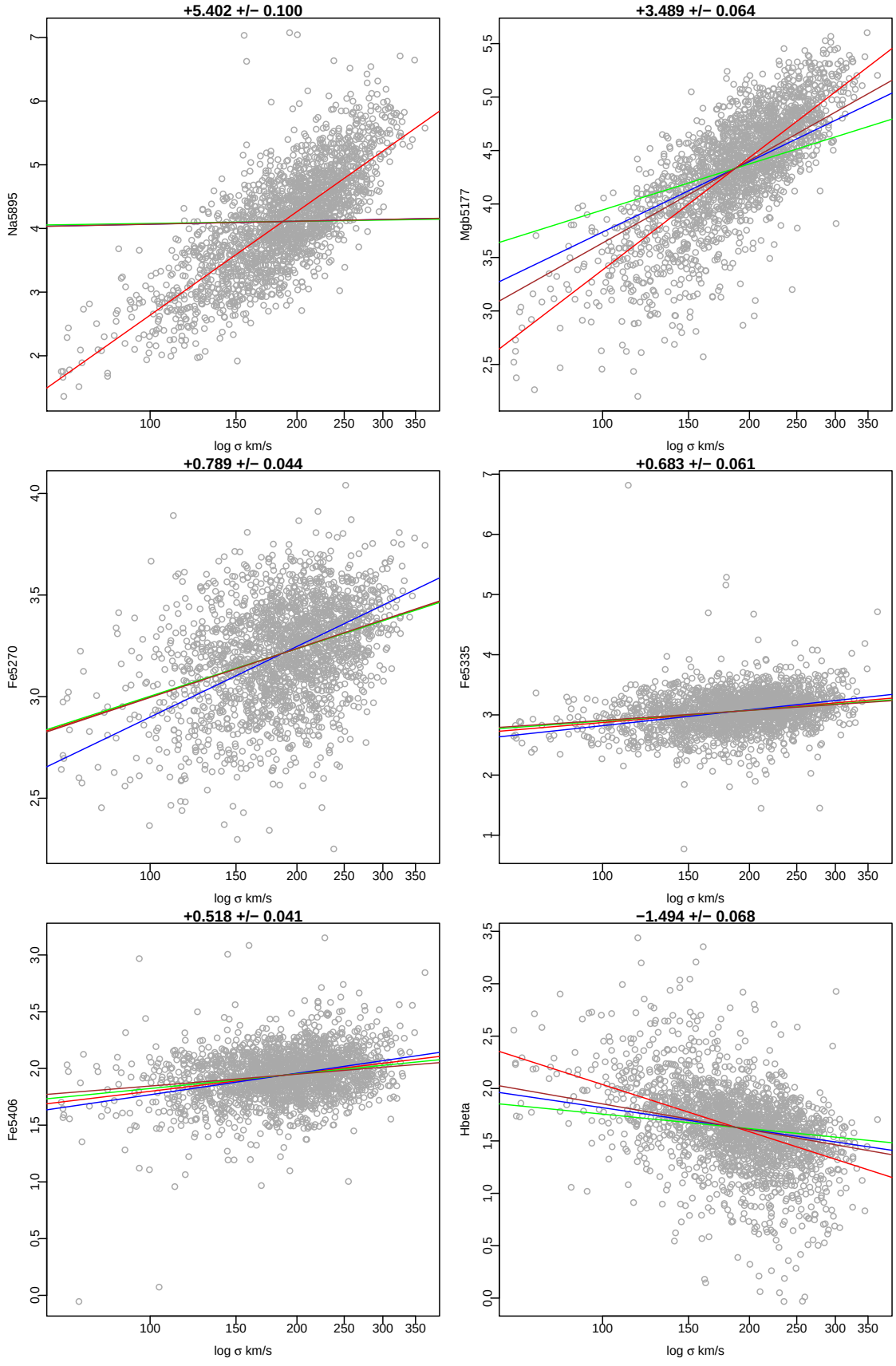

Figure 3.6: Index sigma relations for sodium, magnesium, iron and Hbeta indices. Red lines are linear fits to the observational data (grey points). Blue, brown and green lines are predicted index-sigma slopes according to trends in age, α- and Fe-abundance from published values (Nelan et al. (2005), Smith et al. (2007) and Smith et al. (2009) respectively), combined with model responses from Conroy & van Dokkum (2012a). See Figures 3.5 and 3.7 for other indices and text for discussion.

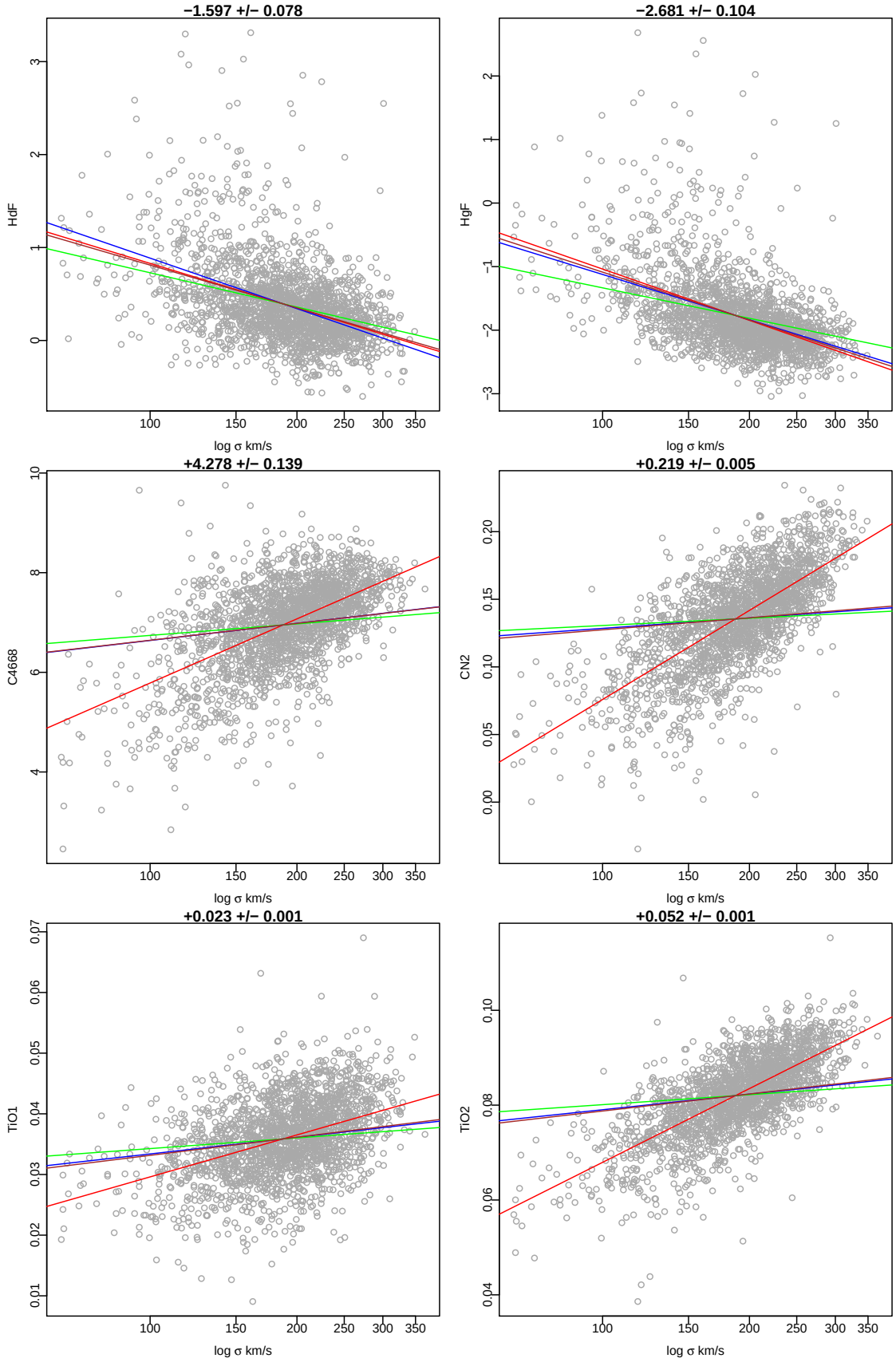

Figure 3.7: Index sigma relations for Hδ, Hγ, carbon and titanium oxide indices. Red lines are linear fits to the observational data (grey points). Blue, brown and green lines are predicted index-sigma slopes according to trends in age, α- and Fe-abundance from published values (Nelan et al. (2005), Smith et al. (2007) and Smith et al. (2009) respectively), combined with model responses from Conroy & van Dokkum (2012a). See Figures 3.5 and 3.6 for other indices and text for discussion.

SLOPES, NORMALISATIONS AND ERRORS FOR INDEX-SIGMA PLOTS

Index	normalisation (b)[1] and error	slope (a)[1] and error	RMS
Ca4227	$+1.323 \pm 0.011$	$+0.883 \pm 0.036$	0.192
Mgb5177	$+3.384 \pm 0.019$	$+3.489 \pm 0.064$	0.342
Fe5270	$+2.999 \pm 0.013$	$+0.789 \pm 0.044$	0.232
Fe5335	$+2.873 \pm 0.018$	$+0.683 \pm 0.061$	0.326
Fe5406	$+1.798 \pm 0.012$	$+0.518 \pm 0.041$	0.221
Na5895	$+2.638 \pm 0.030$	$+5.402 \pm 0.100$	0.536
TiO1	$+0.030 \pm 0.000$	$+0.023 \pm 0.001$	0.006
TiO2	$+0.068 \pm 0.000$	$+0.052 \pm 0.001$	0.006
CaII086a	$+1.225 \pm 0.023$	-0.361 ± 0.076	0.407
CaII086b	$+3.576 \pm 0.027$	-0.700 ± 0.089	0.477
CaII086c	$+2.895 \pm 0.027$	-0.598 ± 0.092	0.485
NaI082	$+0.235 \pm 0.018$	$+1.044 \pm 0.059$	0.312
HdF	$+0.829 \pm 0.023$	-1.597 ± 0.078	0.416
HgF	-1.039 ± 0.031	-2.681 ± 0.104	0.553
CN2	$+0.076 \pm 0.001$	$+0.219 \pm 0.005$	0.027
C4668	$+5.785 \pm 0.041$	$+4.278 \pm 0.139$	0.743
Hbeta	$+2.038 \pm 0.020$	-1.494 ± 0.068	0.365
CaTrip	$+7.695 \pm 0.055$	-1.716 ± 0.185	0.978

[1] where index = a $\log_{10} \frac{\sigma}{100 \text{ km s}^{-1}}$ + b

Table 3.1: Index-sigma relations, normalisations, errors and root mean squares (RMS) for all indices (see Figures 3.5, 3.6 and 3.7). Normalisation is defined as mean index value at σ=100 km s^{-1}.

Both NaI and NaD (see Figures 3.5 & 3.6) have a positive correlation with velocity dispersion. This could indicate an increase in sodium abundance with increasing velocity dispersion, however, the NaI082 doublet feature is also sensitive to age and IMF, complicating the interpretation of the line-strength. There is also the consideration that the NaD spectral feature may be affected by interstellar absorption, this will be discussed later.

The effect of sodium abundance is difficult to interpret because sodium has an influence on the strength of other features due to its role as an electron-contributor in the atmospheres of late-type giants and dwarfs. An increase in the sodium abundance causes a decrease in the ionised species CaII (and therefore has a reducing effect on the size of the CaII feature) this can mimic the effect of the IMF which, as it moves toward more bottom-heavy and therefore more dwarf-dominated values, causes a decrease in the size of the CaII equivalent width.

The magnesium index (Mgb5177) and the three iron indices (Fe5270, Fe5335 and Fe5406), as shown in Figure 3.6, are also positively correlated with velocity dispersion; an indication that the mean metallicity ([Z/H]) increases with galaxy mass as suggested by Worthey (1994). Magnesium is an α-element which could suggest an increase in α-abundance as the galaxy mass increases.

The three hydrogen indices Hbeta, HγF and HδF (see Figures 3.6 and 3.7) show a negative correlation with velocity dispersion. This negative correlation is explained by considering the types of stars in the different sized galaxies. Galaxies that are greater in mass are older, this means that their stars have had more time to evolve than those stars in younger galaxies. The hottest stars are the largest stars and these evolve off the main sequence much quicker than those with lower masses. This means that the hottest stars in the most massive galaxies will be

cooler than the hottest stars in the smaller galaxies. The cooler stars do not have temperatures high enough to excite electrons to higher energy levels. This means that the Balmer lines become less likely to occur the older the galaxy is. This explains the negative correlation between the hydrogen indices and velocity dispersion.

The molecular indices titanium oxide (TiO1 and TiO2) and cyanide (CN2) have a positive correlation with galaxy mass, as does the $C_2$4668 index. The $C_2$4668 and CN2 indices are both strongly sensitive to α-abundance (Conroy & van Dokkum (2012a)), this is because oxygen is an α-element and therefore increases with an increasing α-abundance. With more oxygen in the stellar atmospheres, more carbon is utilised in CO molecules as they have a higher dissociation energy than other carbon molecules. This results in there being less carbon available to form $C_2$4668 and CN2 molecules. Due to the presence of a positive correlation between the molecular indices and velocity dispersion, this may suggest that there is a decreasing α-abundance, or a decrease in oxygen, as the galaxies get more massive.

In order to interpret the trends shown by the spectral features with velocity dispersion in more detail, it is important to consider the effects of different parameters on the slope of the relation by looking at predictions from the models.

3.3 Model Predictions

In order to separate the effects of the abundance and IMF on the observational data, it is important to investigate and account for the effect of changing other parameters such as age, α- and Fe- abundance on the measured equivalent widths of different features, this can be done using stellar population models.

The models used in this study were created by Conroy & van Dokkum (2012a) and have ages, abundances and IMFs that cover a variety of populations and therefore create a versatile set of spectra for comparison with observational data. In order to know which spectral features are characteristic of different parameters, it is important to look at how the measured model equivalent widths vary with different parameters. This is done by plotting the predicted equivalent widths for a certain index against the corresponding parameter to find the response (dI/dP).

Illustrative examples of the strongest and weakest responses for each parameter are shown in the following sections.

3.3.1 Age Responses

Figure 3.8 shows the responses to age (see column 3 of Table 3.2) for the HγF and calcium triplet features (for solar metallicity models and various IMFs). For the hydrogen feature in panel (a), there is a strong negative trend with age; this is as expected from the negative index-sigma relation (see Section 3.2) due to the fact that more massive galaxies are older. The measured equivalent width of the HγF

Index	x	log age	[α/Fe]	[N/Fe]	[Ti/Fe]	[Mg/Fe]	[Si/Fe]	[Na/Fe]	[Ca/Fe]	[Fe/H]	[C/Fe]
Ca4227	$+0.084$	$+1.069 \pm 0.013$	$+4.923 \pm 0.078$	-1.012	-0.047	$+0.402$	-0.255	$+0.025$	$+2.676$	$+0.322$	-2.346
Mgb5177	$+0.144$	$+1.322 \pm 0.011$	$+5.214 \pm 0.093$	-0.044	$+0.044$	$+4.248$	-0.413	-0.162	-0.005	-0.291	-0.269
Fe5270	-0.022	$+0.944 \pm 0.009$	$+0.765 \pm 0.066$	$+0.039$	$+0.109$	-0.635	$+0.140$	-0.042	$+0.402$	$+2.151$	$+0.260$
Fe5335	-0.054	$+0.861 \pm 0.007$	$+0.227 \pm 0.061$	-0.036	-0.052	-0.490	$+0.214$	-0.059	$+0.019$	$+1.847$	$+0.115$
Fe5406	-0.033	$+0.677 \pm 0.007$	-0.045 ± 0.048	-0.002	-0.000	-0.458	-0.116	-0.042	-0.034	$+1.523$	$+0.119$
Na5895	$+0.268$	$+1.043 \pm 0.016$	-0.874 ± 0.075	$+0.052$	-0.561	-0.358	-0.169	$+3.066$	-0.104	-0.061	$+0.768$
TiO1	$+0.006$	$+0.003 \pm 0.000$	$+0.031 \pm 0.001$	-0.000	$+0.015$	-0.003	-0.001	-0.001	-0.003	$+0.003$	-0.013
TiO2	$+0.015$	$+0.009 \pm 0.001$	$+0.040 \pm 0.001$	$+0.003$	$+0.014$	-0.006	-0.000	-0.002	-0.007	$+0.004$	-0.012
CaII086a	-0.127	$+0.005 \pm 0.002$	$+0.882 \pm 0.002$	-0.067	-0.009	-0.350	$+0.010$	-0.054	$+1.274$	-0.226	-0.032
CaII086b	-0.302	$+0.168 \pm 0.003$	$+2.322 \pm 0.012$	-0.080	-0.125	-0.882	-0.087	-0.148	$+3.528$	-0.478	$+0.120$
CaII086c	-0.376	-0.117 ± 0.007	$+1.808 \pm 0.011$	-0.046	$+0.059$	-0.877	-0.121	-0.119	$+2.855$	-0.100	-0.019
NaI082	$+0.531$	$+0.455 \pm 0.007$	-0.328 ± 0.032	-0.074	-0.226	-0.147	-0.049	$+0.559$	$+0.015$	$+0.088$	$+0.170$
HdF	$+0.016$	-2.592 ± 0.029	$+0.102 \pm 0.181$	-0.428	-0.476	$+0.265$	$+1.843$	$+0.014$	$+0.209$	-1.945	-0.825
HgF	-0.031	-3.601 ± 0.046	-1.146 ± 0.253	-0.032	$+0.047$	$+0.482$	$+0.219$	$+0.054$	-0.130	-0.427	-1.082
CN2	-0.007	$+0.090 \pm 0.001$	-0.049 ± 0.006	$+0.212$	$+0.008$	-0.064	$+0.065$	-0.007	-0.024	-0.013	$+0.255$
C4668	-0.034	$+1.910 \pm 0.008$	$+0.479 \pm 0.131$	$+0.038$	$+1.433$	-1.314	-0.824	-0.154	$+0.096$	$+0.551$	$+7.546$
Hbeta	-0.023	-1.273 ± 0.010	-0.343 ± 0.089	$+0.025$	$+0.446$	-0.384	$+0.179$	$+0.007$	-0.027	$+0.302$	-0.604
CaTrip	-0.805	$+0.005 \pm 0.001$	$+5.012 \pm 0.012$	-0.194	-0.075	-2.109	-0.198	-0.321	$+7.657$	-0.803	$+0.068$

Table 3.2: Index-parameter responses for all indices (see Figures 3.8, 3.9, 3.10 and 3.11 for examples). The responses are derived from Conroy & van Dokkum (2012a) models. Note the slopes that are made from only two points do not have errors displayed as these are formally equal to zero.

index decreases more steeply for the younger aged models, and at $\sim$7 Gyr the decrease in the size of the index flattens but continues to decrease at a slower rate as age continues to increase. The trend shown by the models may suggest that the difference between the temperatures for the younger (3 - 7 Gyr) galaxies is more pronounced than the difference between the temperatures of the older (>7 Gyr) galaxies.

For the calcium triplet feature (panel (b) in Figure 3.8) the relationship with age is very different to that of HγF. For CaII there is very little change in index size with increasing age, the slight changes for bottom-light (positive slope) and bottom-heavy (negative slope) are due to the proportional quantities of giant stars for each IMF. Figure 3.1 indicates that galaxies with greater velocity dispersions correspond to a greater age, this means the overall abundance of the CaII species (and therefore the size of the spectral feature) will increase when there are more giant stars (bottom-light IMF) and decrease when there are fewer (bottom-heavy IMF) giant stars. The very weak response of the calcium triplet to age is useful in constraining the IMF and shall be examined in more detail later.

3.3.2 α-Abundance Responses

Column four of Table 3.2 shows the response for each index to a change in α-abundance ([α/Fe]). Figure 3.9 shows the responses of the Mgb5177 and Fe5406 features to an increasing α-enhancement ([α/Fe] = +0.2, +0.3 and +0.4 dex) in models of ages 13.5 Gyr and various IMFs.

Magnesium is an α-element, so unsurprisingly, with an increase in [α/Fe], there is an increase in the size of the Mgb5177 index. The different IMFs show a similar gradient with increasing α-abundance, indicating that the Mgb5177 index is very weakly sensitive to changes in the IMF.

Iron is not an α-element which explains why the Fe5406 index does not show a positive response to α-enhancement. The gradient for the different IMFs is also similar, suggesting that Fe5406 is not particularly sensitive to changes in the IMF.

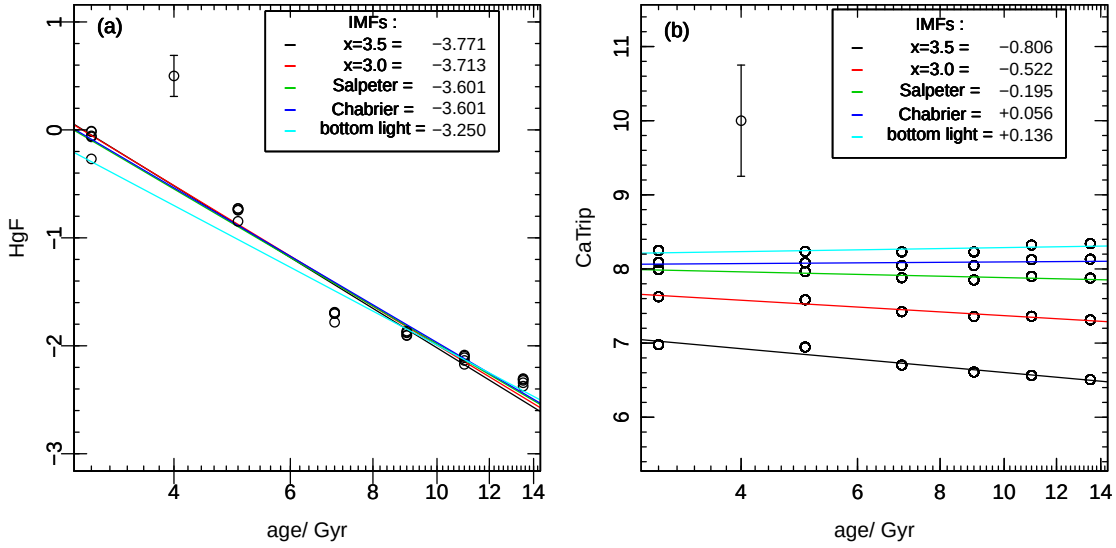

Figure 3.8: The change of the predicted HγF and CaII indices with age for different IMFs (at solar metallicity) from Conroy & van Dokkum (2012a) models. HγF is a strong age indicator whilst the CaII shows a weak response to age. The error bars in the top left of the two panels represent the average observational error for the respective measured index.

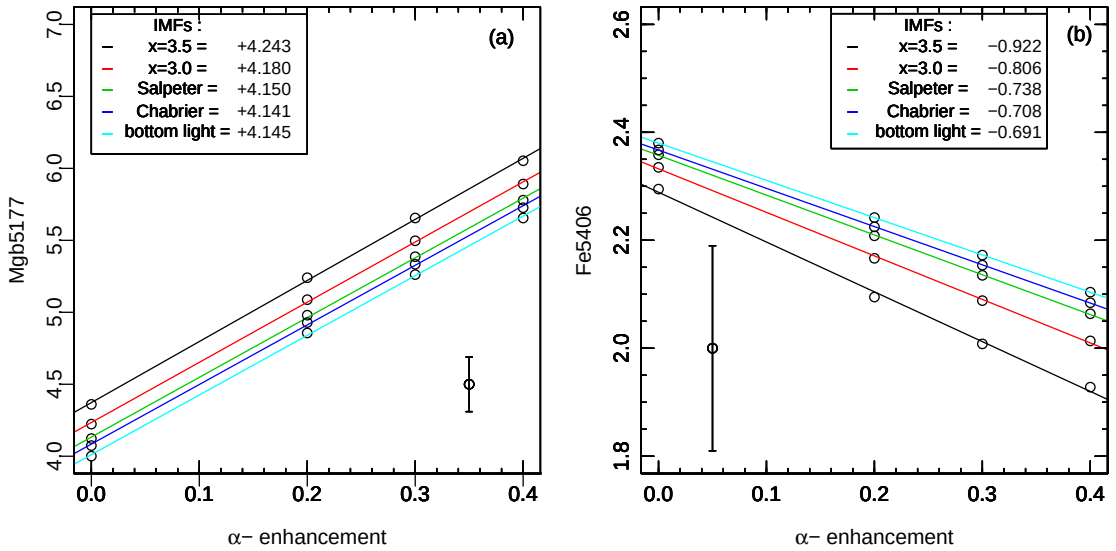

Figure 3.9: The change of the Mgb5177 and Fe5406 indices with increasing [α/Fe] for different IMFs (where age = 13.5 Gyr). Magnesium is an α-element therefore the Mgb5177 index shows a strong positive correlation with α-enhancement. Iron is not an α-element; the Fe5406 index shows a weak response to α-abundance changes. The error bars in the bottom right, and left of panel (a) and (b) respectively, represent the average observational error for the measured Mgb5177 and Fe5406 indices.

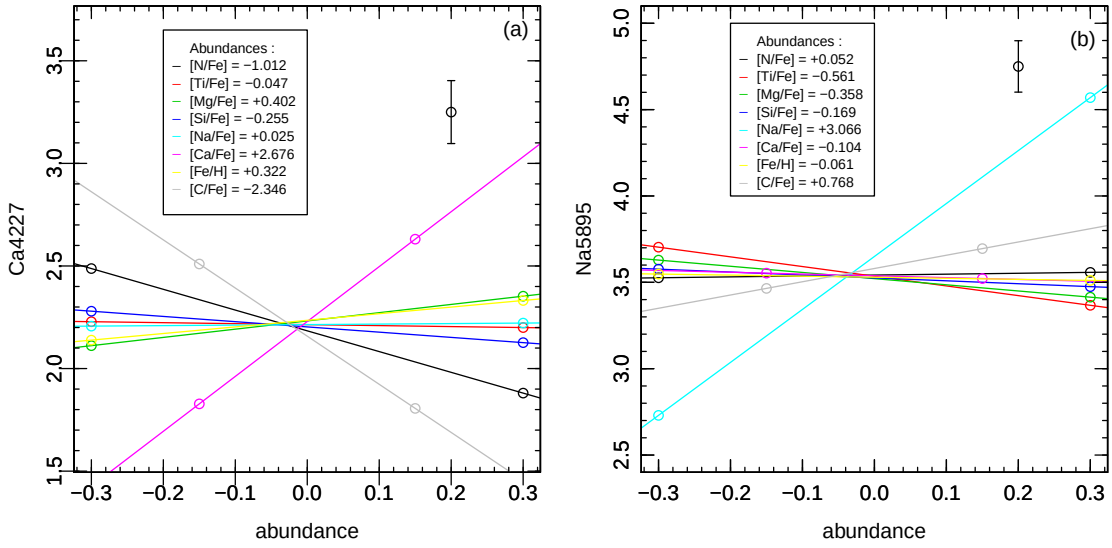

Figure 3.10: The change of the Ca4227 and Na5895 indices with various abundances. The strongest positive response for both indices is to their corresponding elemental abundance; as expected. There is also a strong negative correlation between the Ca4227 index and [C/Fe] and [N/Fe]; possibly due to contamination of the index by a CN band. The error bars in the top right of panels (a) and (b) represent the average observational error for the measured indices.

3.3.3 Various Elemental Abundance Responses

Figure 3.10 shows the relation between the size of the Ca4227 and Na5895 indices with various elemental abundances ([N/Fe], [Ti/Fe], [Mg/Fe], [Si/Fe], [Na/Fe], [Ca/Fe], [Fe/H] and [C/Fe]) for models with ages of 13.5 Gyr and a Chabrier IMF.

The Ca4227 index shows a positive correlation with [Ca/Fe], as expected the index gets larger the more calcium in the stars. There is also a strong negative response with [C/Fe] which may be explained by the presence of a strong CN band in the blue continuum region around the index (Graves et al. (2007)). As the CN feature increases in size with increasing [C/Fe], its strengthening may cause the neighbouring Ca4227 feature to decrease in size. The same can be said for the [N/Fe] which also causes a strong negative response for the Ca4227 feature.

Similarly for the Na5895 index, there is a strong positive correlation between the size of the index and [Na/Fe], this means, in principle, that the Na5895 feature is a good indicator of sodium abundance.

3.3.4 IMF Responses

The final parameter to be considered is the IMF. Figure 3.11 shows the response of the NaI and CaII features to changes in the IMF. The range of IMFs covered are from Salpeter (x = 2.35) to the Conroy & van Dokkum (2012a) 'bottom-heavy' IMF (x = 3.0). The range is limited to these two values because the Chabrier and bottom-light IMFs both have Salpeter-like slopes above 1 $M_{\odot}$ and are more complicated at smaller masses with no single value for the power. The even more bottom-heavy x = 3.5 IMF is also excluded due to its extreme nature. Both plots

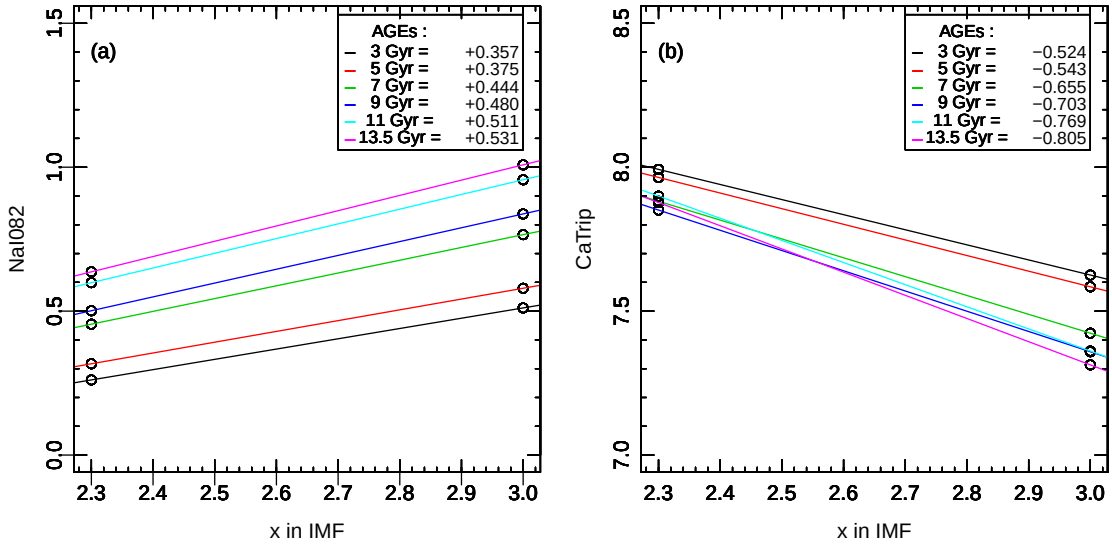

Figure 3.11: The change in NaI and CaII index size with varying IMF; for a range of ages, all at solar abundances. The slope is positive for the NaI index as there are more low-mass stars in bottom-heavy IMF models; the converse for CaII.

show a strong response to IMF; NaI increasing in size with greater values of x in the IMF (representing a trend toward more bottom-heavy populations) and CaII showing the opposite behaviour due to it being characteristic of giant stars.

3.3.5 Sensitivities

The *sensitivity* is defined as the corresponding model *response*; (dI/dP), divided by the average observational *error* for the appropriate feature. This quantity summarises the practical usefulness of each index in constraining the variation of underlying parameters.

Figure 3.12 compares the sensitivity of different indices to age, α abundance, calcium abundance and sodium abundance and IMF. Figure 3.12 clearly highlights the fact that the calcium triplet, TiO2 and NaI features show the greatest sensitivity to the IMF. The TiO2 feature appears to be the most sensitive to the IMF out of all the indices in this study, however, whilst it has been utilised as an IMF indicator (Spiniello et al. (2012)) it has not been used in this piece of work due to the fact that the titanium abundance is not well constrained and currently there is not a titanium-abundance indicative feature that can be combined with TiO2 the way Na5895 can be combined with NaI082, and Ca4227 combined with CaII.

The strongest sensitivities to age are shown by the hydrogen features (see Figure 3.12(a)), including HγF as shown in Figure 3.11. The calcium triplet shows a very weak sensitivity to age as suggested by Conroy & van Dokkum (2012a) and Schiavon et al. (2000), further adding to its appealing properties as an IMF indicator.

The most sensitive features to α-abundance are the calcium feature at 4227 Å and the magnesium feature at 5177 Å. Calcium and magnesium are both α-

elements and are much more sensitive to α-abundance variations than other α-elements (see Figure 3.12(b)). Both the titanium indices are also sensitive to the α-abundance (as titanium is an α-element), and Fe5270 is more sensitive to a change in α-abundance than the other iron indices due to the presence of a calcium feature blending in with the Fe5270 line. Calcium is sensitive to α-enhancement due to its treatment as an α-element in the models, so its contribution to the Fe5270 means that this iron feature is more sensitive to α-abundance changes than the other iron features at 5335 and 5406 Å.

Panel (c) of Figure 3.12 shows the calcium indices are unsurprisingly the most sensitive to calcium abundance changes (Ca4227 the strongest as expected). The iron feature at 5270 Å shows a comparably strong sensitivity to calcium abundance compared to the other iron features; due to calcium contribution to the feature. The Na5895 feature shows a weak sensitivity to calcium abundance, whereas the NaI082 feature shows no sensitivity.

The sodium doublet feature (at 5895 Å) shows the greatest sensitivity to sodium abundance. This is followed by the other sodium feature (NaI at $\sim$8200 Å). The fact that the Na5895 feature is more sensitive than NaI082 to sodium abundance highlights its use as a distinguishing factor for separating effects of the IMF and sodium abundance. It is also interesting to note that the calcium triplet index shows a non-zero response to the sodium abundance (see Figure 3.12(d)), this is due to the role of sodium as an electron donor in stellar atmospheres.

3.4 Abundance or IMF?

The calcium index-sigma slopes in Figure 3.5 pose an interesting question; why do the calcium features behave differently to one another with changes in velocity dispersion? This opposing behaviour can be useful if combined with the knowledge of the features' sensitivities to abundance and IMF (from the previous section); presenting an opportunity to separate the effects of abundance and IMF with increasing velocity dispersion. This can be done by attempting to replicate the linear fit to the index-sigma relations of the observational data (see Section 3.2) by adjusting the variation of age and abundance trends.

To explain the negative slope of the calcium triplet, Cenarro et al. (2004) propose there is either a decrease in calcium abundance with an increase in galaxy size or a variation in the IMF as galaxy mass changes; or simply a combination of both. It is important to investigate whether the negative slope of the CaII triplet with increasing velocity dispersion can be attributed to just a change in IMF or calcium abundance alone. Figure 3.13 is a plot of the calcium triplet combined index against log velocity dispersion (σ). The linear slope fitted to the observed data is the same fit as in Figure 3.5 (and values as in Table 3.2).

Assuming for these purposes that the Ca4227 index responds solely to calcium abundance, Equation 3.1 shows the components that contribute to the slope of the

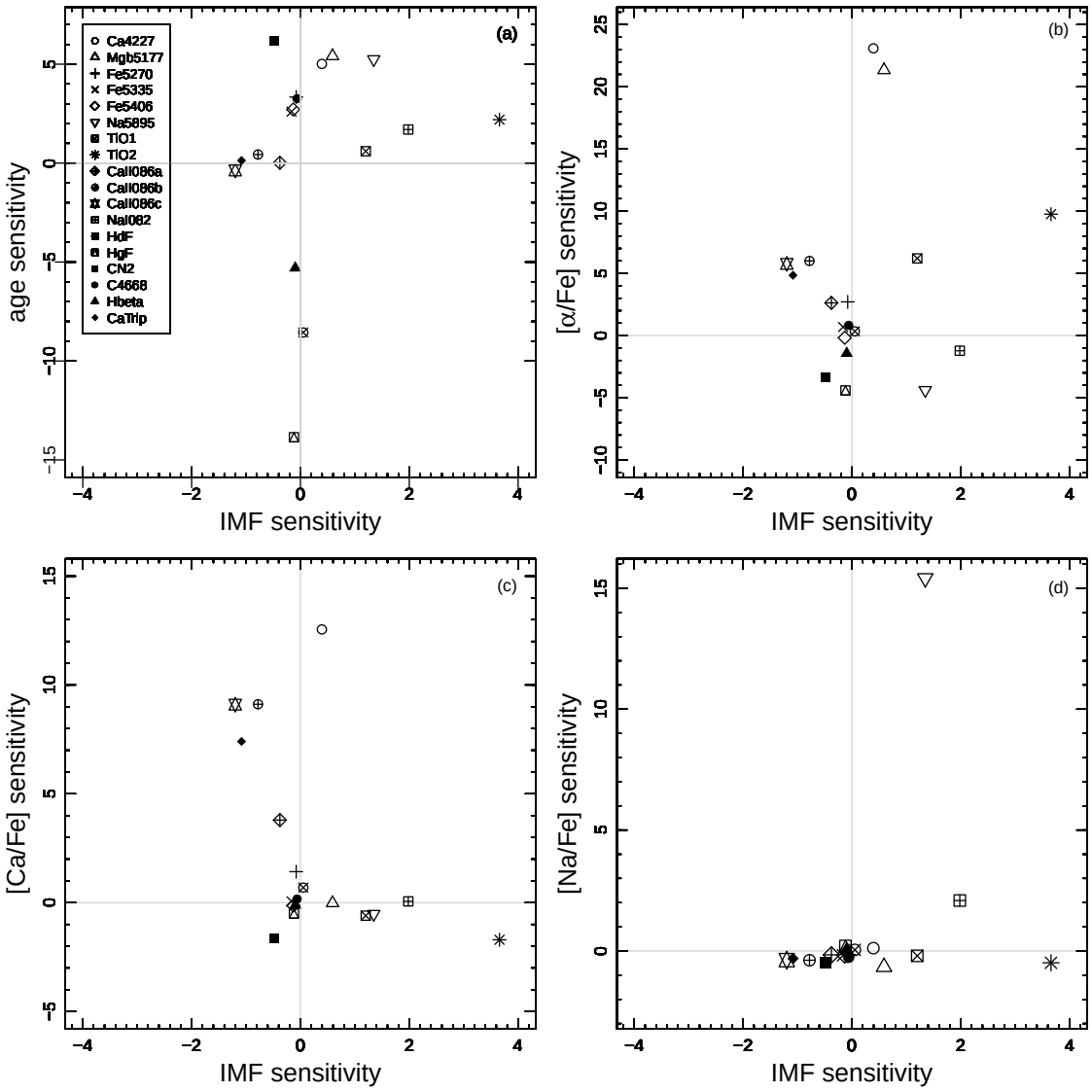

Figure 3.12: Plot of the IMF sensitivity against age (a), α-abundance (b), calcium abundance (c) and sodium abundance (d) sensitivities for all indices. The sensitivity is the response of the index to a given parameter (i.e. age, α-, Fe-, Ca- or Na- abundance) taken from Conroy & van Dokkum (2012a) models, divided by the mean error on the observational measurements. In panel (a) the greatest sensitivity to age is shown by the hydrogen features (HγF, HδF and Hβ) with almost no change due to effects of the IMF. Panel (b) shows the greatest sensitivity for [α/Fe] is by the Ca4227 and Mgb5177 indices; both α-elements. Panel (c) shows that the calcium indices are the most sensitive to changes in [Ca/Fe] (as expected) and the Fe5270 index is also sensitive to the calcium abundance due to a calcium feature blending in with the iron feature. Panel (d) shows the sodium indices are the most sensitive to [Na/Fe] variation (as expected), with Na5895 being the most sensitive. The calcium triplet is also weakly sensitive to changes in [Na/Fe]. The greatest sensitivity to the IMF is shown by the TiO2, NaI082 and calcium triplet features.

Ca4227-sigma relation; a combination of the change in Ca4227 index size with calcium abundance, and the change in calcium abundance with velocity dispersion (in log units).

$$\frac{d\text{Ca4227}}{d\log\sigma} = \frac{d\text{Ca4227}}{d[\text{Ca/Fe}]}.\frac{d[\text{CaFe}]}{d\log\sigma} \tag{3.4}$$

The components of the equation that are used to calculate the change in calcium abundance with velocity dispersion are shown in blue. These terms are then used to predict the slope of the index-sigma relation for the calcium triplet, according to the calcium abundance, shown in Equation 3.2.

$$\frac{d\text{CaTrip}}{d\log\sigma} = \frac{d\text{CaTrip}}{d[\text{Ca/Fe}]}.\left(\frac{d\text{Ca4227}}{d\log\sigma}\frac{d\text{Ca4227}}{d[\text{Ca/Fe}]}\right) \tag{3.5}$$

The new predicted calcium-sigma slope according to the calcium abundance of Ca4227 is shown in Figure 3.13.

Equation 3.1 is repeated for the change in size of the Ca4227 feature according to the power law index, x, in the IMF to calculate a new value for the CaII-sigma scaling relation, this is also shown in Figure 3.13. Neither of the two predicted scaling relations reproduce the slope of the the observed data and neither slope falls within the error margins. The predicted slope for a pure [Ca/Fe] variation, is considerably steeper than the observed slope, whilst the predicted slope according to the IMF is shallower; the opposing nature of the predicted slopes suggests that the observed slope can only be explained by a combination of calcium abundance and IMF effects.

The same process can be repeated with the sodium indices to see if the observed NaI-sigma scaling relation can be reproduced by considering just the sodium abundance or IMF. The change in sodium abundance for NaD (shown in blue in Equation 3.3), is used in the equation for the sodium doublet to calculate a new NaI-sigma scaling relation :

$$\frac{d\text{NaI082}}{d\log\sigma} = \frac{d\text{NaI082}}{d[\text{Na/Fe}]}.\left(\frac{d\text{Na5895}}{d\log\sigma}\frac{d\text{Na5895}}{d[\text{Na/Fe}]}\right) \tag{3.6}$$

The process is then repeated using the response of the NaD index to changes in x (the IMF power law index). Figure 3.14 shows the IMF and sodium abundance constrained scaling relations along with the NaI-sigma scaling relation. There is a clear difference between the sodium abundance and IMF predicted slopes. It is quite obvious that the slope produced by just changing the IMF does not come close to replicating the observational slope. The slope predicted by the sodium abundance, however, does replicate the observed slope if the error margins are taken into consideration. This would seemingly indicate that the effect due to the IMF with increasing velocity dispersion is not as influential on the size of the index equivalent width as the effect due to the sodium abundance. It also has to be appreciated that the effects of other parameters are yet to be taken into consid-

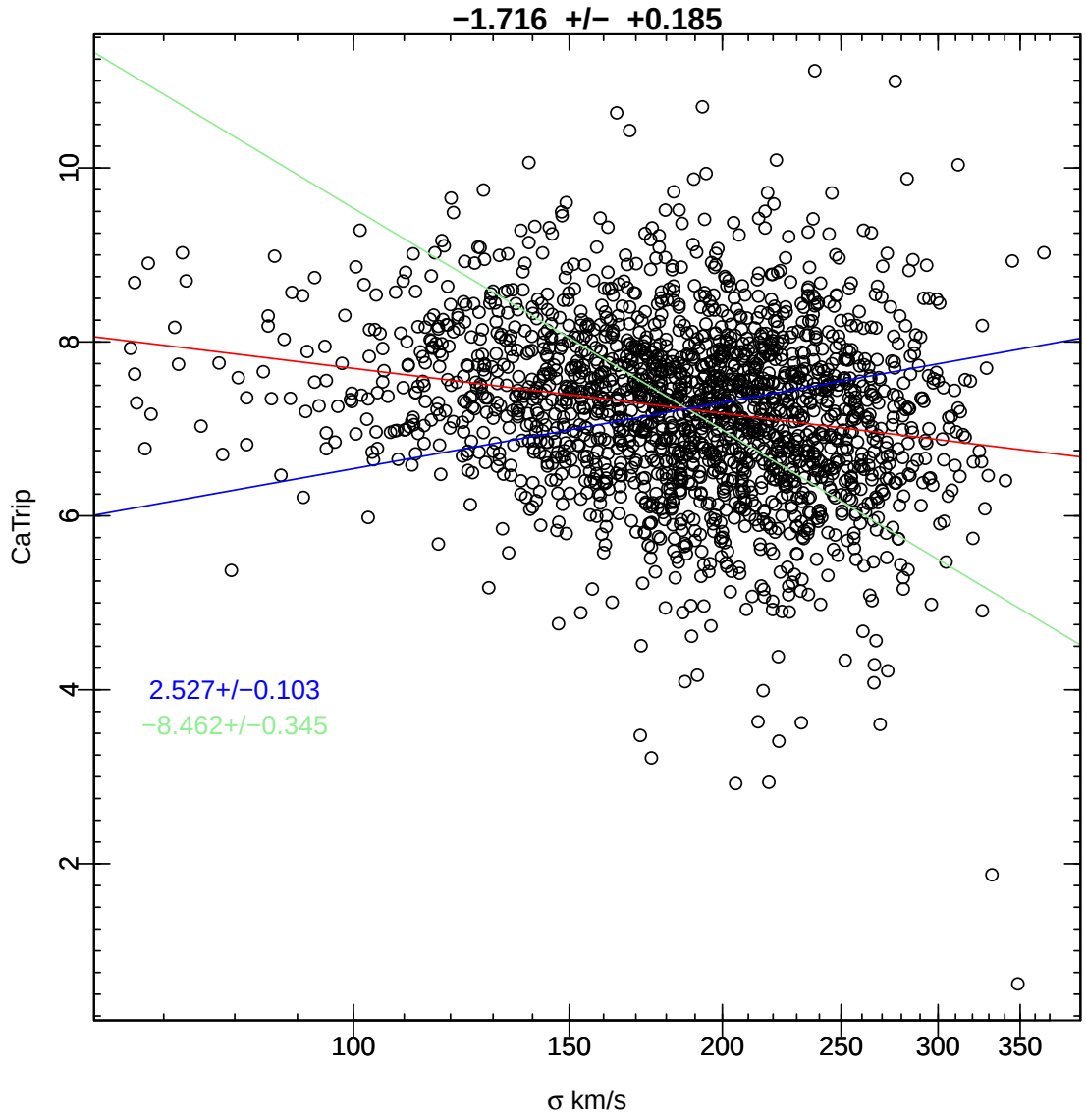

Figure 3.13: Plot of measured equivalent widths for the calcium triplet against velocity dispersion. The red line is the linear fit to the data, the blue line is the predicted slope according to [Ca/Fe] and the light green line is the predicted slope according to the IMF variation. According to the calculated slopes and errors it is not possible to explain the slope of the calcium triplet by IMF or [Ca/Fe] alone.

eration, but by just accounting for the sodium abundance, a good reproduction of the observed scaling relation can be achieved.

In order to carry out a thorough analysis of the effect of the IMF and elemental abundances on stellar populations, it is important to consider all the parameters that have an effect on the size of the measured equivalent widths. Once these parameters are constrained, it is then possible to explore the effects of abundance from abundance characteristic features and the IMF from dwarf- and giant- characteristic features.

3.5 Constraining the index-sigma slope using published and model relations

In this section, the trends of age, α- and Fe-abundance are taken into consideration with respect to the index-sigma scaling relations from the previous section. Three sets of literature scaling relations are used in this piece of work (from Nelan et al. (2005), Smith et al. (2007) and Smith et al. (2009) (see Table 3.3)). These scaling relations are considered to be good representations of the variation of age, α- and Fe-abundance with velocity dispersion in red sequence galaxies. These scaling relations can be combined with model responses (see Figures 3.8 and 3.9; examples for age and α-abundance responses) to predict an index-sigma scaling relation which can be compared to the index-sigma slopes obtained from a linear fit to the observational data.

3.5.1 The change in [α/Fe], [Fe/H] and age with increasing velocity dispersion

It is clear from Figure 3.12 that there are many indices that are sensitive to different parameters, and from the brief investigation in the previous section it is apparent that the scaling relation of the calcium triplet cannot be reproduced with just calcium abundance or IMF effects taken into consideration. For the sodium doublet, the sodium abundance was able to reproduce the index-sigma scaling relation, showing just how large a contribution the sodium abundance makes to the scaling relation.

In order to explore the effects of IMF and abundance individually, it is important to fix the variation of certain parameters that have been constrained directly from other galaxies samples similar to this one. Nelan et al. (2005), Smith et al. (2007) and Smith et al. (2009) measure the variation of the α-abundance ([α/Fe]), age and total metallicity [Z/H] of a group of red sequence galaxies by measuring spectral features at optical wavelengths (Mgb, CN1, Hβ, HδF, HγF and various iron indices between 4500 and 6000 Å). From this information it is also possible to find the iron abundance as [Z/H] $\simeq$ [α/H] = [α/Fe] + [Fe/H], therefore [Fe/H] = [Z/H] - [α/Fe]. The scaling relations are show in Table 3.3.

It is important to bear in mind that the literature values were constrained from

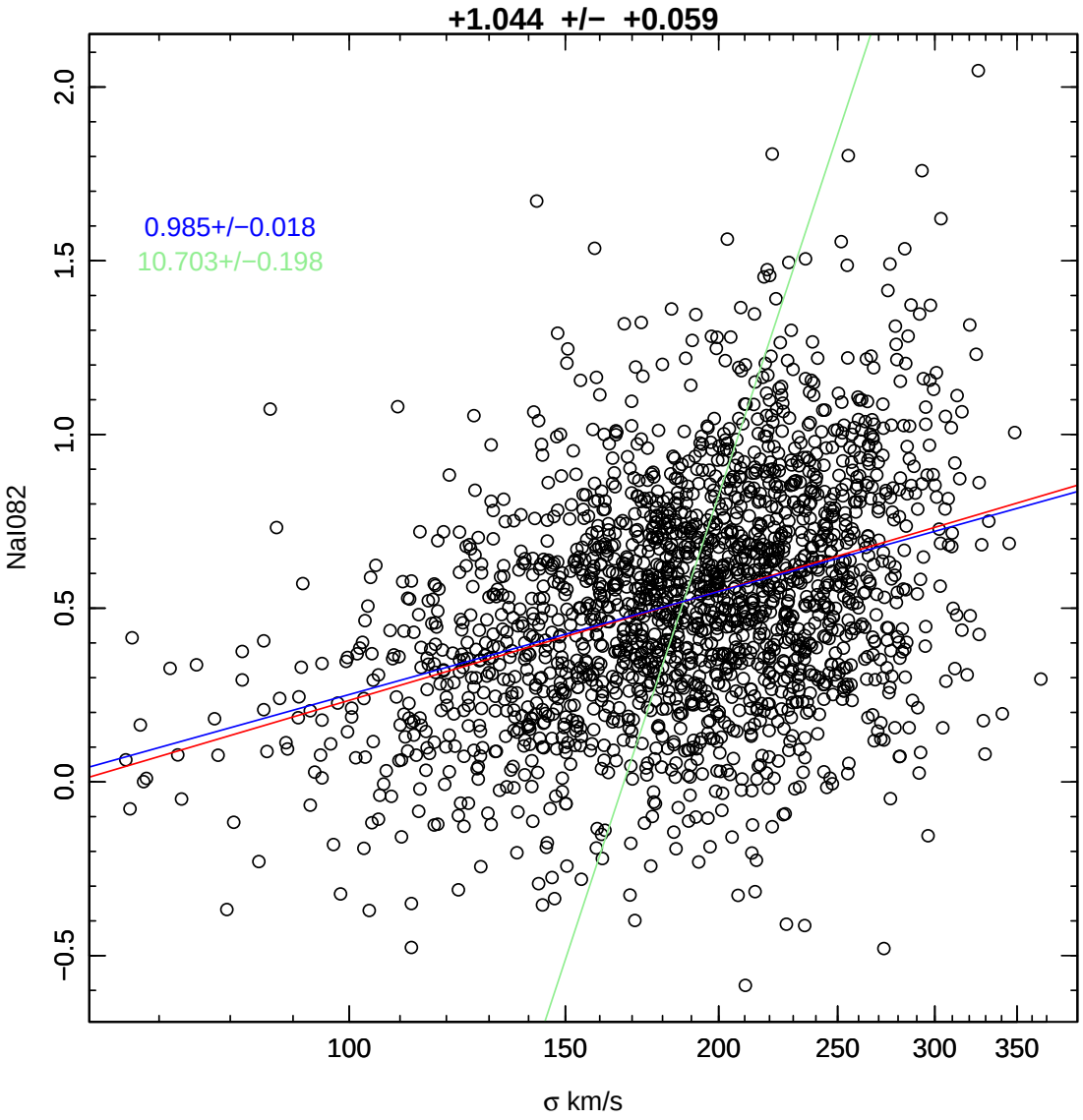

Figure 3.14: Plot of measured equivalent widths for sodium doublet against velocity dispersion. The red line is the linear fit to the data, the blue line is the predicted slope according to [Na/Fe] and the light green line is the predicted slope according to the IMF variation. According to the calculated slopes and errors it is not possible to explain the slope of the sodium doublet by IMF considerations alone, however, when the sodium abundance variation is taken into consideration, it is possible to reproduce the observed NaI-sigma scaling relation without the effect of any other parameters.

LITERATURE VALUES

Origin	[Z/H] $\propto$	age $\propto$	[αFe] $\propto$	[Fe/H] $\propto$
Nelan et al. 2005	$\sigma^{0.53\pm0.08}$	$\sigma^{0.59\pm0.13}$	$\sigma^{0.31\pm0.06}$	$\sigma^{0.22\pm0.14}$
Smith et al. 2007	$\sigma^{0.35\pm0.025}$	$\sigma^{0.40\pm0.028}$	$\sigma^{0.20\pm0.020}$	$\sigma^{0.15\pm0.045}$
Smith et al. 2009	$\sigma^{0.38\pm0.09}$	$\sigma^{0.64\pm0.12}$	$\sigma^{0.36\pm0.07}$	$\sigma^{0.02\pm0.16}$

Table 3.3: Various published age, Fe- and α- abundance scaling relations with velocity dispersion. These scaling relations were measured from optical spectral features. [Fe/H] is constrained from the difference between the total metallicity and the iron abundance ([Z/H] - [α/Fe] = [Fe/H]).

different red-sequence galaxy samples, none of which precisely match the sample of data used in this work. Nelan et al. (2005) constrain their values using ∼4000 red-sequence galaxies from 93 low-redshift galaxy clusters at 0.010 <z <0.067 and covering velocity dispersions of 50 <σ <400 km s^{-1}. The data for the two Smith papers (Smith et al. (2007) & Smith et al. (2009)) are samples of ∼500 and 232 galaxies respectively from the Shapley Supercluster (z = 0.048). Both Smith samples have velocity dispersions spanning 30 <σ <300 km s^{-1}. An important difference is also the fact that in this piece of work the GalaxyZoo defined morphology was used as a selection criterion, whereas morphology was not considered for the Nelan or Smith galaxy samples.

In comparison to the data used in this work, the Nelan data seem to be the most similar sample in both redshift and velocity dispersion ranges (this sample having 0.010 <z <0.057 and 66 <σ <366 km s^{-1}, see Section Two). This similarity in data origin may be reflected in the predicted index-sigma scaling relations.

With these parameters fixed at the constrained values, a value of the slope of the change in index with sigma can be calculated according to the equation:

$$\frac{d\,\mathrm{I}}{d\log\sigma} = \frac{d\log \mathrm{age}}{d\log\sigma}\cdot\frac{d\,\mathrm{I}}{d\log \mathrm{age}} + \frac{d\,[\mathrm{Fe/H}]}{d\log\sigma}\cdot\frac{d\,\mathrm{I}}{d\,[\mathrm{Fe/H}]} + \frac{d[\alpha/\mathrm{Fe}]}{d\log\sigma}\cdot\frac{d\,\mathrm{I}}{d[\alpha/\mathrm{Fe}]} \tag{3.7}$$

For each term on the right hand side of the equation, the first factor is the appropriate literature scaling relation (see Table 3.3) and the second factor is the response from the models (see Table 3.2). The slopes calculated from the scaling relations and model responses are shown in Figures 3.5, 3.6 and 3.7, in comparison to the observed scaling relation.

For the calcium triplet, the literature scaling relations do not reproduce the slope of the observed data; they are all much steeper. This suggests, assuming the literature scaling relations are representative of this sample, that there are one or more additional parameters that cause a decrease in index size as the galaxies become more massive. For the Ca4227 index, the lines predicted by the literature scaling relations also do not reproduce the observed slope. The scaling relations predicted by the three different sets of literature scaling relations are very similar to each other.

The slopes predicted for the two sodium indices are almost completely flat. This would suggest that when taking into consideration just the age, α- and Fe-abundance scaling relations, there is little variation in the size of the sodium equivalent widths with increasing velocity dispersion. This means that there is a large contributory effect due to other factors which causes the gradient of the predicted scaling relation to steepen to match that of the observed scaling relation. From the previous section, it is clear that the sodium abundance has a significant effect on the sodium-sigma scaling relations, without this factor being considered here it is not surprising that the predicted scaling relations are significantly flatter.

The predicted scaling relations for the magnesium index at 5177 Å are shal-

lower than the observed slope, see Figure 3.6. The three different sets of scaling relations predict noticeably different values for the slopes; the set of parameters with the steepest α-abundance scaling relation (Smith et al. (2007)) unsurprisingly predict the steepest Mgb5177-sigma scaling relation (because magnesium is an α-element). The role of magnesium, titanium and calcium as α-elements explains why the predicted index-sigma variations for Mgb5177, Ca4227, CaII, CN2, $C_2$4668, TiO1 and TiO2, at this stage, have a positive gradient (due to the presence of a positive [α/Fe] scaling relation). The scaling relations for the hydrogen indices have negative gradients due to the positive age scaling relation (and the negative correlation between age and Balmer line strength) and the predicted iron scaling relations have a positive gradient due to there being a positive [Fe/H]-sigma scaling relation.

The majority of the iron-sigma scaling relations are well reproduced by the predicted slopes suggesting that the literature Fe-abundance variation is well constrained. The Nelan predicted slope seems to be much steeper for the Fe5270 index (see Figure 3.6) than for the other iron indices.

The observed slopes for the hydrogen indices are fairly well replicated by the constrained slopes, with not much difference between the three separately constrained lines. If anything the Smith 09 data seems to predict a slightly shallower line for HγF; this may be due to the fact that the age-σ relation is the steepest for the Smith 09 data (age$\propto \sigma^{0.64\pm0.12}$) and because the equivalent widths of the hydrogen features decrease in size with increasing age; the greater the age-sigma scaling relation, the shallower the predicted index-sigma scaling relation. The fact that the age-sensitive features are fairly well predicted gives reassurance that the literature values are good representations of this galaxy sample.

The observed slopes of the two carbon indices ($C_2$4668 and CN2) and the two titanium oxide indices (TiO1 and TiO2) are not particularly well reproduced by the predicted lines. This may indicate the need for another factor to be taken into consideration, and in the case of the TiO2 index, which is strongly sensitive to changes in the IMF (see Figure 3.12), it may be effects of the IMF that can account for the difference between the predicted and the observed slopes.

In order to better replicate the observed slopes for the index-sigma relations, particularly for the features of interest, it is crucial to take into consideration the effects of other parameters such as calcium and sodium abundance and the effects of the IMF on the spectral features.

3.6 Constraining parameters from observational data

With the predicted index-sigma slopes showing a poor reproduction of the linear fit to the observed data for the sodium and calcium indices, it is important to consider the effects of abundance. The abundance can be constrained from those features that are strongly responsive to sodium and calcium abundance

(Na5895 and Ca4227 respectively). In this work, the assumption is made that once age, [Fe/H] and [α/Fe] have been taken into consideration, the remaining discrepancy between the observed and predicted scaling relations for Na5895 and Ca4227 is attributable solely to the appropriate abundance.

3.6.1 The change in [Ca/Fe] with increasing velocity dispersion

From the previous section, it is apparent that with just age, [α/Fe] and [Fe/H] constraints the observed calcium-sigma scaling relations cannot be reproduced. From Figure 3.13 it is also clear that the calcium abundance has a significant effect on the size of the Ca4227 and CaII equivalent widths. For this reason it is important to explore the effect of the calcium abundance on the calcium-sigma scaling relations. The calcium abundance is constrained from the Ca4227 index as it is the most sensitive feature in this sample to changes in [Ca/Fe] (see Figure 3.12). The assumption is made that once age, [α/Fe] and [Fe/H] effects have been constrained, the resulting difference between the predicted and observed scaling relations is due to the variation of the calcium abundance (assuming the effect of the IMF and other factors is negligible). The new predicted slope of the Ca4227 index-sigma relation is now described as :

$$\frac{d\,\text{Ca4227}}{d\log\sigma} = \frac{d\log\text{age}}{d\log\sigma}\cdot\frac{d\,\text{Ca4227}}{d\log\text{age}} + \frac{d\,[\text{Fe/H}]}{d\log\sigma}\cdot\frac{d\,\text{Ca4227}}{d\,[\text{Fe/H}]} + \frac{d[\alpha/\text{Fe}]}{d\log\sigma}\cdot\frac{d\,\text{Ca4227}}{d[\alpha/\text{Fe}]} + \frac{d\,[\text{Ca/Fe}]}{d\log\sigma}\cdot\frac{d\,\text{Ca4227}}{d\,[\text{Ca/Fe}]} \tag{3.5}$$

where the green factors represent the scaling relations taken from Nelan and Smith (see Table 3.3), the red factors are model responses and the blue factors are the calcium abundance component from Ca4227 constraints. The difference between the observed and predicted Ca4227-sigma scaling relations (see Figure 3.5), is taken to be the calcium abundance term (see blue factors in Equation 3.5). The difference between the observed and constrained scaling relations divided by the Ca4227 index response to [Ca/Fe] (from the models) gives the variation of the calcium abundance with velocity dispersion :

$$\begin{aligned}\Delta[\text{Ca/Fe}] \propto &\sigma^{-0.502\pm0.116} \text{ (with scaling relations from Nelan et al. (2005))}\\ &\sigma^{-0.216\pm0.039} \text{ (with scaling relations from Smith et al. (2007))}\\ &\sigma^{-0.590\pm0.129} \text{ (with scaling relations from Smith et al. (2009))}\end{aligned}$$

An important subtlety needs consideration here. The models used by Nelan and Smith treat calcium as an α-element, meaning that when the α-abundance constraints were made for their respective galaxy samples, the calcium abundance was already partially taken into consideration. From the previous section it is clear that the α-abundance variation does not replicate the slope of the index-

sigma relation so the independent calcium abundance needs to be considered. This means that the Δ[Ca/Fe] values shown above, need to be combined with the [α/Fe] scaling relations from the literature (see 3.3) to give :

$$\begin{aligned}
\text{[Ca/Fe]} \propto & \sigma^{-0.19\pm0.12} \text{ (with scaling relations from Nelan et al. (2005))} \\
& \sigma^{-0.02\pm0.04} \text{ (with scaling relations from Smith et al. (2007))} \\
& \sigma^{-0.23\pm0.13} \text{ (with scaling relations from Smith et al. (2009))}
\end{aligned}$$

These newly constrained calcium abundance scaling relations can then be used to predict new CaII-sigma slopes with the appropriate CaII model responses :

$$\frac{d\,\text{CaII}}{d\log\sigma} = \frac{d\log\text{age}}{d\log\sigma}\cdot\frac{d\,\text{CaII}}{d\log\text{age}} + \frac{d\,[\text{Fe/H}]}{d\log\sigma}\cdot\frac{d\,\text{CaII}}{d\,[\text{Fe/H}]} + \frac{d[\alpha/\text{Fe}]}{d\log\sigma}\cdot\frac{d\,\text{CaII}}{d[\alpha/\text{Fe}]} + \frac{d\,[\text{Ca/Fe}]}{d\log\sigma}\cdot\frac{d\,\text{CaII}}{d\,[\text{Ca/Fe}]}$$

Figure 3.15 shows the observed and predicted index-sigma scaling relations for the calcium indices (see Table 3.4) with the additional calcium abundance factor. The observed Ca4227-sigma scaling relation is replicated perfectly by the predicted scaling relations as the calcium abundance is constrained directly from that index. With the Nelan data, the CaII-sigma relation predicted with the calcium abundance constrained from the Ca4227 index successfully reproduces the observed CaII-sigma relation. For the two sets of Smith data (2007 & 2009), the predicted CaII-sigma relations are reproducible with 2.4 and 1.2σ confidence respectively.

The sodium-index scaling relations predicted using the Ca4227 constrained calcium abundance do not reproduce the observed scaling relation. This is not surprising considering the fact that the sodium abundance has a considerable effect on the sodium-sigma scaling relations, and this is yet to be taken into consideration in this section.

3.6.2 The change in [Na/Fe] with increasing velocity dispersion

The same procedure can be carried out to find a value for the change in sodium abundance with velocity dispersion. This is done using the Na5895 index as the sodium abundance indicator, and taking the difference between the observed and age, α- and Fe- abundance constrained scaling relations for the Na5895 index. The differences (according to the different literature scaling relations) are then divided by the response of the Na5895 index to the sodium abundance (from the models) to find the [Na/Fe]-sigma scaling relation.

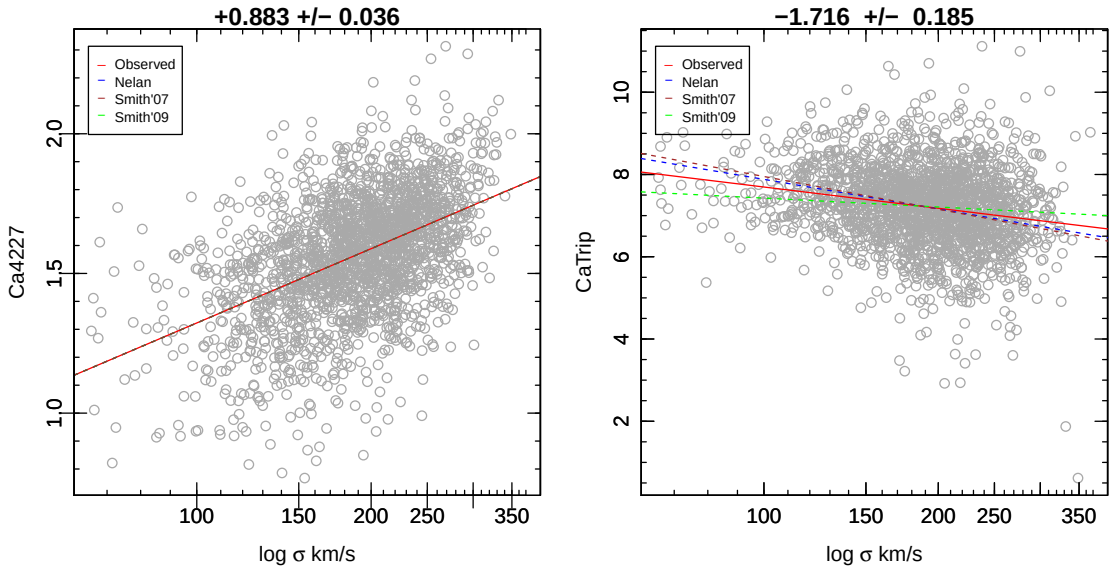

Figure 3.15: Predicted index-sigma relations for the calcium indices (dashed lines) using [Ca/Fe] constraints from the Ca4227 index. Blue = Nelan 2005, brown = Smith 2009 and green = Smith 2007 data. The solid red line represents a linear fit to the data. Panel (a) shows the predicted Ca4227-sigma scaling relations; the observed Ca4227-sigma scaling relation is replicated as the [Ca/Fe] was constrained from this index. Panel (b) shows the predicted CaII-sigma scaling relations (dashed lines), the predicted slopes with Nelan data reproduces the observed slope, the two Smith (2007 & 2009) scaling relations reproduce the observed index-sigma relation with 2.4 and 1.2σ confidence respectively.

$$[\mathrm{Na/Fe}] \propto \sigma^{1.654\pm0.050} \text{ (with scaling relations from Nelan et al. (2005))}$$
$$\sigma^{1.686\pm0.035} \text{ (with scaling relations from Smith et al. (2007))}$$
$$\sigma^{1.647\pm0.047} \text{ (with scaling relations from Smith et al. (2009))}$$

A particular Na5895-predicted [Na/Fe]-sigma scaling relation can then be combined with the response of the NaI index to sodium abundance (from the models) and added to the equation for the predicted NaI-sigma scaling relation :

$$\frac{d\,\mathrm{NaI}}{d\log\sigma} = \frac{d\log\mathrm{age}}{d\log\sigma}\cdot\frac{d\,\mathrm{NaI}}{d\log\mathrm{age}} + \frac{d\,[\mathrm{Fe/H}]}{d\log\sigma}\cdot\frac{d\,\mathrm{NaI}}{d\,[\mathrm{Fe/H}]} + \frac{d[\alpha/\mathrm{Fe}]}{d\log\sigma}\cdot\frac{d\,\mathrm{NaI}}{d[\alpha/\mathrm{Fe}]} + \frac{d\,[\mathrm{Na/Fe}]}{d\log\sigma}\cdot\frac{d\,\mathrm{NaI}}{d\,[\mathrm{Na/Fe}]}$$

Figure 3.16 shows the predicted index-sigma slopes for the Na5895 and NaI082 indices in relation to the observed scaling relations. As expected the predicted Na5895-sigma scaling relations are perfectly reproduced (as the sodium abundance is constrained from the Na5895 index). The predicted NaI082-sigma slopes are slightly shallower than the observed scaling relation, however, all three of the predicted scaling relations reproduce the observed slope. This is not a surprising result considering the sodium abundance has such a strong contribution to the sodium index-sigma relations.

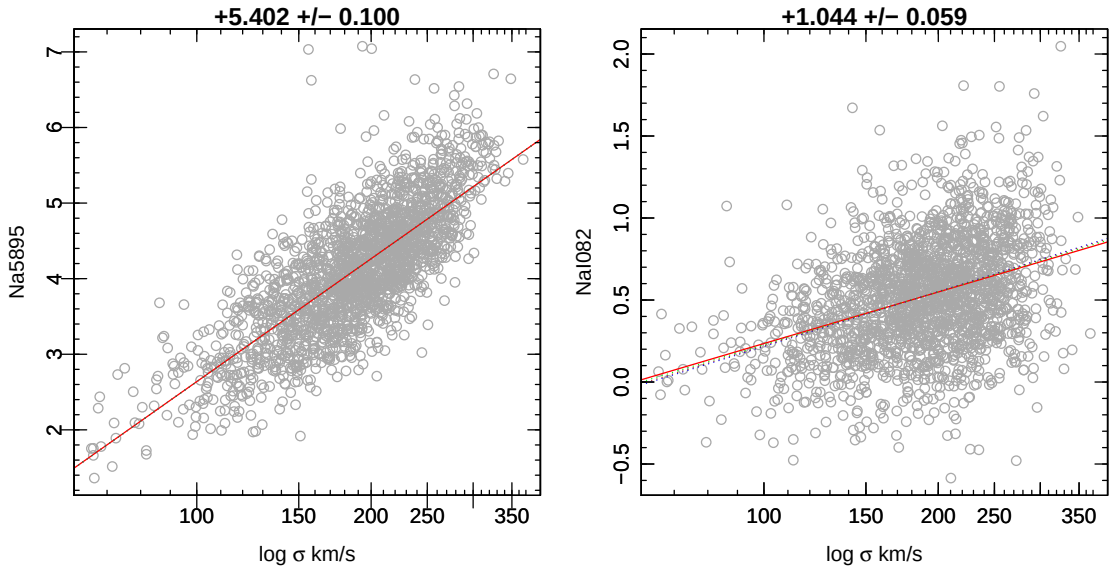

Figure 3.16: Predicted index-sigma relations for the sodium indices (dashed lines) using [Na/Fe] constraints from the Na5895 index. Blue = Nelan 2005, brown = Smith 2009 and green = Smith 2007 data. The solid red line represents a linear fit to the data. Panel (a) shows the predicted NaD-sigma scaling relations, the observed NaD scaling relation is replicated as [Na/Fe] was constrained from this index. Panel (b) shows the predicted NaI-sigma scaling relations (dashed lines) which produce the observed NaI-sigma scaling relation well.

It is not possible to reproduce the two calcium indices with sodium abundance alone; again this is not surprising considering the calcium abundance has been neglected here.

3.6.3 The combined change in [Na/Fe] and [Ca/Fe] with increasing velocity dispersion

In order to consider a more realistic representation of a galaxy population both the sodium and the calcium abundances, predicted from Na5895 and Ca4227 indices respectively, are now considered together. It is important to look at the effects of combining both abundance constraints on both indices to see whether the abundance of one element affects the index-sigma slope of the characteristic features of the other element. This analysis is achieved by adding the previously constrained calcium and sodium abundance variations with velocity dispersion, along with their corresponding response to abundance variation from the models, to equation that predicts the index-sigma relation (see Equation 3.4). This gives another set of predicted index-sigma relations for the calcium triplet and sodium doublet which are shown in Figure 3.17 (and in Table 3.4).

The predicted index-sigma slopes reproduce the observed slopes within the error margins for both the sodium indices and Ca4227. From Figure 3.17 it is clear that the most poorly reproduced index-sigma scaling relation is that of the calcium triplet. For the calcium triplet only the scaling relation predicted using the Smith et al. (2009) data replicates the slope within the error margins, for the scaling relations predicted with the Nelan et al. (2005) and Smith et al. (2007) data, they are only consistent to within 1.5 and 3.8σ respectively. The remaining

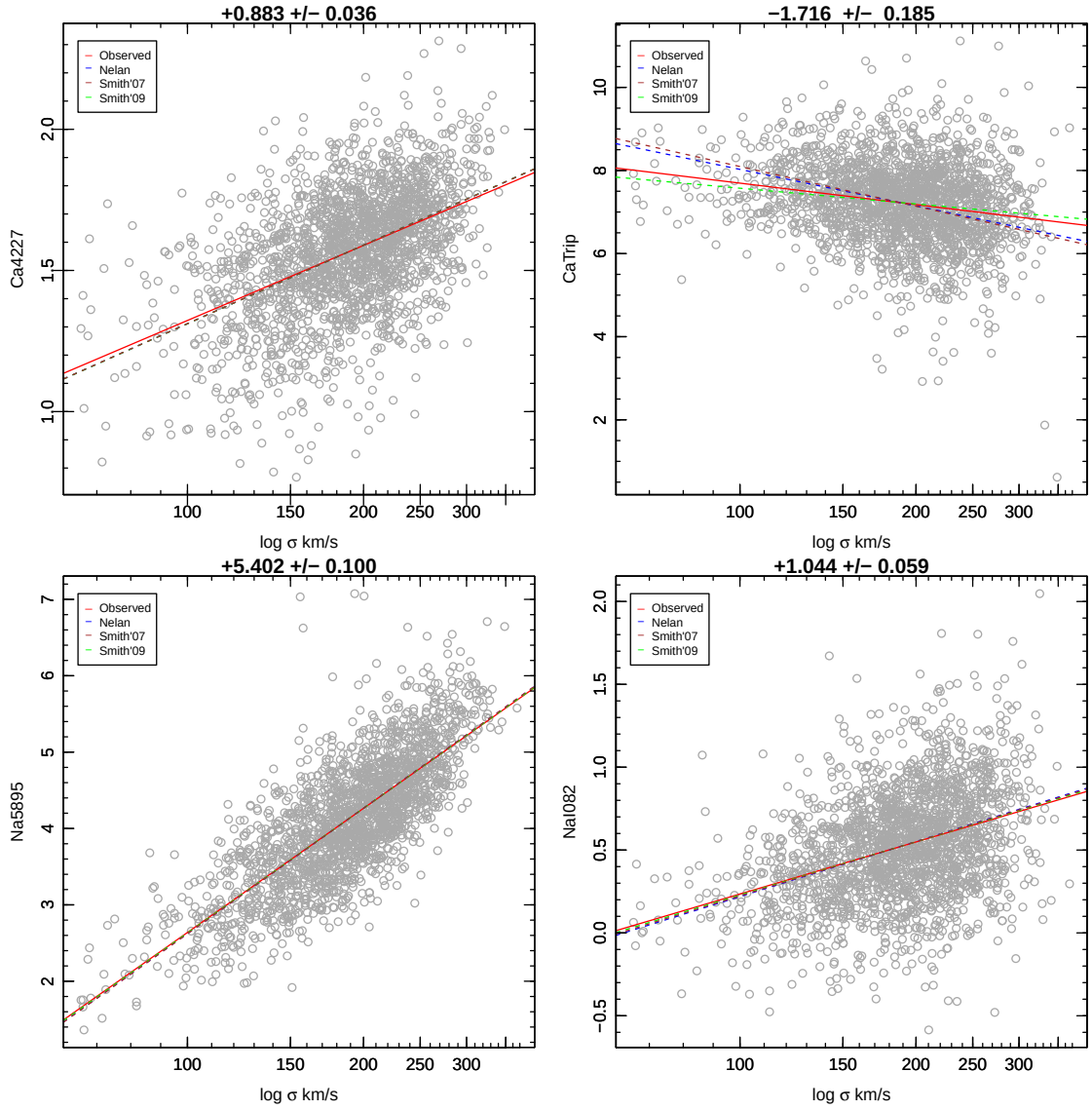

Figure 3.17: Predicted index-sigma relations using combined [Na/Fe] and [Ca/Fe] constraints (dashed lines), along with literature scaling relations and model responses for age, Fe- and α-abundance. Blue lines are constrained with Nelan data, brown with Smith'09 and green with Smith'07. Index-sigma relations for Na5895, NaI082 and Ca4227 are reproduced within the errors and for the calcium triplet the Smith'09 data reproduces the slope whilst Nelan'05 and Smith'07 data reproduce the slope with 1.5 and 3.8σ confidence respectively.

deviation between the predicted and observed scaling relations is now attributed to the IMF variation.

3.6.4 The change in IMF with increasing velocity dispersion

In the following section, the remaining deviations between the predicted and observed index-sigma relations are interpreted as IMF variation, with the assumption that there are no other contributing factors. The IMF variation can be investigated by looking at the indices that are most sensitive to changes in the IMF; from Figure 3.12 it is evident that the calcium triplet and NaI doublet are two of the most sensitive features to IMF variation. For reasons previously discussed the TiO2 index is not used in this study.

With a similar method to constraining the sodium and calcium abundance from the data, the IMF contribution is taken as the difference between the observed slope and the sodium or calcium constrained slope (depending on which index is used). This is then divided by the IMF response of that index (from the models) to get the change in IMF with velocity dispersion. This factor is then added to the index-sigma equation :

$$\frac{d\,\mathrm{I}}{d\log\sigma} = \frac{d\log\mathrm{age}}{d\log\sigma}\cdot\frac{d\,\mathrm{I}}{d\log\mathrm{age}} + \frac{d\,[\mathrm{Fe/H}]}{d\log\sigma}\cdot\frac{d\,\mathrm{I}}{d\,[\mathrm{Fe/H}]} + \frac{d[\alpha\,/\mathrm{Fe}]}{d\log\sigma}\cdot\frac{d\,\mathrm{I}}{d[\alpha\,/\mathrm{Fe}]} + \frac{d\,[\mathrm{e/Fe}]}{d\log\sigma}\cdot\frac{d\,\mathrm{I}}{d\,[\mathrm{e/Fe}]} + \frac{d\,\mathrm{IMF}}{d\log\sigma}\cdot\frac{d\,\mathrm{I}}{d\,\mathrm{IMF}}$$

where I is the IMF characteristic index (NaI or CaII) and e in [e/Fe] is the corresponding abundance for the given IMF characteristic feature.

The IMF variation can be described in the form of $\Delta x = \mu.\Delta\log\sigma$ where μ is the IMF scaling relation. With this notation, the results with different published scaling relations are :

$$\begin{aligned}\mu^{\mathrm{NaI}} = &-0.126 \pm 0.071 \text{ (with scaling relations from Nelan et al. (2005))}\\ &-0.053 \pm 0.119 \text{ (with scaling relations from Smith et al. (2007))}\\ &-0.097 \pm 0.069 \text{ (with scaling relations from Smith et al. (2009))}\end{aligned}$$

As the IMF variation for sodium is constrained from the NaI index, the NaI-sigma slope is reproduced exactly with each of the literature scaling relations (see panels (a) and (b) in Figure 3.18). Adding the IMF variation found from the NaI082 index along with the Na5895 index response to IMF from the models, to the predicted slope using the sodium abundance (and age, α- and Fe- constraints) the Na5895-σ slope can also be reproduced (see Figure 3.18). Unsurprisingly, the observed slopes of the calcium indices are not reproduced by predicting the slope

PREDICTED INDEX-SIGMA SLOPES WITH ERRORS
ACCORDING TO NELAN α, FE, NA, CA, IMF AND AGE CONSTRAINTS

Index	Origin	observed index-sigma slope	slope1 = α, age and Fe constrained	slope1 + [Ca/Fe]	slope1 + [Na/Fe]	slope1 + [Ca/Fe] + [Na/Fe]	slope1+ [Ca/Fe] + IMF	slope1 + [Na/Fe] + IMF	slope1 + [Na/Fe] + [Ca/Fe] + IMF (from CaTrip)	slope1 + [Na/Fe] + [Ca/Fe] + IMF (from NaI)
CaTrip	N05	-1.716±+0.185	+1.457±0.359	-2.391±0.619	+0.926±0.355	-2.921±0.614	-1.716±0.340	+1.067±0.189	-1.716±0.189	-2.797±0.602
	S07		+1.875±0.118	-2.645±0.202	+1.347±0.117	-3.174±0.202	-1.716±0.167	+1.456±0.183	-1.716±0.183	-3.084±0.244
	S09		+0.936±0.409	-0.716±0.638	+0.395±0.404	-1.257±0.636	-1.716±0.384	+0.454±0.185	-1.716±0.185	-1.205±0.638
Ca4227	N05	+0.883±+0.036	+2.228±0.309	+0.883±0.022	+2.269±0.309	+0.924±0.022	+0.832±0.309	+2.258±0.055	+0.834±0.055	+0.915±0.023
	S07		+2.463±0.097	+0.883±0.037	+2.504±0.097	+0.924±0.037	+0.813±0.098	+2.496±0.048	+0.815±0.048	+0.917±0.038
	S09		+1.461±0.344	+0.883±0.022	+1.503±0.344	+0.925±0.022	+0.958±0.345	+1.498±0.056	+0.960±0.056	+0.921±0.023
Na5895	N05	+5.402±+0.100	+0.331±0.144	+0.383±0.146	+5.402±0.051	+5.454±0.053	+0.222±0.052	+5.368±0.167	+5.166±0.152	+5.424±0.053
	S07		+0.352±0.033	+0.413±0.033	+5.402±0.101	+5.463±0.101	+0.191±0.096	+5.376±0.071	+5.115±0.117	+5.442±0.096
	S09		+0.233±0.136	+0.256±0.136	+5.402±0.053	+5.424±0.055	+0.495±0.052	+5.388±0.182	+5.534±0.154	+5.412±0.055
NaI082	N05	+1.044±+0.059	+0.186±0.065	+0.179±0.065	+1.111±0.041	+1.103±0.041	-0.141±0.033	+1.044±0.412	+0.532±0.415	+1.044±0.033
	S07		+0.175±0.015	+0.166±0.015	+1.096±0.021	+1.087±0.021	-0.275±0.060	+1.044±0.132	+0.396±0.133	+1.044±0.060
	S09		+0.130±0.061	+0.126±0.062	+1.072±0.039	+1.069±0.039	+0.600±0.033	+1.044±0.436	+1.286±0.436	+1.044±0.033
Mgb5177	N05	+3.489±+0.064	+2.332±0.371	+2.335±0.372	+2.064±0.373	+2.067±0.373	+2.248±0.372	+2.046±0.305	+1.912±0.306	+2.051±0.373
	S07		+2.717±0.117	+2.720±0.117	+2.450±0.117	+2.453±0.117	+2.601±0.119	+2.436±0.100	+2.266±0.100	+2.442±0.119
	S09		+1.528±0.413	+1.529±0.413	+1.255±0.413	+1.256±0.413	+1.658±0.414	+1.247±0.340	+1.315±0.339	+1.249±0.415
Fe5270	N05	+0.789±+0.044	+1.267±0.297	+1.065±0.299	+1.198±0.298	+0.996±0.300	+1.079±0.299	+1.201±0.301	+1.020±0.302	+0.998±0.300
	S07		+0.923±0.066	+0.685±0.071	+0.853±0.066	+0.616±0.071	+0.703±0.067	+0.856±0.070	+0.645±0.070	+0.618±0.071
	S09		+0.853±0.242	+0.766±0.254	+0.782±0.243	+0.696±0.255	+0.747±0.244	+0.784±0.253	+0.687±0.254	+0.697±0.256
Fe5335	N05	+0.683±+0.061	+0.985±0.266	+0.975±0.266	+0.887±0.268	+0.878±0.268	+1.008±0.270	+0.894±0.276	+0.936±0.277	+0.884±0.270
	S07		+0.670±0.061	+0.658±0.061	+0.573±0.062	+0.561±0.062	+0.703±0.063	+0.578±0.062	+0.632±0.062	+0.566±0.063
	S09		+0.667±0.224	+0.663±0.224	+0.567±0.225	+0.563±0.226	+0.615±0.228	+0.570±0.227	+0.541±0.228	+0.566±0.228
Fe5406	N05	+0.518±+0.041	+0.721±0.223	+0.738±0.223	+0.651±0.224	+0.668±0.224	+0.757±0.225	+0.655±0.228	+0.704±0.229	+0.672±0.225
	S07		+0.448±0.053	+0.468±0.052	+0.378±0.053	+0.398±0.053	+0.495±0.054	+0.382±0.052	+0.441±0.052	+0.401±0.053
	S09		+0.490±0.191	+0.498±0.190	+0.419±0.192	+0.427±0.191	+0.468±0.194	+0.421±0.191	+0.413±0.191	+0.428±0.193
Hbeta	N05	-1.494±+0.068	-0.791±0.174	-0.777±0.172	-0.779±0.174	-0.766±0.173	-0.764±0.174	-0.776±0.164	-0.741±0.165	-0.763±0.172
	S07		-0.932±0.039	-0.916±0.038	-0.921±0.039	-0.905±0.039	-0.897±0.039	-0.918±0.036	-0.875±0.037	-0.903±0.038
	S09		-0.532±0.160	-0.527±0.158	-0.521±0.160	-0.515±0.158	-0.547±0.159	-0.519±0.149	-0.524±0.150	-0.514±0.157
HdF	N05	-1.597±+0.078	-1.926±0.428	-2.031±0.433	-1.902±0.428	-2.007±0.433	-2.040±0.429	-1.904±0.437	-2.025±0.438	-2.009±0.434
	S07		-1.661±0.096	-1.784±0.095	-1.638±0.096	-1.761±0.096	-1.798±0.096	-1.640±0.096	-1.782±0.096	-1.763±0.096
	S09		-1.308±0.379	-1.353±0.380	-1.285±0.380	-1.330±0.381	-1.339±0.381	-1.285±0.383	-1.323±0.383	-1.330±0.381
HgF	N05	-2.681±+0.104	-2.574±0.429	-2.508±0.421	-2.484±0.431	-2.419±0.423	-2.490±0.430	-2.481±0.409	-2.386±0.412	-2.416±0.422
	S07		-2.726±0.103	-2.649±0.101	-2.637±0.103	-2.560±0.101	-2.623±0.103	-2.634±0.098	-2.520±0.099	-2.558±0.101
	S09		-1.734±0.390	-1.706±0.382	-1.643±0.392	-1.615±0.384	-1.733±0.391	-1.641±0.371	-1.627±0.374	-1.613±0.383
TiO1	N05	+0.023±+0.001	+0.012±0.002	+0.014±0.002	+0.010±0.002	+0.012±0.002	+0.010±0.002	+0.010±0.002	+0.005±0.002	+0.011±0.002
	S07		+0.013±0.001	+0.015±0.001	+0.011±0.001	+0.013±0.001	+0.010±0.001	+0.011±0.001	+0.005±0.001	+0.013±0.001
	S09		+0.008±0.002	+0.008±0.002	+0.006±0.002	+0.007±0.002	+0.014±0.002	+0.006±0.002	+0.009±0.002	+0.007±0.002
TiO2	N05	+0.052±+0.001	+0.019±0.002	+0.022±0.003	+0.015±0.003	+0.019±0.003	+0.013±0.003	+0.013±0.006	+0.003±0.006	+0.017±0.003
	S07		+0.020±0.001	+0.024±0.001	+0.017±0.001	+0.021±0.001	+0.012±0.002	+0.015±0.003	+0.002±0.003	+0.020±0.002
	S09		+0.012±0.003	+0.014±0.004	+0.009±0.003	+0.010±0.004	+0.027±0.003	+0.008±0.006	+0.016±0.006	+0.010±0.004
CN2	N05	+0.219±+0.005	+0.035±0.012	+0.047±0.013	+0.023±0.012	+0.036±0.013	+0.051±0.013	+0.024±0.016	+0.043±0.016	+0.036±0.014
	S07		+0.040±0.003	+0.054±0.003	+0.028±0.003	+0.042±0.003	+0.060±0.003	+0.029±0.004	+0.051±0.004	+0.043±0.003
	S09		+0.024±0.011	+0.029±0.012	+0.012±0.011	+0.018±0.012	+0.023±0.012	+0.013±0.014	+0.015±0.015	+0.018±0.012
C4668	N05	+4.278±+0.139	+1.397±0.258	+1.348±0.253	+1.142±0.264	+1.094±0.259	+1.369±0.266	+1.146±0.265	+1.130±0.271	+1.097±0.261
	S07		+1.406±0.055	+1.349±0.054	+1.152±0.057	+1.096±0.056	+1.377±0.058	+1.155±0.057	+1.140±0.059	+1.098±0.057
	S09		+0.942±0.231	+0.922±0.227	+0.683±0.237	+0.662±0.233	+0.891±0.239	+0.685±0.238	+0.648±0.244	+0.664±0.235

Table 3.4: Table of constrained slopes with errors. Slope 1 is constrained using literature age, Fe- and α-abundance scaling relations combined with model responses. [Ca/Fe], [Na/Fe] and IMF scaling relations are constrained from Ca4227, NaD and CaII and NaI respectively. See text for more detailed discussion.

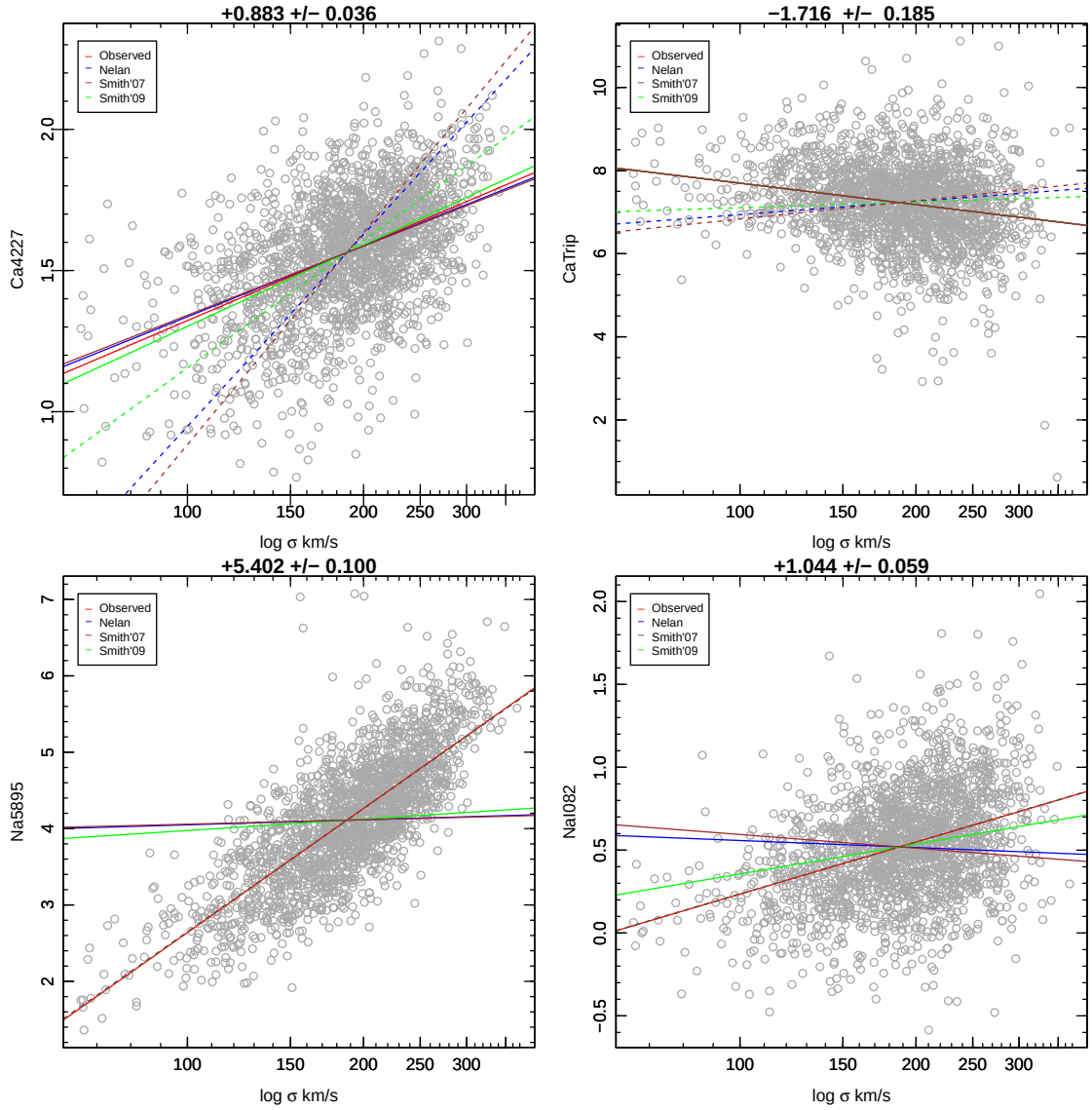

Figure 3.18: Predicted index-sigma slopes for the calcium and sodium indices. The solid lines are predicted slopes according to the calcium abundance (from Ca4227) and the IMF (from CaII). The dashed lines are predicted slopes according to the sodium abundance (from Na5895) and the IMF (from NaI082). The blue lines are Nelan'05 data, brown lines are Smith'07 data and green lines are Smith'09 data. The NaI082 and CaII slopes are constrained directly so are perfectly replicated. The Na5895 index is reproduced by the NaI082 constrained slope but not by the CaII slope. The converse is true for the Ca4227 index which is reproduced by the CaII constrained slope and not by the NaI constrained slope.

using the sodium abundance and IMF from sodium indices.

The predicted IMF-sigma scaling relations are shallower for higher mass galaxies which suggests that as galaxies get more massive, they have fractionally lower quantities of dwarf stars than that of lower mass galaxies. This result is not in agreement with Ferreras et al. (2012) who find the IMF scaling relation steepens for more massive galaxies. This is an interesting result and will be discussed in Section 4.

The process is repeated for the calcium triplet; the difference between the predicted and observed index-sigma scaling relation for the calcium triplet feature gives an IMF variation of :

$$\begin{aligned}\mu^{\mathrm{CaII}} = &-0.602 \pm 0.578 \text{ (with scaling relations from Nelan et al. (2005))} \\ &+0.893 \pm 0.247 \text{ (with scaling relations from Smith et al. (2007))} \\ &-0.830 \pm 0.593 \text{ (with scaling relations from Smith et al. (2009))}\end{aligned}$$

It is interesting to note that the IMF scaling relation predicted by the CaII index is also shallower at greater masses for the Nelan and Smith 2009 data. The IMF scaling relation is combined with the model index response to IMF variation and added to the index-sigma equation, along with the abundance and literature constraints. The predicted calcium index-sigma scaling relations are shown in Figure 3.18.

The observed slope of the CaII-sigma relation is reproduced perfectly as the IMF variation was constrained directly from this index. The Ca4227 index is also reproduced well by the calcium abundance and IMF predicted index-sigma slope, whilst the observed slopes of the sodium indices cannot be reproduced using just calcium abundance and IMF variations.

The variation of the IMF in a real galaxy sample is subject to both the calcium and the sodium abundance. For this reason, and to investigate the effect of the different abundances on the predicted IMF variation, the factors for the both the sodium and calcium abundances are now combined in the equation for the index-sigma scaling relation :

$$\begin{aligned}\frac{d\,\mathrm{I}}{d\log\sigma} = &\frac{d\log\mathrm{age}}{d\log\sigma}\cdot\frac{d\,\mathrm{I}}{d\log\mathrm{age}} + \frac{d\,[\mathrm{Fe/H}]}{d\log\sigma}\cdot\frac{d\,\mathrm{I}}{d\,[\mathrm{Fe/H}]} + \frac{d[\alpha/\mathrm{Fe}]}{d\log\sigma}\cdot\frac{d\,\mathrm{I}}{d[\alpha/\mathrm{Fe}]} \\ &+ \frac{d\,[\mathrm{Na/Fe}]}{d\log\sigma}\cdot\frac{d\,\mathrm{I}}{d\,[\mathrm{Na/Fe}]} \\ &+ \frac{d\,[\mathrm{Ca/Fe}]}{d\log\sigma}\cdot\frac{d\,\mathrm{I}}{d\,[\mathrm{Ca/Fe}]} \\ &+ \frac{d\,\mathrm{IMF}}{d\log\sigma}\cdot\frac{d\,\mathrm{I}}{d\,\mathrm{IMF}}\end{aligned}$$

The difference between the "double abundance"predicted index-sigma relation

and the observed scaling relation for both of IMF sensitive features in turn is interpreted as the IMF variation (shown in violet), with the following results :

$$\mu^{\mathrm{NaI}} = -0.111 \pm 0.071 \text{ (with scaling relations from Nelan et al. (2005))}$$
$$-0.047 \pm 0.119 \text{ (with scaling relations from Smith et al. (2007))}$$
$$-0.081 \pm 0.069 \text{ (with scaling relations from Smith et al. (2009))}$$

$$\mu^{\mathrm{CaII}} = -1.076 \pm 0.574 \text{ (with scaling relations from Nelan et al. (2005))}$$
$$+0.409 \pm 0.247 \text{ (with scaling relations from Smith et al. (2007))}$$
$$-1.302 \pm 0.591 \text{ (with scaling relations from Smith et al. (2009))}$$

With these variations added to the index-sigma equation, along with the calcium and sodium abundance constraints, the index-sigma relations for the two sodium and two calcium indices are well reproduced. The observed NaI-sigma scaling relations are perfectly reproduced using the NaI (as expected) and well reproduced from the CaII index, with the exception of the Smith 2007 data relation which is still consistent within $\sim 3\sigma$. The observed Na5895-sigma scaling relation is well reproduced by both the NaI and CaII predicted scaling relations; this is presumably because the sodium abundance has been taken into consideration which has been shown to have the greatest contribution to the NaD-sigma relation. The observed Ca4227-sigma scaling relation is well reproduced by both the NaI and CaII predicted relations. The observed CaII-sigma scaling relation is perfectly reproduced by the CaII predicted scaling relations (as expected) and for the scaling relations predicted from the NaI index, the Nelan, Smith 2007 and Smith 2009 values are consistent to within 1.4, 3.1 and 0.6σ respectively.

A summary of the results found in this section are shown in Table 3.5.

VARIATION OF IMF, [CA/FE] AND [NA/FE] WITH LOG σ

Variation with σ (μ)[1]	Nelan	Smith 07	Smith 09
[Na/Fe]	$+1.654 \pm 0.050$	$+1.686 \pm 0.035$	$+1.647 \pm 0.047$
[Ca/Fe]	-0.19 ± 0.12	-0.02 ± 0.04	-0.23 ± 0.13
μ^{NaI} (with [Na/Fe])	-0.126 ± 0.071	-0.053 ± 0.119	-0.097 ± 0.069
μ^{CaII} (with [Ca/Fe])	-0.602 ± 0.578	$+0.893 \pm 0.247$	-0.830 ± 0.593
μ^{NaI} (with [Ca/Fe] & [Na/Fe])	-0.111 ± 0.071	-0.047 ± 0.119	-0.081 ± 0.069
μ^{CaII} (with [Ca/Fe] & [Na/Fe])	-1.076 ± 0.574	$+0.409 \pm 0.247$	-1.302 ± 0.591

[1] where $\Delta x = \mu\ \Delta \log\sigma$ (and x is $\xi(m) \propto m^x$)

Table 3.5: Results from index-sigma analysis; the variation of [Ca/Fe], [Na/Fe] and IMF with velocity dispersion. Columns Two - Four show predicted values using parameters constrained by Nelan et al. (2005), Smith et al. (2007) and Smith et al. (2009) respectively. The four separate IMF variation values are constrained from lines predicted with different parameters; with [Na/Fe], with [Ca/Fe] and with both abundances (constrained separately from CaII and NaI082).

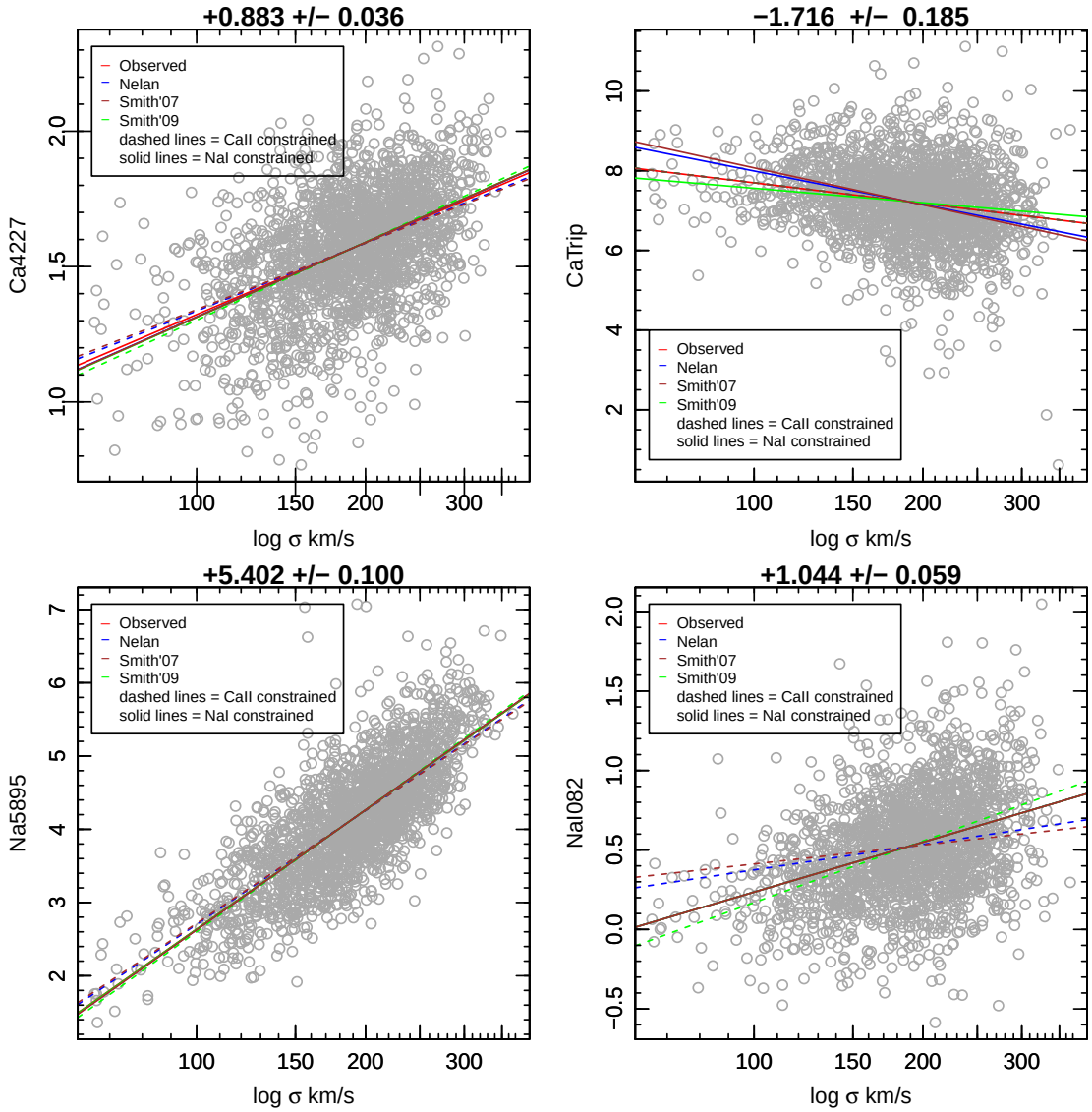

Figure 3.19: Predicted index-sigma relations with calcium and sodium abundances considered and constraining the IMF variation from the CaII and NaI indices. The solid lines represent NaI predicted scaling relations, dashed lines are from CaII. The blue slopes are constrained with Nelan data, green with Smith 2007 and brown with Smith 2009 data. The predicted scaling relations from the CaII index predict the calcium-sigma relations very well, also reproducing the sodium indices within the error margins with the exception of the NaI-sigma relation with Smith 2007 data which is within $\sim 3\sigma$ confidence. For the NaI predicted slopes, again, the sodium index-sigma relations are well reproduced, as are those for the Ca4227 index. The calcium-sigma slopes for Nelan, Smith 2007 and Smith 2009 data are consistent within 1.4, 3.1 and 0.6σ respectively.

Chapter 4

Discussion

The following section is split into two halves. The first half will discuss and reiterate the various caveats, assumptions and limitations associated with this work. The second half will then continue to discuss the results found in Section 4 and compare these results to those found in similar studies.

4.1 Caveats, Assumptions and Limitations

The results found in this piece of work are subject to certain assumptions and limitations. It is important to briefly discuss these factors in order to consider the reliability of the values in Table 3.5.

The basis of the investigation is that there are certain features that are characteristic of specific parameters (such as abundance or IMF), and once basic considerations of galaxy environment have been adopted, the remaining variation of the characteristic index with velocity dispersion is due to that specific parameter. With the effect of velocity dispersion broadening corrected for, it is assumed that the variation in size of the equivalent width of the calcium triplet, for example, is wholly attributable to five factors; age, [α/Fe], [Fe/H], [Ca/Fe] and the IMF (with the Ca4227 index being constructed of just the first four). It is important to bear in mind it may be the case that other factors that are not considered in this piece of work have an effect on the size of the spectral feature, the broad assumption is made that if there are contributory factors then they do not have a significant effect on the results of this work.

It is apparent from Figure 3.12 that the abundance-sensitive features are also sensitive to the IMF to a certain extent, however, in this work the assumption is made that the abundance variation is taken as the difference between the age, [α/Fe] and [Fe/H] scaling relation and the observed slope (without the effect of the IMF being considered).

In addition to this major assumption, the other considerations are; the assumptions made when making linear fits to observational and model data, the models themselves, the data used in this work and the effect of sample selection on comparing results from other studies.

4.1.1 Fitting and model assumptions

In this piece of work a large proportion of the results depend upon the interpretation of linear fits to the observational and model data. For the study of the scaling relation between measured equivalent widths for certain indices and the SDSS measured velocity dispersion, linear fits are made to the observational data and the success of the replication of these observed slope by literature and model predicted slopes is often reliant on the errors of the linear fit and errors calculated by random Gaussian selection (see Section 2.4.1). Whilst the systematic errors on the linear fits are taken into consideration, the individual errors on each measured data point are neglected and it is assumed that they are equivalent to the intrinsic scatter. It is possible to account for these errors individually by giving the data points a weighting according to their `indexf` errors (from SDSS error spectra), however, this investigation remains for further study.

There is also a strong reliance on linear fits for the interpretation of the information from the models. It has been assumed that the responses shown by the models for various parameters are linear and can be described by a linear fit to the data. This is not the case in reality, as Conroy & van Dokkum (2012b) state, the variation of spectral features with a given abundance variation is not linear over a wide range of abundances. For most of the elemental abundances, the non-linearity of the index-abundance response is not important, because the range of abundance variation is so small (variations $\pm$0.3 dex for most elements). However, for the sodium abundance, Conroy & van Dokkum (2012b) found values of up to 1.0 dex for an individual galaxy. This greater variation shown by sodium means that the non-linearity of the response of the sodium-characteristic spectral features leads to errors when extrapolating the sodium abundance. Conroy & van Dokkum (2012b) have new stellar population models that account for the non-linear variation sodium abundance, and have abundances up to +1.0 dex. The difference they find between the new models and extrapolating from the old models is -0.2 dex for the most extreme cases; the new models are to be used in their future work.

Another caveat to be aware of is that some of the model responses are a linear fit from just two data points; this is the case for the response to the IMF and various abundances (see Figures 3.10 and 3.11), posing the question whether this is descriptive enough as an interpretation of the response of a given index to a certain parameter. Three of the five different IMFs used by Conroy & van Dokkum (2012a) to compile their models are easily described by a simple power-law index (Salpeter x = 2.35, x = 3.0 and bottom-heavy x = 3.5) with no breaks at certain masses (unimodal). The bottom-light and Chabrier IMFs have a bimodal description with a turnover at $\sim$2 and $\sim$0.08 $M_{\odot}$ respectively. This makes it more difficult to describe the IMF across the whole mass range with a single power-law index value in order to include it in the IMF response. For this reason, the IMF response from the models is constrained from the x = 3.0 and Salpeter IMFs, the x = 3.5

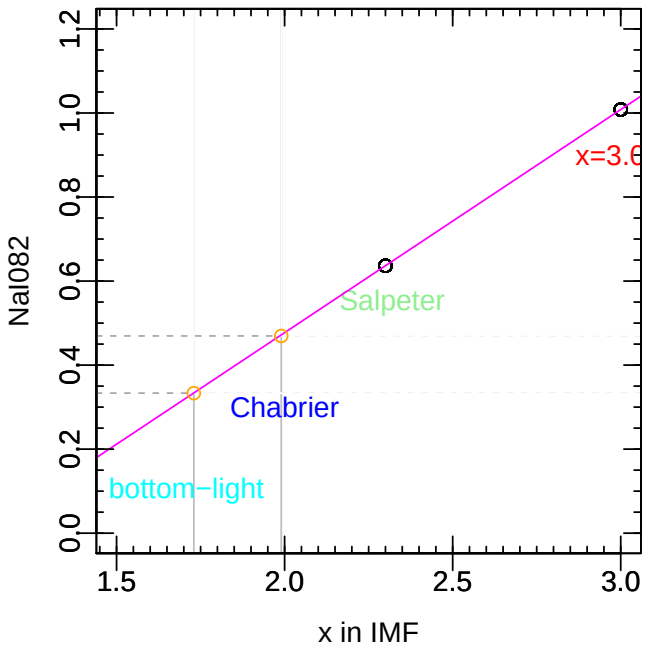

Figure 4.1: Predicted x values for Chabrier and bottom-light IMFs. The magenta line is the linear fit to the black points x = 3.0 and Salpeter points for the age = 13.5 Gyr, solar metallicity model (shown in Figure 3.11). The horizontal dashed grey lines represent the measured model equivalent width values for NaI082 and the representative power-law value in the IMF is extrapolated from the magenta linear fit. The values are x = 1.99 for the Chabrier IMF and x = 1.73 for the bottom-light IMF.

power-law point being removed from the relation due to its extreme equivalent width predictions making the slope a steeper gradient.

It is possible to extrapolate from the model IMF response, for a particular age, to find the 'equivalent' power-law index value for the Chabrier and bottom-light IMFs. This is done using the model predicted equivalent width value for a given index and finding the corresponding x value from the slope of the response.

For the NaI082 index, the extrapolated values (see Figure 4.1) are x = 1.99 for Chabrier IMF and x = 1.73 for bottom-light. Although this is a crude representation of the IMFs due to their log-normal behaviour at lower-masses, it is still a useful approximation for comparing the different IMFs used in this work.

4.1.2 Model selection

Of equal influence on the results are the responses from the model relations. The basis of the analysis of the observational data is to make comparisons with model spectra, this means that the model predictions are assumed to be accurate and representative of a given population. Any changes to the models will subsequently affect the predicted equivalent widths for certain features and therefore change the best-fitting metallicities, ages and IMFs.

The model responses are taken as the slope of the relation between a certain equivalent width and a particular parameter. From Figures 3.8, 3.9 and 3.11 it is apparent that for each parameter there are multiple responses according to dif-

ferent IMFs or ages. In this work, the response that is combined with literature scaling relations to predict an index-sigma scaling relation, is the slope for the Chabrier IMF or 13.5 Gyr age model (where appropriate). The assumption is made that the selection of a different response would not have a considerable effect on the final predicted index-sigma scaling relation. This is a reasonable assumption if the average error bars are considered (see Figures 3.8, 3.9 and 3.11), in most cases the average error bar is greater than the range covered by the various responses.

The responses and literature scaling relations are used to explore the abundance and IMF trends for the observational galaxies in this data sample by means of comparison between model and observed spectral features. However, if the equivalent width values predicted by the models are changed (by editing the nature of stellar evolutionary isochrones, or changing the treatment of a certain element in the calculations), this can have a fundamental effect on the results. An example of this is shown by comparing the current and preceding versions of the Conroy & van Dokkum models.

The preceding version of the Conroy & van Dokkum models, as shown in the `arXiv` pre-release of the Conroy & van Dokkum (2012a) paper (Conroy & van Dokkum (2011)), differs primarily, if not exclusively, in the predicted equivalent widths for the Ca4227 index. The difference between the two models is shown in Figure 4.2 where the current version of the models predicts almost identical values to the preceding model for the calcium triplet (the current models predicting values between 0.02 and 0.1 Å smaller than the preceding models). For the Ca4227 index, the predicted equivalent widths for the current models are between 0.3 and 0.4 Å greater than the preceding models. This is equal to $\sim$10% of the Ca4227 measured equivalent width, compared to the difference in the calcium triplet values being closer to $\sim$1% of the measured value.

This difference is interesting as it does not have an equal effect on the two calcium characteristic features. Whilst this difference could be attributed to a change in the treatment of calcium in the models (because the difference between the two model versions affects primarily the calcium sensitive feature), it is actually due to an improved technique in the model-creation process. There is a lack of information about stars on the red- and super-giant branches of the Hertzsprung-Russell diagram. This means that when a model population is formed, interpolation is required to predict the quantity of those giant stars in a given model population. In the most up-to-date models, the turnoff and subgiant stars undergo a more thorough treatment where they are interpolated from the MILES library rather than being taken as the star with the closest effective temperature to the IRTF star. This results in greater values for the predicted equivalent widths of Ca4227 (Conroy (private communication)).

With the analysis being reliant on the predicted values of the models, the change in size of these predicted equivalent widths (due to the improvement

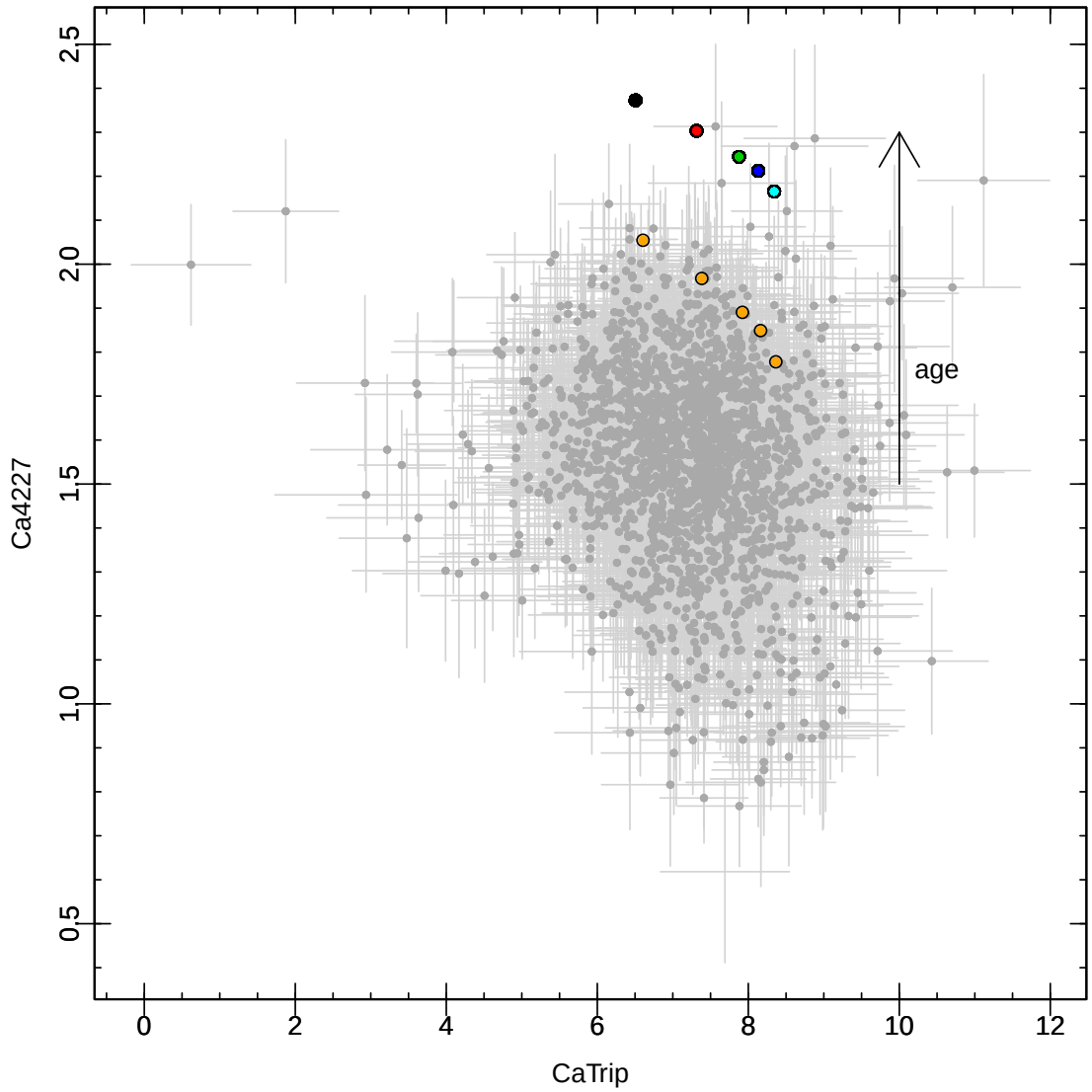

Figure 4.2: The difference between preceding and current Conroy models. Coloured points represent line strengths for calcium indices for current models of 13.5 Gyr, solar metallicity and various IMFs. The orange points below are the same points for the previous van Dokkum & Conroy models. The current models (various coloured points) are subject to an improved model-creation process (see text for details).

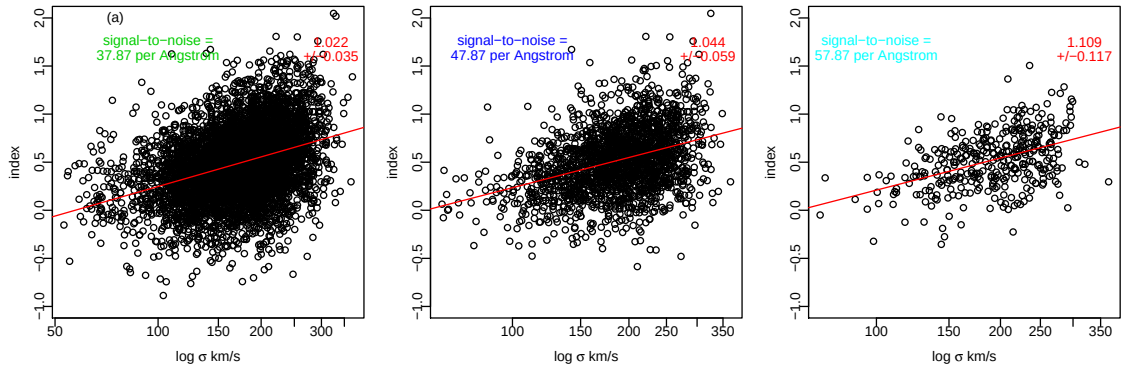

Figure 4.3: Signal-to-noise cut comparison for observational data for the NaI index. Despite the effect on the sample size (5890, 2024 and 367 galaxies for signal-to-noise $\approx$ 38, 48 and 58 Å^{-1}), the effect on the scaling relation is minimal and can be disregarded in comparison to the errors on the fits.

of the model-formation process) means the interpretation of the observational data is different to what it would have been with the preceding models. The calcium abundance is constrained from the Ca4227 index, so it is possible that with greater Ca4227 equivalent widths (than the preceding models) there could have been an effect on the resulting predicted calcium abundance. Conroy & van Dokkum (2012a) find good agreement between their current models and the stellar population models of other authors (Vazdekis et al. (2010), Schiavon (2007), Thomas et al. (2011)), this suggests that the models used in this work are good representations of observed stellar populations.

4.1.3 Data selection

For a large majority of the results in this piece of work, the final quoted scaling relations for abundance and IMF are dependent on the ability of the model responses and literature scaling relations to replicate the observed index-sigma slope. This observed slope is taken as a linear fit to the equivalent width measurement for each index against the SDSS measured velocity dispersion. When the galaxy sample was selected from SDSS data, a given signal-to-noise criterion was specified. A further signal-to-noise cut was introduced on visual inspection of the spread of data in order to create a cleaner galaxy sample (see Section 2). It is important to know what effect the signal-to-noise cut has on the data sample, and consequently whether it drastically changes the linear fit to the data. The higher signal-to-noise cut, theoretically, removes more of the outlier galaxies from the plot, but does this change the gradient of the linear fit to the data? If there is a great difference between the linear fits according to different signal-to-noise cuts then this will have a substantial impact on the trends taken from the linear relationship. The index-sigma relations for the NaI doublet are shown in Figure 4.3. The selection cut used in this piece of work ($\gtrsim$48 Å^{-1}) is shown in panel (b) whilst panels (a) and (c) show lower and higher signal-to-noise cuts (respectively).

There is a marked difference between the sample size for each of the signal-

Author	# of galaxies	Redshift range	Median velocity dispersion
Nelan et al. (2005)	4097	0.010<z <0.067	225
Graves et al. (2007)	∼6000	0.06<z <0.08	185
Smith et al. (2007)	∼500	z≈0.048	165
Smith et al. (2009)	232	z≈0.048	165
Johansson et al. (2012)	∼4000	0.05<z <0.10	215
Spiniello et al. (2012)	∼250	z≈0.1642	268
Jermak (this work)	2047	0.010<z <0.057	216

Table 4.1: Comparison of sample sizes and redshift and velocity dispersion ranges for a selection of similar studies. Nelan et al. (2005) have selection criteria that are closest in redshift and velocity dispersion range to the sample used in this work.

to-noise cuts, with 5890, 2024 and 367 galaxies for signal-to-noise $\approx$ 38, 48 and 58 Å^{-1} respectively. Whilst this change in adopted signal-to-noise cut has a significant effect on sample size, the effect on the slope of the linear fit to the data is not significant. The linear fits for the smallest and largest samples can be accounted for by the error margins on the sample with signal-to-noise of $\gtrsim$48 Å^{-1} (used in this work). This shows that the linear fit to the observational data is not substantially affected by the signal-to-noise limit of the galaxy sample.

4.1.4 Comparing Galaxy Samples

When comparing and contrasting results from different studies it is important to bear in mind the fact that whilst the type of galaxy in the sample may be equivalent (i.e. red sequence galaxies) the other properties of the sample may differ and therefore have an effect on the comparability of the different results. Table 4.1 shows the redshift and velocity dispersion values for this and other similar studies. It is apparent that the closest matched galaxy sample to the sample used in this work is that used by Nelan et al. (2005), the selection criteria used by Smith et al. (2007 & 2009) are similar to those used in this piece of work but the velocity dispersion range is <300 km s^{-1} meaning the greatest mass galaxies are not present in their sample. Spiniello et al. (2012) cover the higher end of the velocity dispersion range and study a sample of galaxies at greater redshift than the other samples. It is also important to bear in mind the selection criteria for the galaxies in the different samples; Nelan and Smith select red sequence galaxies according to low emission Balmer lines, whilst the galaxies in this piece of work are selected by morphological cuts (galaxies that are voted by GalaxyZoo users to be elliptical and therefore assumed to be red sequence galaxies) with a further cut according to Balmer lines. The two different selection methods may affect the different types of galaxies that go into the samples and subsequently have an effect on the resulting scaling relations.

It is also possible to compare the results from some recent studies by comparison of index-sigma scaling relations for common indices. In Figure 4.4 the index-sigma scaling relations for Nelan et al. (2005) and Smith et al. (2007) are plotted

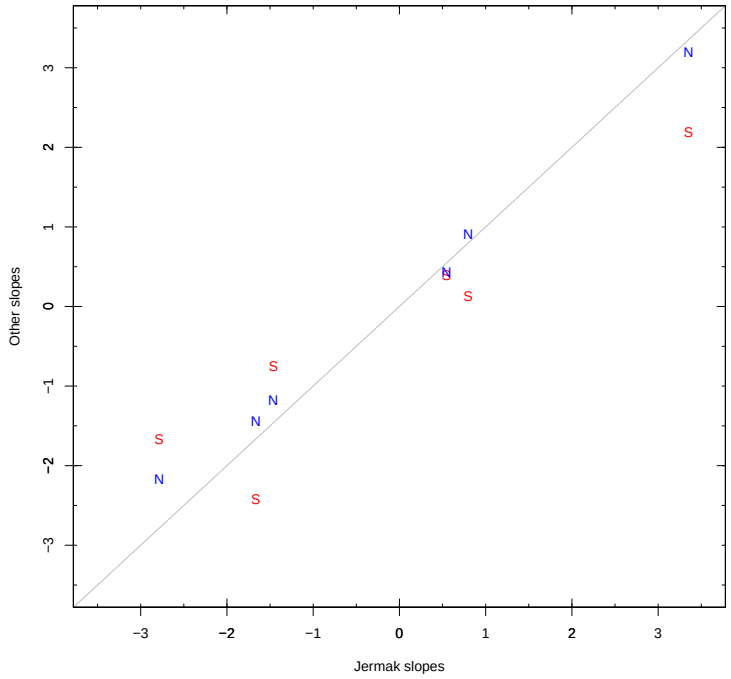

Figure 4.4: Comparison of index-sigma scaling relations for Smith et al. (2007), Nelan et al. (2005) and this work. Red 'S' for Smith data, blue 'N' for Nelan data. Grey line represents 1:1 ratio. The scaling relations found in this piece of work (Jermak slopes) are closer to the scaling relations found by Nelan et al. (2005) which is not surprising considering the Nelan data sample is most similar to the galaxy sample used in this piece of work.

against the scaling relations from this work (shown in Column Three of Table 3.4), this comparison clearly shows that the Nelan relations are a closer match to the relations found in this piece of work.

4.2 Interpretation of results

For the index-sigma scaling relation analysis there are three different sets of results for each parameter according to the origin of the scaling relations used to predict the slope. From comparisons between galaxy sample selection criteria and common index-sigma scaling relations for Nelan et al. (2005) and Smith et al. (2007), it is evident that the Nelan galaxy sample is more similar to the sample used in this piece of work and for that reason interpretation will be made with predicted slopes using the Nelan-scaling relations rather than the Smith-scaling relations.

4.2.1 Sodium Indices

The positive correlation between the NaI082 feature and velocity dispersion has been investigated by various recent studies including Conroy & van Dokkum (2012b), Spiniello et al. (2012) and Ferreras et al. (2012). In principle this increase in NaI line strength can be explained by either variations in [Na/Fe], IMF or a

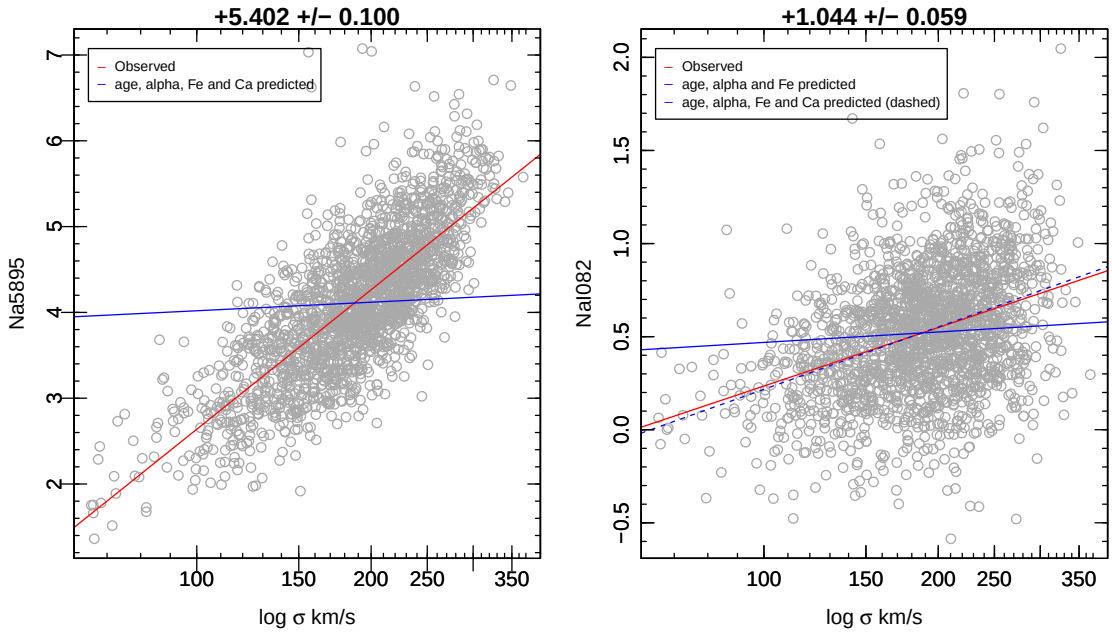

Figure 4.5: The predicted index-sigma slopes for both the sodium indices are practically flat when only age, α- and Fe- abundance are considered. When the sodium abundance is constrained from the Na5895 index, the index-sigma slope is reproduced to 0.7σ significance. This suggests that the effect of the IMF on the NaI082 index is minimal in comparison to the effect of the sodium abundance.

combination of both. In this study, the effect of both the IMF *and* [Na/Fe] variation have been considered with an interesting result. From the index-sigma analysis for the sodium indices it has been found that with the [Na/Fe] variation taken into consideration, the subsequent IMF variation is small with a slope that is shallower at higher masses and also consistent with zero. This suggests that there is no systematic correlation between the IMF and velocity dispersion. This result agrees with Smith et al. (2012), who find no clear evidence for an increase in dwarf-star content with velocity dispersion, and is contradictory to other studies that favour a steepening IMF with increasing velocity dispersion (Ferreras et al. (2012), Spiniello et al. (2012), Conroy & van Dokkum (2012b)).

Comparing the predicted index-sigma relations for the NaI082 index before and after the abundance is constrained from Na5895 (see Figure 4.5), shows just how influential the sodium abundance is. The predicted index-sigma scaling relations for both sodium indices are practically flat when only age, α- and Fe- abundances are considered, but with [Na/Fe] accounted for by the deviation from the Na5895 slope, the NaI082 scaling relation can be reproduced; without considering the effect of the IMF. This highlights just how little contribution is made by IMF variation to the NaI-sigma scaling relation compared to that of the sodium abundance variation. It is possible that if the sodium abundance is not taken into consideration, the remaining deviation of the NaI-sigma scaling relation can be interpreted as an increasing IMF-sigma variation.

There is a consideration to be made with regards to constraining the sodium abundance from the Na5895 spectral feature. It has been suggested that Na5895 is affected by absorption from interstellar dust lanes which can make it unreli-

able when using measured equivalent widths to constrain the sodium abundance (Spiniello et al. (2012)). The interstellar absorption at 5895 Å would result in an increase in the measured Na5895 index strength (Sparks et al. (1997)) and appear on the index-sigma plot as upwards scatter (because the interstellar dust associated with galaxies in the same velocity dispersion bin will vary stochastically). On independent grounds, it might be expected that the amount of interstellar material contributing to an increased Na5895 absorption feature should be less for galaxies with greater masses. This is because large galaxies tend to be ellipticals and have less interstellar medium than smaller galaxies. If the Na5895 feature is in fact affected by interstellar absorption, then the Na5895-sigma plot should show upward scatter at lower velocity dispersions which lessens with increasing velocity dispersions. This trend is not seen in the Na5895-sigma plot (see Figure 3.6) which has a considerably tight correlation.

Ferreras et al. (2012) find an IMF variation of μ = 3.8 which is significantly steeper than the results from this work, but as already mentioned, they do not take the [Na/Fe] into consideration. Theoretically, to find an IMF variation that is positive, the Na5895-sigma scaling relation would have to be shallower than what is observed (to find a smaller sodium abundance variation and therefore require an increasing IMF variation with sigma to account for the rest of the NaI082 trend). For the Na5895 interstellar absorption to be prominent, it would have to have the effect of steepening the Na5895-sigma slope as to cause an otherwise smaller sodium abundance to steepen. However, as argued above, the effect of Na5895 absorption is more likely to be a greater amount of upward scatter at lower velocity dispersions (more Na5895 interstellar absorption where there is more dust) and therefore cause the scaling relation to flatten. This would not reproduce the observed Na5895-sigma slope which is steeper than that required to predict an IMF variation that is positive. For this reason, the result from Ferreras et al. (2012) cannot be reconciled from the present work by allowing for the interstellar absorption of Na5895.

The sodium abundance variation from this piece of work cannot be directly compared to the results found by Conroy & van Dokkum (2012b), where for an individual galaxy (NGC 4261), which has a velocity dispersion of 229 km s^{-1}, they find a best-fitting sodium abundance value of $\sim$1.0 dex. Without knowing the best-fitting sodium abundance for a lower-velocity dispersion galaxy in their sample it is difficult to comment on whether the sodium abundance variation found in this sample is consistent, however, it is not inconceivable.

From a visual inspection of the first panel of Figure 5 in Conroy & van Dokkum (2012b), the IMF variation is $\mu \approx 1.8$, this is steeper than the IMF variation found in this study but shallower than the μ = 3.8 found by Ferreras et al. (2012). The technique used by Conroy & van Dokkum (2012b) is to replicate their high signal-to-noise observational spectral data using stellar population models and adjusting the sodium abundance accordingly in order for the spectral features of in-

terest in the models to fit the observational spectra. An important difference in their analysis is their choice of spectral features to replicate when matching the model to observed spectra; they use the Wing-Ford band, NaI doublet and calcium triplet but not the Na5895 feature. From Figure 3.12 it is the Na5895 feature that has the strongest sensitivity to sodium abundance, and with the assumption that the interstellar absorption does not have a pronounced effect on the values, it should be the best feature to constrain the sodium abundance from. It is not unreasonable to imagine that if they had used Na5895 as one of the spectral features to replicate with the model data, they may have found a shallower result for the IMF variation.

The sodium index-index plot (see Figure 3.4) in Section 3.1.2 clearly shows that with increasing velocity dispersion, the galaxy data follow a trend of increasing [Na/Fe] and do not correspond with the vector for increasing x values in the IMF. The observational data cover a wide range of [Na/Fe] with the majority suiting Chabrier and Salpeter-like IMFs and some outlying points corresponding to enhanced [Na/Fe] and bottom-heavy IMFs. The data with velocity dispersions >200 km s^{-1} agree with a similar plot in Spiniello et al. (2012) (their Figure 2b) (after accounting for different index definitions), where they use the same stellar population models as this work. They find that massive galaxies require [Na/Fe]>0.3 dex and correspond with bottom-heavy model IMFs, this is in agreement with this work as although the majority of the data suit a Salpeter-like IMF, there are outlying massive galaxies in the sodium index-index plot that require bottom-heavy IMFs. The spectral features of these outlying galaxies could be affected by errors in the sky subtraction technique that are not accounted for in the given error bars, or they may just be rare galaxies with more low mass stars. The same can be said for those galaxies that appear to require a more bottom-light IMFs than those used in the Conroy models.

4.2.2 Calcium Indices

The IMF variation predicted from the calcium triplet index is consistent with that predicted from the sodium doublet within $\sim 2\sigma$ significance. This is an encouraging result as the variation from calcium was constrained independently from the sodium abundance (which is reported to be affected by Na5895 interstellar absorption). The IMF variations predicted with consideration of the calcium and sodium abundances separately are consistent with each other, this is encouraging that the Na5895 interstellar absorption does not have a fundamental effect on the Na5895-sigma relation.

The calcium abundance variation measured from the index-sigma analysis is [Ca/Fe]$\propto \sigma^{-0.19\pm0.12}$ and is consistent with zero with a significance of 1.6σ. Graves et al. (2007) find [Ca/Fe]$\propto \sigma^{0.130\pm0.039}$, the value from this work is consistent with the Graves' value within 2σ significance. Johansson et al. (2012) find [Ca/Fe] values that are close to solar ([Ca/Fe]$\propto \sigma^{0.15\pm0.01}$), our value is consis-

tent with theirs with a significance of 2.6σ. With the calcium abundance variation being roughly consistent with published values, there is more confidence in the IMF scaling relation found in this study. The fact that the IMF variations predicted from the NaI and CaII indices are consistent with each other, gives more gravitas to the idea that the interstellar absorption of sodium does not have a significant effect on the sodium abundance variation determination.

From the calcium index-index plots (see Figures 3.1 and 3.2) it is evident that in order for the models to correspond with ages that concur with the morphological constraints placed on the sample (i.e. elliptical galaxies which are older) there needs to be a sub-solar average calcium abundance. With a sub-solar calcium abundance, the index-index plot suggests the best-fitting IMFs will be bottom-light, Chabrier-light IMFs which agrees with the sodium index-index plot. Although interpretation of the index-index plots is complicated, the implication from analysis of the plots is that the best-fitting IMF for this galaxy sample is approximately Chabrier or Salpeter like. Due to the incompatible age relations for the calcium index-index plot, there is no strong evidence for the best-fitting IMF for this galaxy sample being bottom-heavy, there are some galaxies in both the calcium and sodium index-index plots that do suit bottom-heavy IMFs, however, it does appear that these are the minority.

The predicted IMF variations constrained from the calcium triplet feature have errors that are five times larger than those errors for the variations constrained from NaI. For the predicted calcium abundance variation, the errors are $\sim$2.5 greater than those for the sodium abundance variation (see Table 3.5). This implies that the calcium indices are less sensitive than the sodium indices and will result in the final quoted value for the IMF variation being that constrained by the NaI index.

4.2.3 Implications of Results

In light of the preceding caveats and assumptions, the results have the following implications. The results from this piece of work suggest that as early-type galaxies get more massive, the sodium abundance increases considerably. At the same time the calcium abundance either shows no variation, or a slight decrease at greater masses. With these abundance variations taken into consideration, the subsequent IMF variation is minimal and consistent with zero. If the galaxies in this sample are considered to be characteristic of early-type galaxies, then for star-formation theories this result suggests that when stars are formed in the progenitors to early-type galaxies, the distribution of stars, as a function of mass, were very similar, if not the same.

The index-index plots (see Figures 3.1, 3.2, 3.3 and 3.4), whilst difficult to interpret due to the crowding around the Salpeter, Chabrier and bottom-light IMF values, suggest that the best-fitting IMF for the average galaxies in this sample (with average abundances taken into consideration) is an approximately Chabrier-like

IMF. Whilst it is not possible to give an accurate estimate of the power-law IMF index for this study, it is unlikely that the average IMF is bottom-heavy (i.e. x$\gtrsim$3). From studies of various stellar populations in the field, young clusters and associations and old globular clusters, it has been suggested that the vast majority have a universal IMF with a power law index of α = 2.35 above a few solar masses, and a log normal or shallower power law ($\alpha \approx$1 - 1.25) for lower mass stars (Bastian et al. (2010)). This is not inconsistent with the results from this piece of work which would suggest there is tentative evidence for a universal IMF.

Current galaxy evolution models use a universal IMF for predicting the properties of galaxies. If the IMF were in fact proven to be universal and equal to the IMF of Galactic populations, these theoretical models would be able to have the IMF as a solid constraint and not have to account for the effect of a varying IMF. Although theoretical studies predict a varying IMF due to the complicated nature of the physics of star formation, it is possible that the multitude of contributory factors that come into assembling stars during epochs of formation are so complicated that the resulting distribution is in fact very similar.

Chapter 5

Conclusion

A variety of spectral features have been measured in SDSS observational and Conroy & van Dokkum (2012a) model galaxy spectra. The combination of dwarf- and giant-characteristic features, along with calcium- and sodium-abundance indicators, is a useful technique for separating the effects of the IMF from those of the different elemental abundances. With model responses from this work and literature scaling relations constrained from optical spectral features it has been possible to predict the variations of calcium and sodium abundances and IMF with increasing galaxy mass. The measured equivalent widths from the observational data are also compared to the predicted equivalent widths from models with different IMFs and elemental abundances to be able to comment on the best-fitting parameters for the galaxies in this sample. The results are summarised as follows :

- The sodium abundance increases strongly with velocity dispersion and dominates the Na-sigma scaling relations. Without considering the variation in sodium abundance, the IMF can be interpreted as having a strong positive trend with velocity dispersion, but with the sodium abundance constrained from the Na5895 index, the resulting IMF variation is minimal in comparison.

- The predicted IMF variation suggests a trend towards slightly more dwarf-depleted populations at greater masses, with a variation of $\mu^{\mathrm{Na}} \propto \sigma^{-0.11\pm0.07}$ (constrained from the NaI index with both calcium and sodium abundances taken into consideration) over the range of a whole decade in sigma. This is also consistent with no systematic IMF variation for increasing velocity dispersion to the significance of $<2\sigma$ which is not in agreement with recent studies which report an IMF variation which is steeper at greater masses.

- The best-fitting IMF for the average galaxies in this sample is Chabrier-like, future work is required to find a more accurate estimate of the low-mass IMF. There are outlier galaxies that appear to require IMFs, ages and abundances outside the range covered by the models. It is expected that in some cases these galaxies represent minority or unique cases where extreme parameters

are required to describe that particular stellar population, or they may be complicated due to their formation history (for reasons that are beyond the scope of this work). It is also possible that due to the significant number of different factors used in this work, the equivalent widths for these outlier galaxies are subject to errors that have not been accounted for by the systematic error bars. Because of the many possible factors affecting the outlier galaxies, this work has focused on the average galaxy population of this sample.

- The IMF variations predicted from different indices (CaII and NaI) with different abundances ([Na/Fe], [Ca/Fe] or combined abundances) are in good agreement with each other and all suggest a decreasing IMF trend with increasing galaxy mass. The sensitivity of sodium is greater than that of calcium, so the IMF variation constrained from the NaI index is quoted as the final value.

- The sodium abundance is constrained from the Na5895 spectral feature. It is thought that this index is substantially affected by interstellar absorption, however, no evidence of prominent upwards scatter is found in this piece of work. With more interstellar dust for lower mass galaxies, it is expected that the effect of interstellar absorption would be to flatten the Na5895-sigma slope, however, evidence of this is not found in this work. For this reason it is assumed that the effect of Na5895 interstellar absorption is minimal and can be ignored. When considering calcium and sodium abundances separately, the predicted IMF variations are consistent with one another, suggesting that the Na5895 feature is suitable for constraining the sodium abundance.

- The calcium abundance variation is found to be slightly shallower for more massive galaxies with [Ca/Fe]$\propto \sigma^{-0.19\pm0.12}$ and is also consistent with zero (to within $<2\sigma$). The result for the calcium abundance scaling relation is consistent with that found by Graves et al. (2007) ([Ca/Fe]$\propto \sigma^{0.130\pm0.039}$) to the significance of 2σ.

It has not been possible to accurately determine the best-fitting IMF for this sample of galaxies in this work, however, the index-index plots for the calcium and sodium indices indicate that the average IMF is centred around the Salpeter, Chabrier and bottom-light IMFs, with some outlier galaxies requiring more bottom-heavy IMFs. Once the sodium abundance has been taken into consideration, there is no evidence for a steepening IMF variation with galaxy mass.

This work has shown that the sodium abundance is a crucial factor to consider when predicting the variation of the IMF. When the sodium abundance is not taken into consideration or is underestimated, the results can indicate a steepening IMF variation. The recent studies that have reported a steepening IMF trend with velocity dispersion from measurement of spectral features either neglect (Ferreras et al. (2012)) or only partially account for (Conroy & van Dokkum

(2012b)) the sodium abundance variation. This is directly due to the exclusion of the Na5895 spectral feature from their sample. This work has endeavoured to provide evidence that the effect of the interstellar sodium absorption at 5895 Å does not have a considerable effect on the Na5895-sigma scaling relation and therefore poses no obstacle to using Na5895 as a method for constraining sodium abundance variations.

Bibliography

Abazajian K. N. et al., 2009, ApJS, 182, 543

Banerji M. et al., 2010, MNRAS, 406, 342

Baraffe I., Chabrier G., Allard F., Hauschildt P. H., 1998, A&A, 337, 403

Bastian N., Covey K. R., Meyer M. R., 2010, ARA&A, 48, 339

Burstein D., Faber S. M., Gaskell C. M., Krumm N., 1984, ApJ, 287, 586

Cappellari M. et al., 2012, Nature, 484, 485

Cardiel N., 2010, Astrophysics Source Code Library, 10046

Cenarro A. J., Gorgas J., Vazdekis A., Cardiel N., Peletier R. F., 2003, MNRAS, 339, L12

Cenarro A. J., Sánchez-Blázquez P., Cardiel N., Gorgas J., 2004, ApJ, 614, L101

Chabrier G., 2003, PASP, 115, 763

Chabrier G., Baraffe I., 1997, A&A, 327, 1039

Conroy C., van Dokkum P., 2011, ArXiv e-prints

Conroy C., van Dokkum P., 2012a, ApJ, 747, 69

Conroy C., van Dokkum P., 2012b, ArXiv e-prints

Dotter A., Chaboyer B., Jevremović D., Kostov V., Baron E., Ferguson J. W., 2008, ApJS, 178, 89

Einstein A., 1936, Science, 84, 506

Faber S. M., Friel E. D., Burstein D., Gaskell C. M., 1985, ApJS, 57, 711

Ferreras I., La Barbera F., de Carvalho R. R., de la Rosa I. G., Vazdekis A., Falcon-Barroso J., Ricciardelli E., 2012, ArXiv e-prints

Graves G. J., Faber S. M., Schiavon R. P., Yan R., 2007, ApJ, 671, 243

Henry T. J., McCarthy, Jr. D. W., 1993, AJ, 106, 773

Johansson J., Thomas D., Maraston C., 2012, MNRAS, 421, 1908

Jones J. E., Alloin D. M., Jones B. J. T., 1984, ApJ, 283, 457

Kroupa P., 2001, MNRAS, 322, 231

Kroupa P., 2002, Science, 295, 82

Kroupa P., Tout C. A., Gilmore G., 1993, MNRAS, 262, 545

Kuntschner H., 2000, MNRAS, 315, 184

Lintott C. J. et al., 2008, MNRAS, 389, 1179

Nelan J. E., Smith R. J., Hudson M. J., Wegner G. A., Lucey J. R., Moore S. A. W., Quinney S. J., Suntzeff N. B., 2005, ApJ, 632, 137

Nordh H. L., Lindgren B., Wing R. F., 1977, A&A, 56, 1

Oey M. S., 2011, ApJ, 739, L46

Saglia R. P., Maraston C., Thomas D., Bender R., Colless M., 2002, ApJ, 579, L13

Salpeter E. E., 1955, ApJ, 121, 161

Scalo J., 1998, 142, 201

Schiavon R. P., 2007, ApJS, 171, 146

Schiavon R. P., Barbuy B., Bruzual A. G., 2000, ApJ, 532, 453

Smith R. J., Lucey J. R., Carter D., 2012, ArXiv e-prints

Smith R. J., Lucey J. R., Hudson M. J., 2007, MNRAS, 381, 1035

Smith R. J., Lucey J. R., Hudson M. J., 2009, MNRAS, 400, 1690

Sonnenfeld A., Treu T., Gavazzi R., Marshall P. J., Auger M. W., Suyu S. H., Koopmans L. V. E., Bolton A. S., 2012, ApJ, 752, 163

Sparks W. B., Carollo C. M., Macchetto F., 1997, ApJ, 486, 253

Spiniello C., Koopmans L. V. E., Trager S. C., Czoske O., Treu T., 2011, MNRAS, 417, 3000

Spiniello C., Trager S. C., Koopmans L. V. E., Chen Y. P., 2012, ApJ, 753, L32

Thomas D., Maraston C., Johansson J., 2011, MNRAS, 412, 2183

Trager S. C., Worthey G., Faber S. M., Burstein D., Gonzalez J. J., 1998, ApJS, 116, 1

Treu T., Auger M. W., Koopmans L. V. E., Gavazzi R., Marshall P. J., Bolton A. S., 2010, ApJ, 709, 1195

van Dokkum P. G., Conroy C., 2010, Nature, 468, 940

Vazdekis A., Sánchez-Blázquez P., Falcón-Barroso J., Cenarro A. J., Beasley M. A., Cardiel N., Gorgas J., Peletier R. F., 2010, MNRAS, 404, 1639

Warner B., 1961, PASP, 73, 439

Wild V., Hewett P. C., 2005, MNRAS, 358, 1083

Wild V., Hewett P. C., 2010, ArXiv e-prints

Wing R. F., Ford, Jr. W. K., 1969, PASP, 81, 527

Worthey G., 1994, ApJS, 95, 107

Worthey G., Ottaviani D. L., 1997, ApJS, 111, 377

Zoccali M., Cassisi S., Frogel J. A., Gould A., Ortolani S., Renzini A., Rich R. M., Stephens A. W., 2000, ApJ, 530, 418